5-2020

The effects of intercalating molecules on the polymer properties of DNA

Joseph Tibbs
University of Northern Iowa

THE EFFECTS OF INTERCALATING MOLECULES ON THE POLYMER PROPERTIES OF DNA

A Thesis Submitted

in Partial Fulfillment

of the Requirements for the Designation

University Honors with Distinction

Joseph Tibbs

University of Northern Iowa

May 2020

This Study by: Joseph Tibbs

Entitled:

THE EFFECTS OF INTERCALATING MOLECULES ON THE POLYMER PROPERTIES OF DNA

has been approved as meeting the thesis or project requirement for the Designation

University Honors with Distinction or University Honors (select appropriate designation)

5/4/2020	Dr. Justin Peters
_____	_____
Date	Honors Thesis Advisor
5/4/2020	Dr. Ali Tabei
_____	_____
Date	Honors Thesis Advisor
_____	_____
Date	Dr. Jessica Moon, Director, University Honors Program

Acknowledgements:

The author would like to acknowledge the lab of Dr. Timothy Kidd at the University of Northern Iowa for the use of his Atomic Force Microscope, and for the assistance of Taylor Harris in calibration and technical assistance. This work was funded by the Student Opportunities for Academic Research (SOAR) Award from the University of Northern Iowa. This thesis was guided jointly by Dr. Justin Peters of the UNI Department of Chemistry & Biochemistry and Dr. Ali Tabei of the UNI Department of Physics.

Abstract:

This project used Atomic Force Microscopy (AFM) imaging to examine the effects of different intercalation conditions upon the elastic properties of intrinsically straight DNA molecules. Three intercalating molecules (chloroquine, ethidium bromide, and acridine) were used to demonstrate the dependence of persistence length and mean polymer extension on the intercalator type. It was found that all three intercalators significantly increased persistence length, and that this effect was most pronounced for ethidium bromide. In addition, an analysis of the normal bending modes of the static molecules corroborated these results. The only intercalator which resulted in significant extension of the DNA polymers was ethidium bromide. By measuring these properties for a model system of DNA, the understanding of binding effects of intercalators and the bending properties of generic DNA molecules will be improved.

Introduction:

Deoxyribonucleic acid (DNA) is a polymer which is essential to life, composed of base pair units in chains extending thousands or even millions of monomers in length. The genetic code contained in this fundamental molecule has been analyzed by countless studies, but the physical structure providing the scaffold for that information is still revealing new properties of biological significance (Peters et al., 2014). Like most polymers, this long chain can bend and twist; the simple "Worm-like Chain" (WLC) model accounts for the energetics of many of these conformations (Peters & Maher, 2010). However, unlike most polymers, when DNA bends, coils, or wraps itself around other objects, significant biological activity is the result (Hogan & Austin, 1987). Single-molecule studies have done much in recent years to examine both the protein-dependent property changes as well as the importance of the bending properties themselves in the regulation of protein binding. For example, Han et al. (2009) investigated the important impact of DNA bending on the function of the *lac* operon. In essence, the simple regulatory act of bending DNA can change the behavior of gene transcription, the process by which DNA acts as the "blueprint" for cells, tissues, and entire organisms. Thus, it is essential to understand the chemical and physical behavior of this fundamental building block of biology.

The bending of DNA in regulatory mechanisms can also assume nonequilibrium dynamics, driven by protein activity (Ross et al., 2018). These types of systems are ubiquitous across disciplines and are under active research by physicists searching for new models to explain far-from-equilibrium behavior. For example, in studies of nonequilibrium bending, Seara et al. (2018) drew conclusions about fundamental balances between system energy and entropy dissipation using the polymer properties of biomolecules called actin filaments. Thus,

knowing quantitative details about the flexibility of DNA and other biopolymers promises to advance the understanding of both biological mechanisms and non-equilibrium polymer physics.

One important parameter in characterizing the flexibility of molecules is the *persistence length* of a polymer chain, a measurement of its resistance to bending. Persistence length, *P*, for a chain confined to two dimensions is defined rigorously as

$$\langle \cos\left(\theta(s)\right)\rangle = \exp(-s/2P) \tag{1}$$

In essence, the rate of decay of the correlation of the angle between two locations on the chain is proportional to the arc length (*s*) separating them and inversely proportional to the persistence length of the polymer (Gittes et al., 1993). Figure 1 illustrates an example of a θ measurement on a chain composed of discrete linear elements. However, the determination of *P* stated above is only one way of extracting the persistence length of a flexible rod. Peters and Maher (2018) demonstrated a variety of methods for calculating the persistence length using higher-order moments of θ and end-end distance (R). Each of these provides an independent estimate of *P* from discrete chain data.

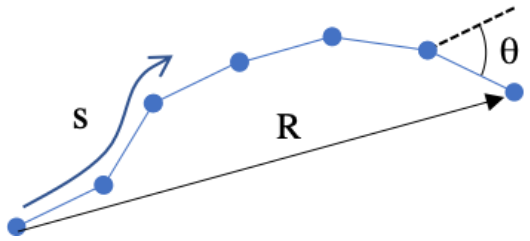

Figure 1: Discrete Freely-Rotating Chain

The discrete freely-rotating chain model assumes that the polymer is made of linear segments. The worm-like chain (WLC) is the limit of this model in which the length of the segments approaches zero while the contour length is unchanged. Labeled in the figure are the contour length measured from the left end (*s*), the end-end vector between two points (**R**, with magnitude R), and the change in angle (θ) between the first and last segment. By measuring θ and R between a variety of intervals, the functions θ(*s*) and R(*s*) may be defined.

Extracting shape data from a biopolymer requires the ability to probe and visualize biological molecules at the single-molecule level. The advent of Atomic Force Microscopy (AFM) technology resulted in the ability to image surfaces at resolutions approaching the size of molecules. These methods use highly precise positioning and sensing mechanisms to feel, rather than see, their targets. An AFM instrument uses a cantilever with a precisely machined tip to scan over a surface. In tapping mode, the cantilever is driven to vibrate near its resonance frequency, causing the amplitude of these vibrations to be highly sensitive to any forces acting on the tip from the surface. An internal feedback loop running a z-dimension piezoelectric actuator maintains the tip at a constant height above the surface. Thus as the tip scans over the surface it records height changes as a reflection of the underlying topography of the surface, and anything on it. A sensitive AFM with a sharp silicon tip can resolve structures with resolution exceeding 10 nm, on the order of the 2-nm width of DNA molecules. Thus by depositing DNA onto a sufficiently flat surface, AFM measurements can accurately show the shape of the molecules (Figure 2). Rivetti, Guthold, and Bustamante (1996) showed that the images produced by this technique can be robustly analyzed to produce DNA bending profiles.

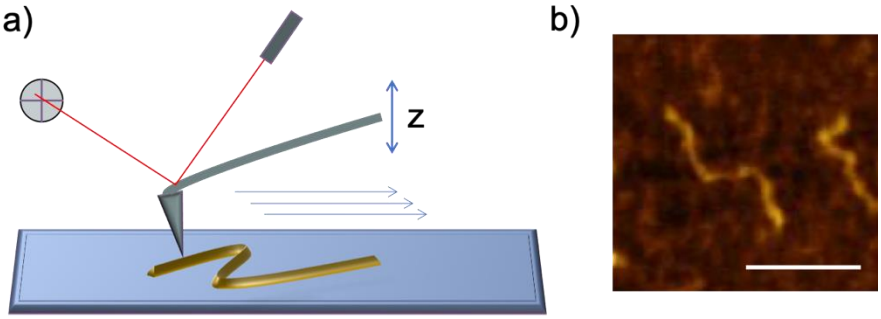

Figure 2: Atomic Force Microscopy
a) A cartoon schematic of an AFM setup. The tip scans over the surface, vibrating near its resonant frequency. This vibration is measured by the motion of a laser reflecting off of the cantilever. When features on the surface (such as molecules) alter the forces on the tip, a z piezo adjusts the vertical position of the cantilever. b) An example image of a DNA molecule; scale bar is 100 nm, maximum height contrast is ~ 2 nm.

To understand the material properties of DNA, it is useful to build models of DNA's behavior under contrived experimental conditions, which then inform on the behavior of DNA in its native state. One perturbation to DNA molecules commonly encountered in the biochemical laboratory is the influence of intercalating molecules. Intercalation, in this context, is the process of insertion of hydrophobic molecules into the spaces between the "rungs" of the DNA double helix. The flat, aromatic molecules find a favorable environment in the slots between the closely-spaced aromatic DNA bases (Lerman, 1964). This ability to disrupt DNA's structure gives these molecules mutagenic and carcinogenic properties. However, upon binding to DNA, some intercalators become fluorescent, allowing the specific detection of DNA, making intercalating dyes an essential quantitative tool for biochemistry (Hong & Piette, 1976). Ethidium bromide is one example of such a dye, and is consistently used in biochemistry labs today. Other intercalators, from organic molecules to organometallic complexes (Mihailovic et al., 2006), do not have the fluorescent properties necessary to stain DNA, but still bind preferentially between the bases of DNA.

However, certain aspects of intercalation by these molecules are still not well understood, especially regarding how they alter the physical properties of the DNA molecules. Smith, Finzi, and Bustamante (1992) used direct force spectroscopy methods to determine length extension upon intercalation, and Pope et al. (2000) observed changes in the supercoiling structure of closed-loop plasmids. Hards (2005) used force spectroscopy, focused on double-stranded cohesion properties in the presence of intercalator. However, quantitation of persistence length changes by AFM imaging have been attempted only for limited systems despite the importance of DNA bending properties (Moukhtar, et al., 2007). As a result, there is a need for data on DNA bending under intercalation conditions on linear molecules which have been corrected for

sequence-dependent curvature (called *intrinsically straight* molecules). Further, using the methods of Gittes et al. (1993) an expanded set of physical properties can be extracted from such a system, including static bending energy. These methods involve modeling the molecules' flexibility as being composed of distinct, orthogonal bending modes corresponding to the normal modes of a classical oscillating rod. This process is illustrated schematically in Figure 3.

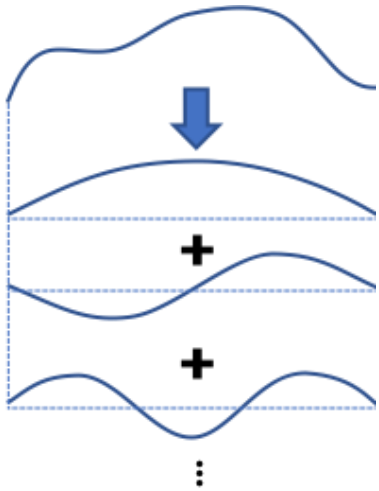

Figure 3: Bending Modes Illustration
A simplified picture of the bending modes decomposition process. A chain is modeled as being composed of distinct modes of bending which are orthogonal (energy is not transferred between the modes in the course of motion).

The aim of this project is to use Atomic Force Microscopy imaging to observe the physical and energetic properties of intrinsically straight DNA molecules under the influence of several intercalating molecules. By observing the changes in contour length and persistence length of the molecules, differences in the binding behavior of the intercalators can be determined. This in turn will further elucidate the elastic properties of DNA as a physical polymer and as an important biological molecule.

Experimental Methods

A region of intrinsically straight DNA 752-bp in length was amplified from plasmid pUNI18 using standard polymerase chain reaction (PCR) conditions with a 60°C annealing temperature, *Taq* polymerase, and the primers UNI8 (5′-CGGTGATGACGGTGAAAA) and UNI7 (5′-TGTGAGTTAGCTCACTCATTAGG). The amplified DNA was screened for nonspecific products by running a portion of the sample on a 2% agarose gel, and the remaining product was purified using a PCR purification kit and quantified using UV-Vis spectroscopy. A 12.6 ng/µL stock was used for the creation of all further DNA samples.

All samples (including a control condition lacking intercalator) were prepared in AFM buffer (5 mM Tris-HCl at pH 8.4 supplemented with 5 mM magnesium chloride and 12.5 mM potassium chloride) with an added DNA concentration of 2-4 ng/µL. For the experimental conditions, a molar excess of intercalator (relative to the DNA base pair concentration) was added. Three intercalators were used: ethidium bromide, acridine, and chloroquine (Figure 4).

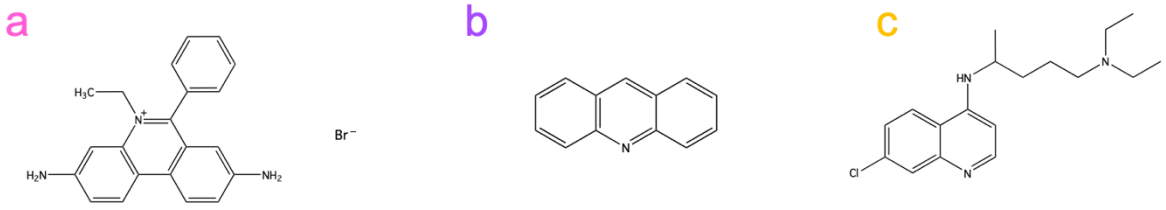

Figure 4: Intercalators used in Experimental Conditions
The chemical structure of the three intercalators mixed with the DNA. a) ethidium bromide, b) chloroquine, c) acridine. The labels are color-coded to match the colors used in all later figures; the control condition is indicated by the color blue.

Just prior to imaging, a 10 µL droplet of sample was deposited onto a freshly-cleaved mica surface and adsorption allowed for 2-3 minutes. Then the mica surface was gently rinsed

with ~5 mL of autoclaved water, and dried with a stream of air. For the ethidium bromide condition only, the mica was pre-treated with a 50 mM solution of magnesium chloride prior to deposition.

An Agilent 5500 SPM Atomic Force Microscope equipped with an A-type scanner and MAC Mode III controller operating in alternating current (AC) tapping mode was used to scan the mica surface. Samples were imaged with silicon cantilevers (PPP-NCHR, NanoAndMore) at a resonance frequency near 320 kHz. Scans were collected in air at room temperature and

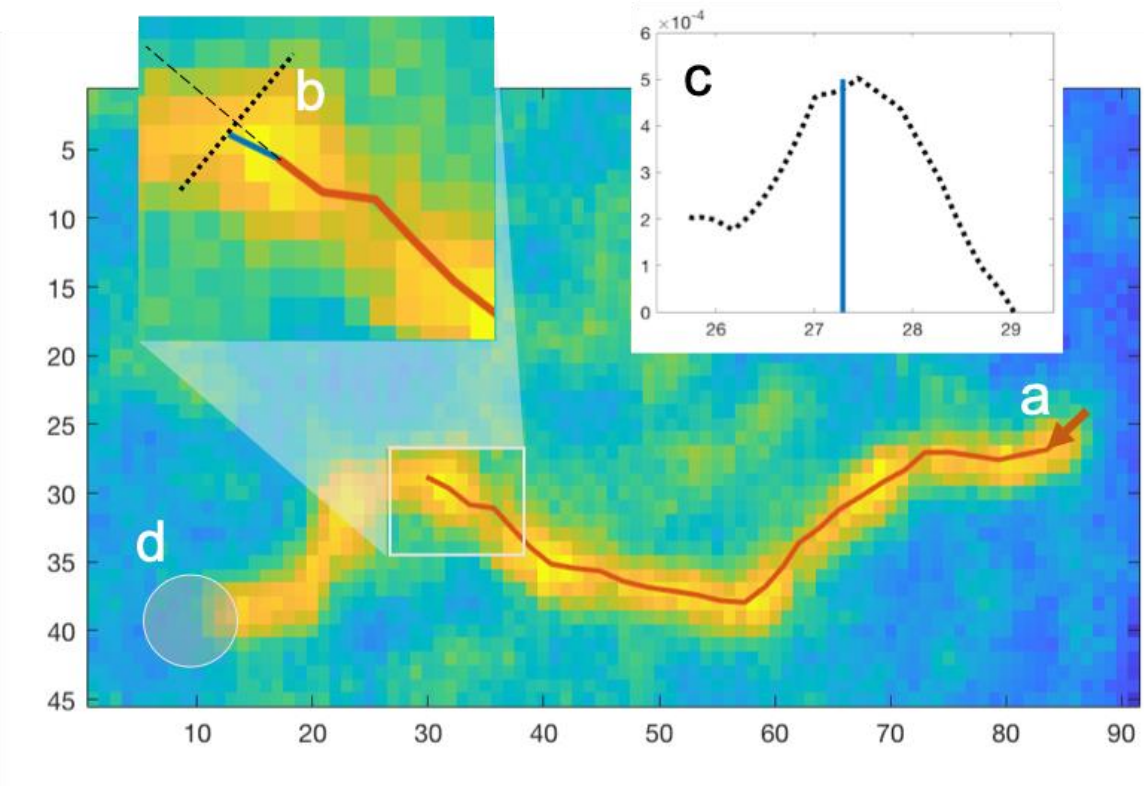

Figure 5: Chain-Stepping Procedure

a) The user selects the beginning point and direction of the chain. b) For each successive step, MATLAB's gridded interpolant function is used to extract a section of the height profile at a right angle (dotted line) to the current trajectory (dashed line). c) A graph of the height profile along the section. The center of mass (first moment) of the profile is determined (blue line). This determines the direction of the next step (blue segment in inset b). d) This continues until a step enters the user-identified end region, defined by a central point and a radius.

humidity and had a resolution of 256 × 256 pixels and dimensions of 600 nm × 600 nm. The resulting topography images were either processed for figures using Gwyddion software or imported into MATLAB where a custom tracing script was used to digitize the molecules into discrete chains. First, the user specified a step size for the length of chain segments. The user then selected the beginning point and end point region of a particular isolated molecule where both ends were visible. From there, the code automatically stepped from one end of the molecule to the other until the chain was extended into the user-identified end region. Stepping along the polymer was done in a manner similar to that of Wiggins et al. (2006), and is illustrated in Figure 5.

The digitized traces from a set are analyzed using the method of Peters and Maher (2018) to determine the persistence length (P) using eight independent estimation methods. These methods involve using WLC-derived models for the functional form of an experimentally-determined value as a function of the separation distance. Each WLC model has only one parameter, dependent on the persistence length, and thus a non-linear least-squares (cost-minimizing) fit to the experimental data creates an estimate of P. The list of quantities and functional forms used is listed in Supplemental Table 1. The contour lengths of the molecules are estimated by sums of the linear chain segments.

Fourier bending mode analysis was conducting using the methods of Gittes et al. (1993) but with an algebraic alteration to the method of calculating θ_k, the angular direction of each segment, to allow for polymers with significant curvature. The resulting bending mode amplitudes were used to estimate the persistence length of each experimental group.

Results and Discussion

AFM scanning resulted in images such as those seen in Figure 6. The AFM tip was changed between datasets, and the acridine dataset was composed of fewer (and lower-quality) images due to constraints on data collection at the time of the thesis completion. Nevertheless, each condition had at least 40 molecules which could be digitized and subjected to analysis.

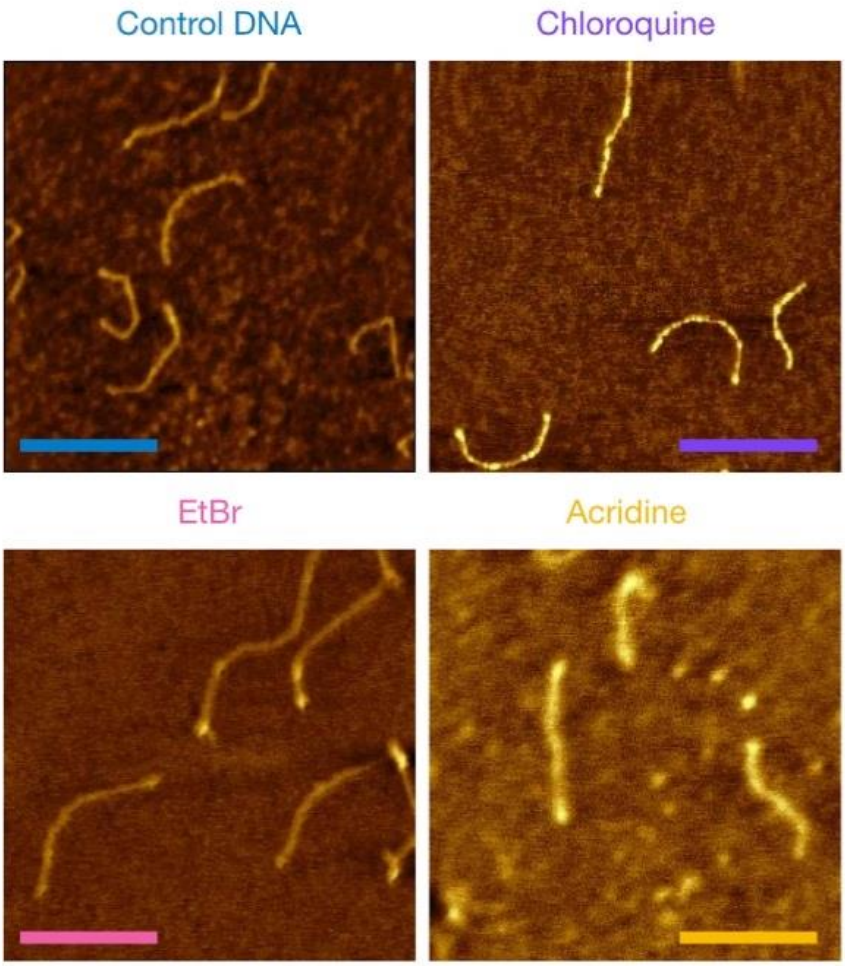

Figure 6: Representative Images
These images are taken from the datasets used in the analysis. The scale bars (color-coded to the condition, as in Figure 4) are all 200 nm and the gold color gradient reflects a sample height from 0 nm to 1.7 nm.

The molecules used for analysis are compiled in the flower plots shown in Figure 7. In these plots, the first segment of each digitized trace is aligned, and the resulting evolution of the ensemble can be seen at a glance. Figures 8-11 show the results of fitting the data using the WLC models in order to obtain estimates for the persistence length. Table 1 summarizes the results of the persistence length and contour length for the experimental conditions.

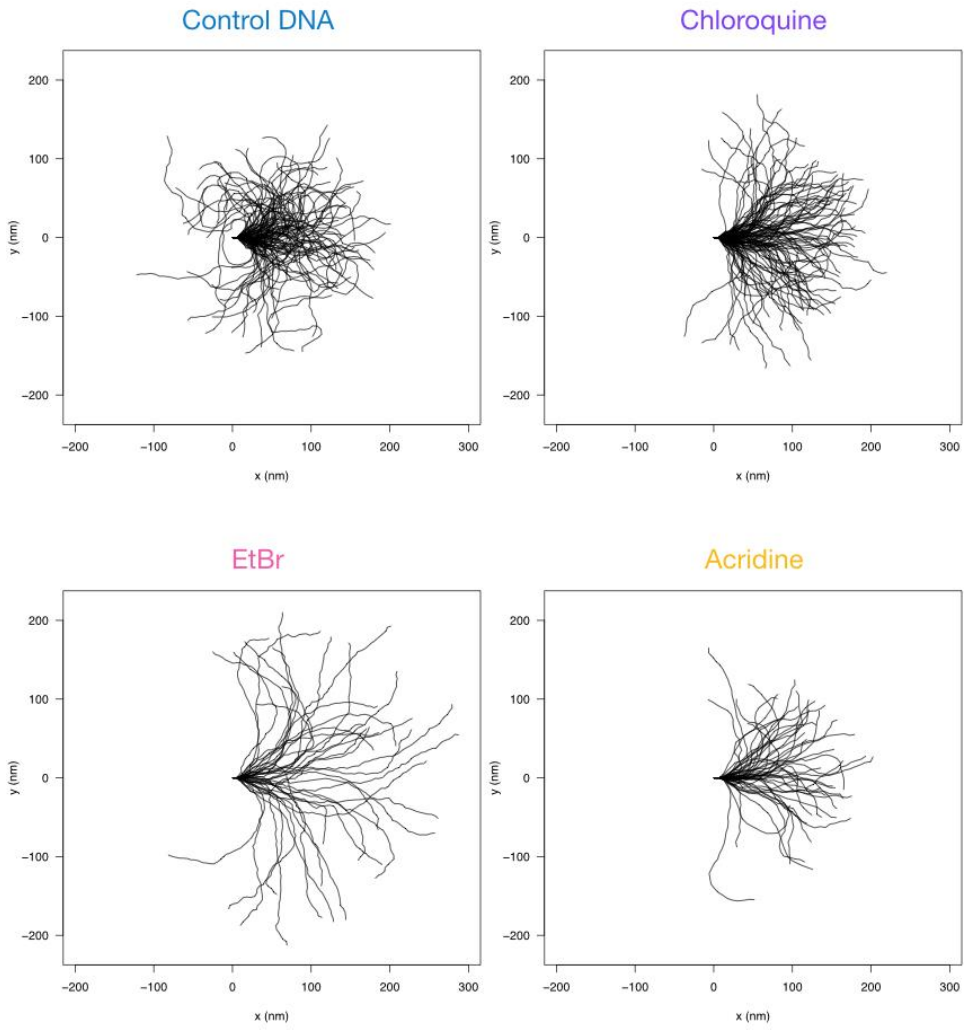

Figure 7: Flower Plots

The four datasets are illustrated using flower plots, in which all chains are rotated such that the first segment of each chain is aligned. Qualitatively, it appears that the Control DNA has a greater tendency to curve, and that the EtBr DNA molecules are comparatively the most elongated and straightened.

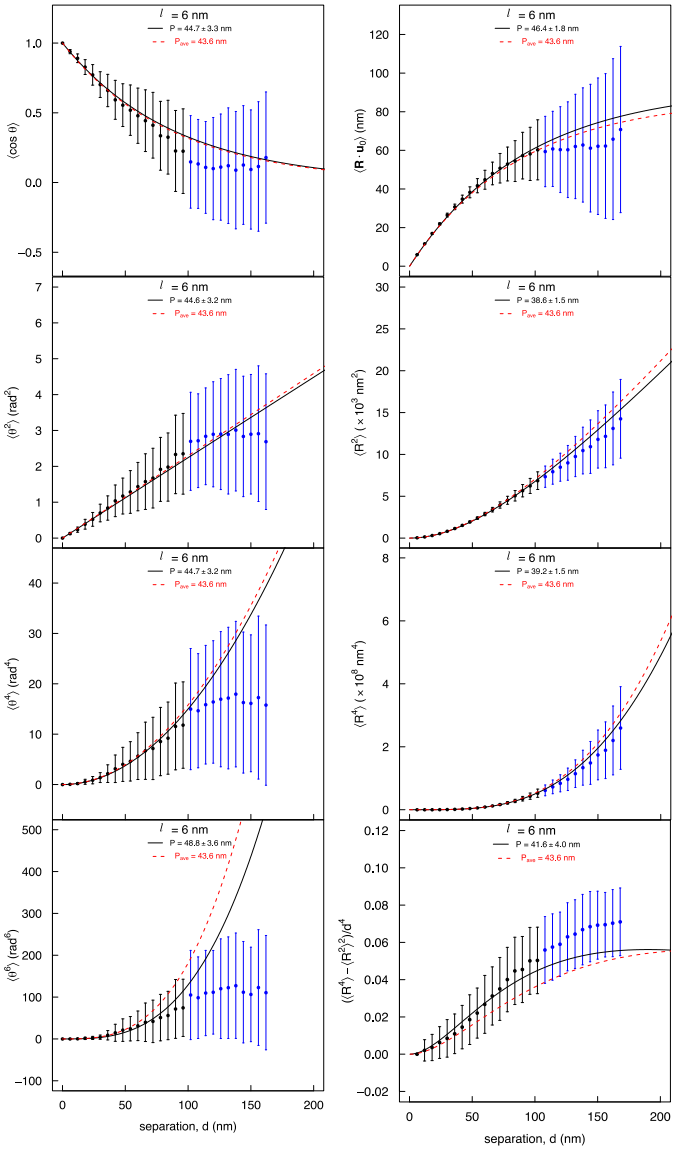

Figure 8: Control Persistence Length Estimates

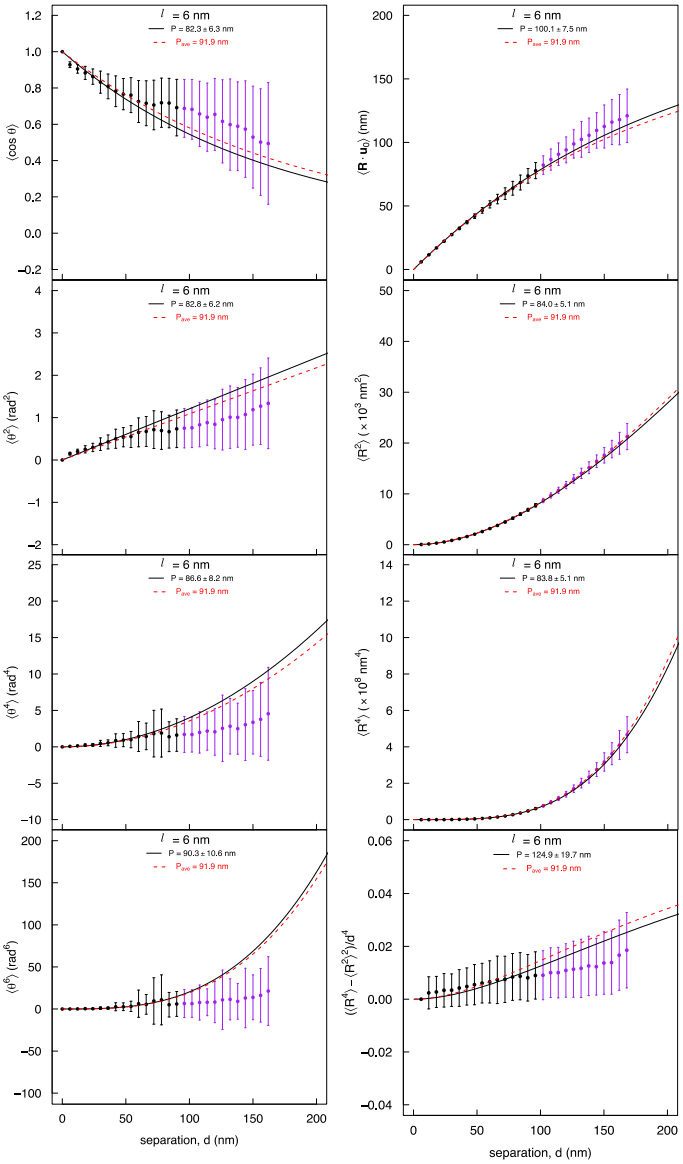

Figure 9: Chloroquine Persistence Length Estimates

In Figures 8-11, the experimental data is subjected to analysis by angular correlation and other statistical moment fitting, informed by an idealized WLC polymer. Each WLC model relates the statistical ensemble quantity on the vertical axis to the separation distance *d* along the chain contour. Values calculated from experimental data are plotted (dots and error bars) along with the best-fit model (solid line) with the estimate of persistence length (*P*) listed at the top in black.

(continued on next page)

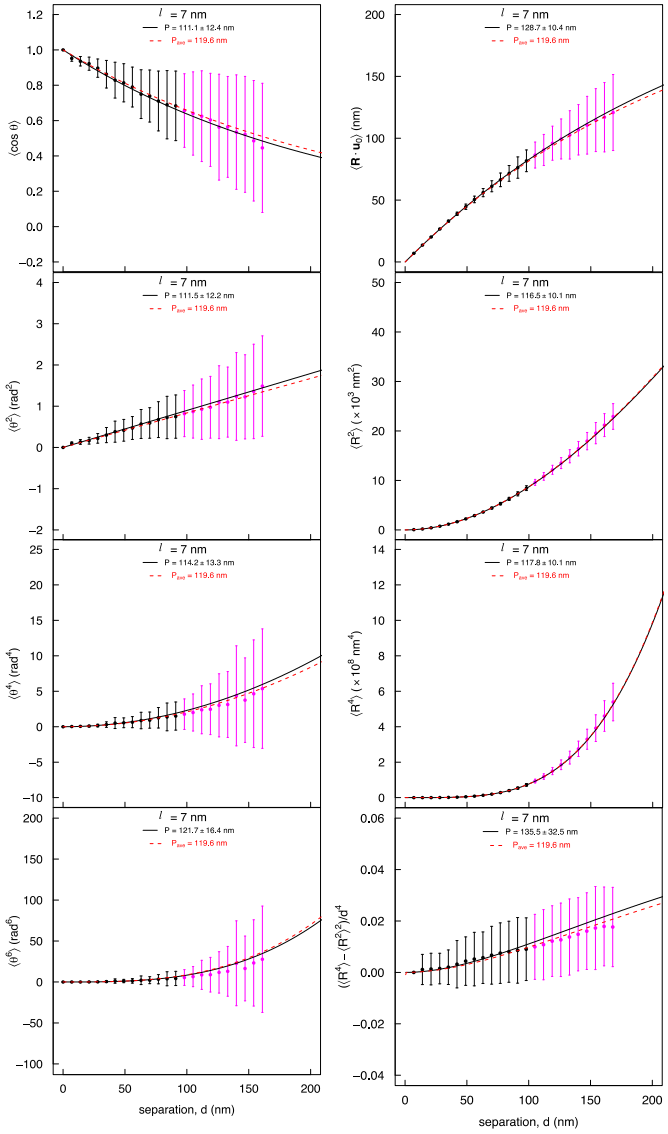

Figure 10: Ethidium Bromide Persistence Length Estimates

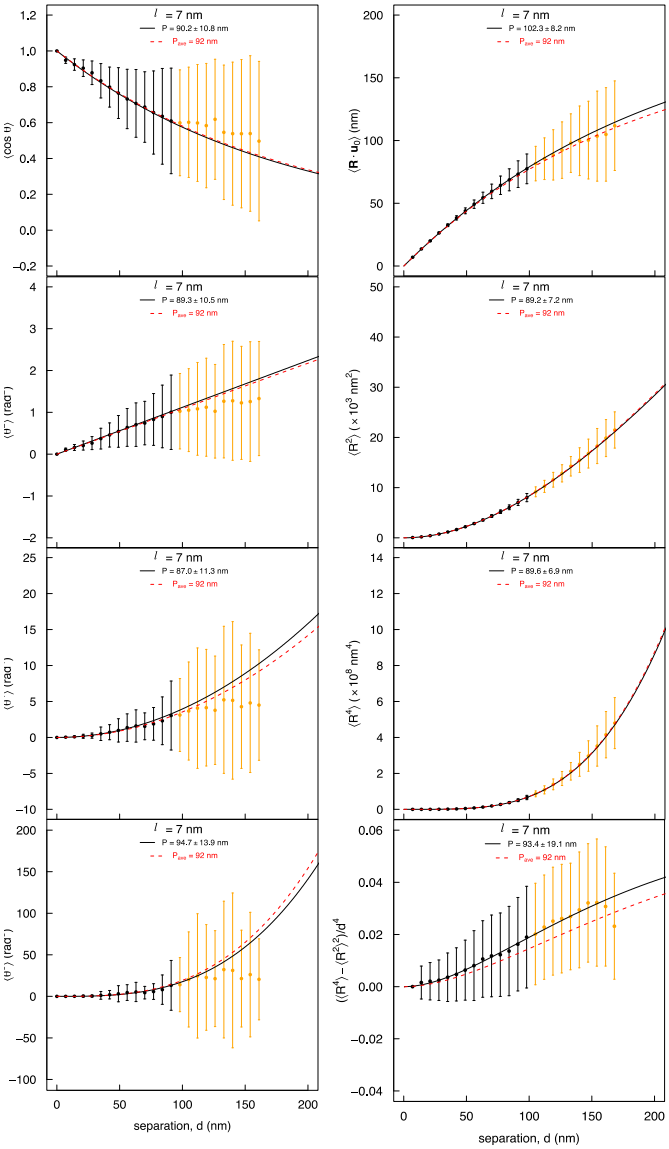

Figure 11: Acridine Persistence Length Estimates

(continued from previous page)

At the top in red is the P_{ave} determined by an average of all eight estimation methods, and the red dashed line is the model prediction using the parameter corresponding to P_{ave}. The color-coded data were excluded from fitting (longer separation distances d are known to exhibit volume-exclusion effects and thus deviate from the WLC model) but are shown for comparison.

Table 1: Summarized Persistence Length Results

Parameter	Symbol	Control	Chloroquine	Ethidium Bromide	Acridine
Number of molecules	N	96	93	41	49
Optimal step size	l (nm)	6	6	7	7
Contour length	L_C (nm)	194 ± 37	185 ± 30	250 ± 34	176 ± 26
Persistence length	P (nm)	43.6 ± 3.5	91.9 ± 14.6	119.6 ± 8.6	92.0 ± 4.8

In the previous figures, the data is plotted for each experimental quantity as a function of the contour separation distance d, with error bars generated from 1000 random nonoverlapping samplings of the datasets). The solid black line shows the best fit to the black dataset. The color-coded data points are not included in the fit because, for larger d, the models become unreliable due to volume exclusion effects. The top of each plot lists the estimated value of the persistence length obtained from that model, as well as the averaged value of all estimations for that experimental condition (P_{ave} in red). The red dotted line on each plot shows the expected trend of the data given a persistence length equal to P_{ave}.

The results, summarized in Table 1, show clear trends in the persistence length. Addition of the intercalating molecules significantly increased the persistence length of the DNA molecules. The ethidium bromide condition appeared to increase the persistence length by the greatest amount; this is qualitatively visible in the flower plot of Figure 7, where the EtBr traces tend to appear smoother and less curved than the other molecules. Despite the lower number of sampled molecules, the error estimations of persistence length were relatively small for the EtBr and acridine conditions.

The contour length (L_C) results were more difficult to interpret, since the only molecules which exhibited a clear increase in contour length were those treated with ethidium bromide. It is well-known that EtBr, upon binding, causes the spreading of the bases in DNA, lengthening

and somewhat unwinding the molecule (Krautbauer et al., 2002). Since the other intercalating molecules did not display an increase in contour length, it is possible that the bases were not forced apart to the same extent by the insertion of the planar acridine or chloroquine. This puzzling result for contour length warrants further study of the system to identify the possible mechanisms of intercalation.

Analysis of the Fourier bending modes also identified the intercalated molecules as having a greater bending modulus, which is directly proportional to the persistence length. For the intercalated molecules, significant agreement was found between the experimentally-determined bending energies and the equipartition theorem. That is, the energy contributions of all modes were roughly equivalent regardless of bending mode number *n*. These promising results suggest that further exploration with bending mode analysis is warranted to extract quantitative information about energetics.

Gittes et al. (1993) found that the variance in the amplitude (*a*) of each mode in a time series was an independent estimator of *P*, such that:

$$P = \frac{L_C^2}{n^2\pi^2 \mathrm{var}(a_n)} \qquad (2)$$

.

Here, L_C refers to the contour length of the polymer – the total length measured along the curvature of the molecule. The number *n* refers to the mode number under consideration, a_n represents the set of amplitudes of that mode for all of the molecules under consideration, and "var" refers to the variance of the set. Although the present data are not a time series over a single molecule, the ensemble of molecules does provide a population which has a distribution of mode amplitudes and a mean contour length which can be used in the above equation. The results of this analysis for each mode amplitude in the four datasets is shown in Figure 12.

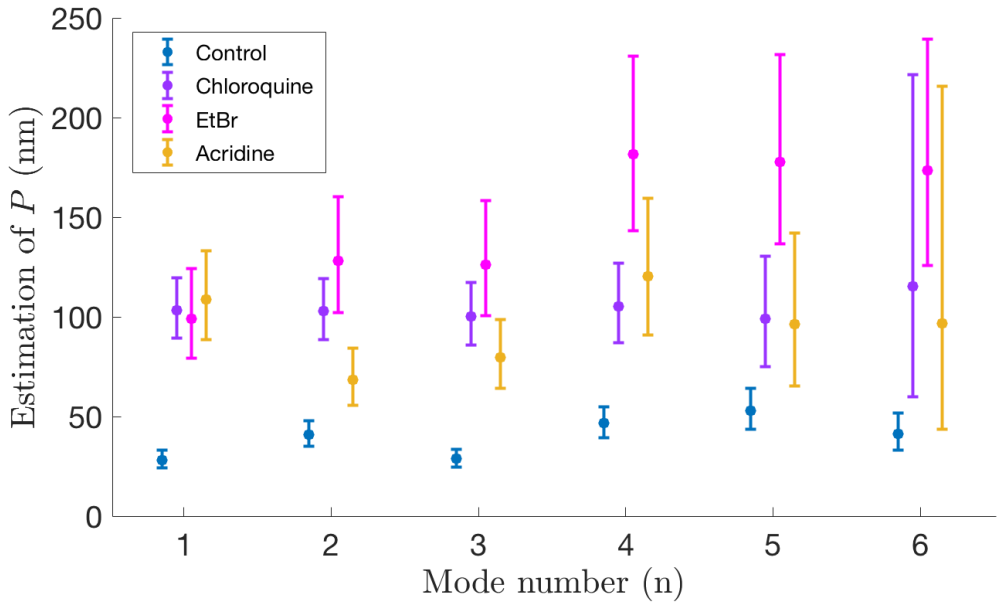

Figure 12: Normal Mode Estimation of *P* by Mode Number

For each condition (control or intercalator), each of the first six modes (*n*) were used to estimate the persistence length (*P*). The average contour length (from Table 1) as well as the variance of the set of amplitudes calculated for a given mode across all molecules was used in these estimations. The error bars were calculated based on an instrument uncertainty equal to the size of a pixel and other error dependencies detailed in the supplement.

The estimations display a certain amount of variation between the modes (only the first six modes were used for purposes of averaging), but taken in aggregate they produce qualitatively similar results to the previous WLC-based method. Table 2 summarizes the estimations obtained from both methods. The values obtained from the Normal Modes method vary somewhat from the WLC estimations, and the margins of error are also generally larger. However, the two estimation methods are qualitatively consistent with each other.

Table 2: Comparison of Estimation Methods

***P* Estimations (nm)**	**Control**	**Chloroquine**	**Ethidium Bromide**	**Acridine**
WLC	44 ± 3.5	92 ± 14.6	120 ± 8.6	92 ± 4.8
Normal Modes (6 modes)	40 ± 10	104 ± 6	148 ± 34	95 ± 19

Future Work and Conclusions:

This thesis used Atomic Force Microscopy to probe the physical properties of DNA under the influence of intercalating molecules. The major result was showing an increase in persistence length for DNA molecules upon intercalation with chloroquine, ethidium bromide, or acridine. Results were less clear for the effect on polymer length. Finally, bending mode analyses yielded results that were qualitatively in agreement with both the WLC method and theoretical models of energetics. Further bending mode analysis shows promise in future exploration of this system.

This study was restricted by a limited amount of data and some inconsistency in AFM image quality, as mentioned for the acridine case specifically. In the future, work would ideally involve multiple datasets of each condition being aggregated to reduce the effects of environmental and other transient factors. Moreover, future experiments could be rigorously performed as a function of intercalator concentration. This approach may be limited in the acridine experimental condition, as the concentration used in this study was already nearing the solubility of acridine, and precipitation may result.

In the future, this work could be extended to examine more types of intercalating molecules and additional examples of the various types. Because the extent of bending (and the bending energies calculated in the bending mode analysis) depend on temperature, depositing the molecules at a range of temperatures might provide more insight on the nature of the molecules' flexibility, and add robustness to the results.

In summary, this project identified important properties of DNA molecules under the influence of intercalating molecules. These properties are tied to DNA's ability to engage in regulatory mechanisms dependent on its flexibility. The DNA binding and insertion ability of

intercalators also makes this class of molecules particularly carcinogenic (Lerman, 1961). Understanding the mechanisms of this carcinogenesis depends on relating the physical and chemical properties of the DNA molecule to its biological function. Analogously, the flexible nature of DNA is not merely a necessity for the polymer to fit inside a cell, but an important factor in the regulation and activity of this fundamental molecule of life. By understanding the physical properties of DNA as a polymer, applications significant to DNA's biological function may be developed, and basic research is the first step in achieving this kind of understanding.

References

Gittes, F., Mickey, B., Nettleton, J. & Howard, J. (1993) Flexural rigidity of microtubules and actin-filaments measured from thermal fluctuations in shape. *J. Cell. Biol.*, 120, 923–934.

Hards, A., Zhou, C., Seitz, M., Bräuchle, C., & Zumbusch, A. (2005). Simultaneous AFM manipulation and fluorescence imaging of single DNA strands. *ChemPhysChem*, *6*(3), 534-540.

Han, L., Garcia, H. G., Blumberg, S., Towles, K. B., Beausang, J. F., Nelson, P. C., & Phillips, R. (2009). Concentration and length dependence of DNA looping in transcriptional regulation. *PloS one*, *4*(5), e5621.

Hogan, M. E., & Austin, R. H. (1987). Importance of DNA stiffness in protein–DNA binding specificity. *Nature*, *329*(6136), 263.

Hong, S. J., & Piette, L. H. (1976). Electron spin resonance spin-label studies of intercalation of ethidium bromide and aromatic amine carcinogens in DNA. *Cancer research*, *36*(3), 1159-1171.

Krautbauer, R., Pope, L. H., Schrader, T. E., Allen, S., & Gaub, H. E. (2002). Discriminating small molecule DNA binding modes by single molecule force spectroscopy. *FEBS letters*, 510(3), 154-158.

Lerman, L. S. (1961). Structural considerations in the interaction of DNA and acridines. *Journal of molecular biology*, *3*(1), 18-IN14.

Lerman, L. S. (1964). Acridine mutagens and DNA structure. *Journal of cellular and comparative physiology*, *64*(S1), 1-18.

Mihailovic, A., Vladescu, I., McCauley, M., Ly, E., Williams, M. C., Spain, E. M., & Nuñez, M. E. (2006). Exploring the interaction of ruthenium (II) polypyridyl complexes with DNA using single-molecule techniques. *Langmuir*, 22(10), 4699-4709.

Moukhtar, J., Fontaine, E., Faivre-Moskalenko, C., & Arnéodo, A. (2007). Probing persistence in DNA curvature properties with atomic force microscopy. *Physical review letters*, *98*(17), 178101.

Peters, J. P., & Maher III, L. J. (2010). DNA curvature and flexibility in vitro and in vivo. *Quarterly reviews of biophysics*, *43*(1), 23-63.

Peters, J. P., & Maher III, L. J. (2018). Approaches for Determining DNA Persistence Length Using Atomic Force Microscopy. In *Bacterial Chromatin* (pp. 211-256). Humana Press, New York, NY.

Peters, J. P., Mogil, L. S., McCauley, M. J., Williams, M. C., & Maher III, L. J. (2014). Mechanical properties of base-modified DNA are not strictly determined by base stacking or electrostatic interactions. *Biophysical journal*, *107*(2), 448-459.

Pope, L. H., Davies, M. C., Laughton, C. A., Roberts, C. J., Tendler, S. J. B., & Williams, P. M. (2000). Atomic force microscopy studies of intercalation-induced changes in plasmid DNA tertiary structure. *Journal of microscopy*, *199*(1), 68-78.

Rivetti, C., Guthold, M., & Bustamante, C. (1996). Scanning force microscopy of DNA deposited onto mica: Equilibration versus Kinetic trapping studied by statistical polymer chain analysis. *Journal of molecular biology*, *264*(5), 919-932.

Ross, D., Strychalski, E. A., Jarzynski, C., & Stavis, S. M. (2018). Equilibrium free energies from non-equilibrium trajectories with relaxation fluctuation spectroscopy. *Nature Physics*, *14*(8), 842-847.

Seara, D. S., Yadav, V., Linsmeier, I., Tabatabai, A. P., Oakes, P. W., Tabei, S. A., ... & Murrell, M. P. (2018). Entropy production rate is maximized in non-contractile actomyosin. *Nature communications*, *9*(1), 4948.

Smith, S. B., Finzi, L., & Bustamante, C. (1992). Direct mechanical measurements of the elasticity of single DNA molecules by using magnetic beads. *Science*, *258*(5085), 1122-1126.

Wiggins, P. A., Van Der Heijden, T., Moreno-Herrero, F., Spakowitz, A., Phillips, R., Widom, J., Dekker, C., & Nelson, P. C. (2006). High flexibility of DNA on short length scales probed by atomic force microscopy. *Nature nanotechnology*, *1*(2), 137.

Supplementary Material

Normal Mode amplitude calculations:

Each mode amplitude (a_n) for the individual discretized molecules was calculated according to the following equation:

$$a_n = \sqrt{\frac{2}{L_C}} \sum_{k=1}^{k_{max}} \theta_k l \cos\left(\frac{nl\pi}{2L_C}(2k-1)\right)$$

where L_C is the contour length of the molecule (approximated by summing the lengths of the discrete linear elements), k_{max} is the number of linear segments, θ_k is the angle (mod π) of the kth segment, and l is the length of each segment. The above was repeated for each molecule and for various n to obtain an ensemble of amplitudes for each mode.

Error calculations in Normal Mode P estimations:

The error in the natural logarithm of P is estimated by the following formula:

$$\delta \ln(P) = \frac{\sqrt{\frac{2}{N-1}\mathrm{var}(a_n)^2 + (\langle \delta a_n^2 \rangle)^2}}{\mathrm{var}(a_n) - \langle \delta a_n^2 \rangle}$$

Here, N is the number of molecules being averaged over, a_n is the set of amplitudes of mode n, and δa_n^2 is defined as:

$$\left\langle \delta a_n^2 \right\rangle = \frac{4}{L_C} \left\langle \epsilon_k^2 \right\rangle \left[1 + \left(\frac{L_C}{l} - 1\right) \sin^2\left(\frac{nl\pi}{2L_C}\right)\right]$$

where L_C is the average contour length of the set of molecules, l is the length of the discretized segments, and $\langle \epsilon_k^2 \rangle$ is based on the estimated error in fitting the discretized chain to the molecule.

Determination of the optimal segment length, *l*:

The chain discretization was undertaken for multiple values of *l*, based on the same set of AFM images. Each of these resulted in a different set of estimated *P* values, using the WLC-derived models for the functional forms given in Supplemental Table 1. The variation among the estimates of *P* was taken as a measure of the consistency of the estimations, and the *l* which resulted in the lowest standard deviation of *P* was used for subsequent calculations. For these data sets, the optimal *l* was consistently near 6-7 nm, corresponding to a distance of about 3 pixels on the microscope images.

Supplemental Table 1:

Experimentally measured quantity, as a function of separation distance *d*	Predicted functional form with respect to *d* and single parameter *a*	Relationship of model parameter to persistence length *P*
$\langle\theta^2\rangle$	ad	$a = \frac{1}{P}$
$\langle\theta^4\rangle$	ad^2	$a = \frac{3}{P^2}$
$\langle\theta^6\rangle$	ad^3	$a = \frac{15}{P^3}$
$\langle cos\ \theta\rangle$	$e^{-d/a}$	$a = P$
$\langle \boldsymbol{R}\cdot\boldsymbol{u_0}\rangle$	$a(1-e^{-d/a})$	$a = P$
$\langle R^{\mathbf{2}}\rangle$	$2da[1-\frac{a}{d}(e^{-d/a})]$	$a = 2P$
$\langle R^{\mathbf{4}}\rangle$	$8d^2a^2-30da^3+\frac{87}{2}a^4-\frac{40}{3}da^3e^{-d/a}-\frac{392}{9}a^4e^{-d/a}+\frac{1}{18}a^4e^{-4d/a}$	$a = 2P$

The following figures show the complete WLC estimation results for each data set, conducted at a variety of values of *l*. The figures remain color-coordinated in the same way as the main-text figures. The value of *l* used is listed at the top of each figure. The additional plots on each page (those not shown in Figures 8-11) are illustrations of certain normality conditions of the WLC assumptions, consisting of products of the moments of θ which should not depend on *P*.

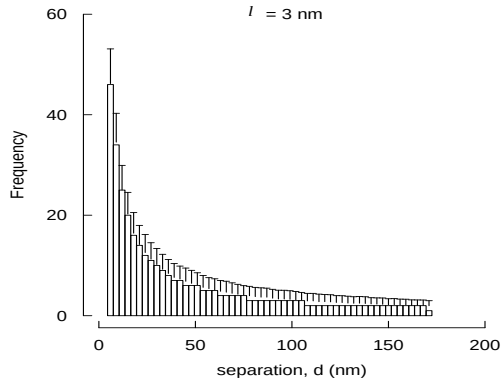
l = 3 nm
Frequency
separation, d (nm)

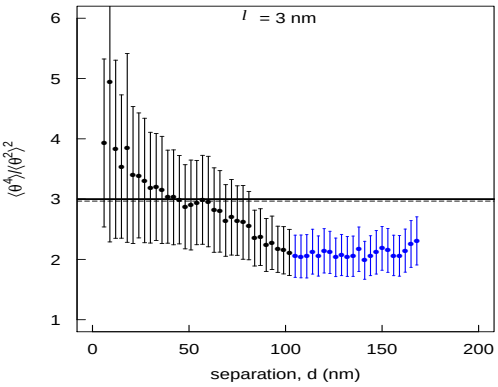
l = 3 nm
⟨θ⁴⟩/⟨θ²⟩²
separation, d (nm)

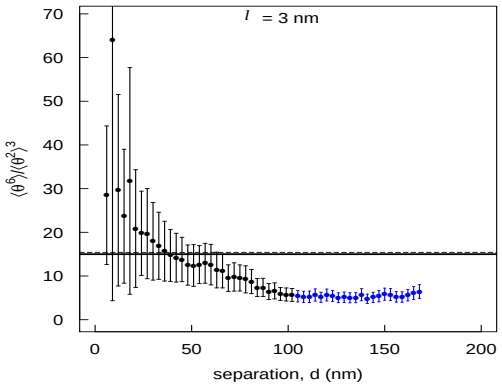
l = 3 nm
⟨θ⁶⟩/⟨θ²⟩³
separation, d (nm)

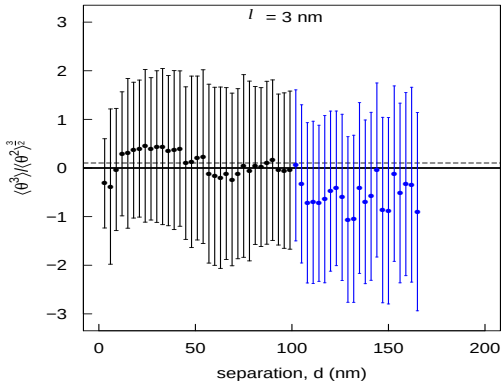
l = 3 nm
⟨θ³⟩/⟨θ²⟩^3/2
separation, d (nm)

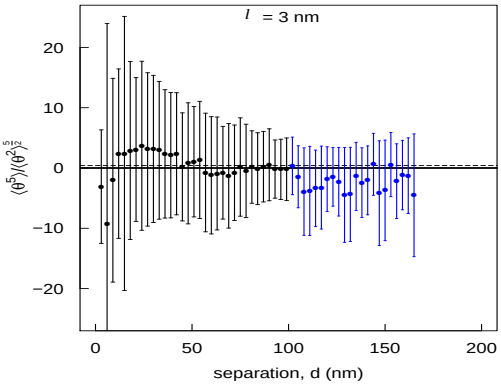
l = 3 nm
⟨θ⁵⟩/⟨θ²⟩^5/2
separation, d (nm)

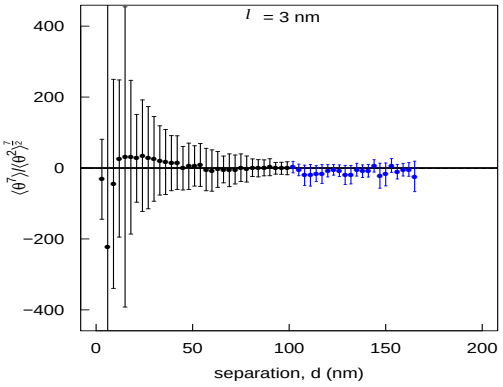
l = 3 nm
⟨θ⁷⟩/⟨θ²⟩^7/2
separation, d (nm)

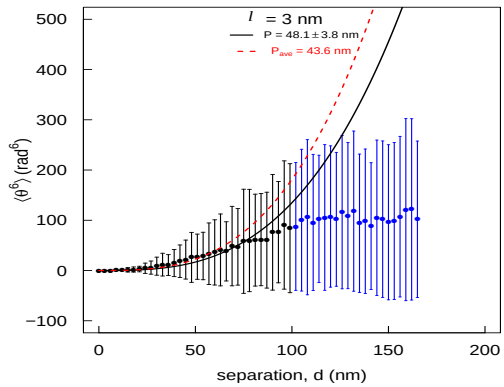
l = 3 nm
P = 48.1±3.8 nm
P_ave = 43.6 nm
⟨θ⁶⟩ (rad⁶)
separation, d (nm)

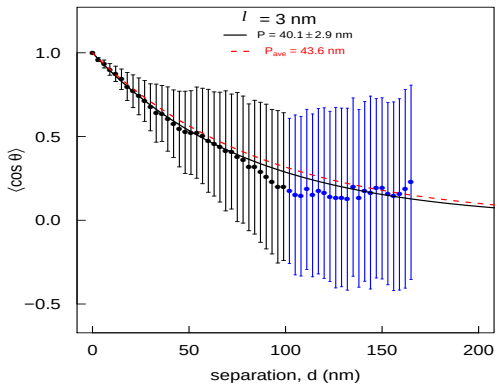
l = 3 nm
P = 40.1±2.9 nm
P_ave = 43.6 nm
⟨cos θ⟩
separation, d (nm)

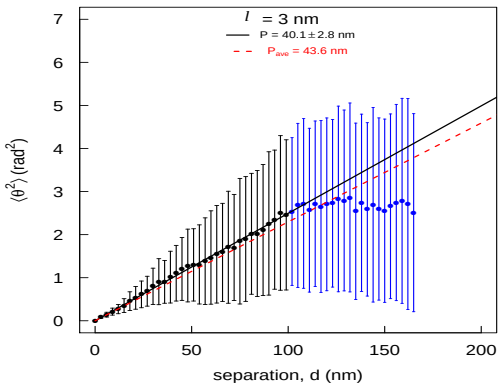
l = 3 nm
P = 40.1±2.8 nm
P_ave = 43.6 nm
⟨θ²⟩ (rad²)
separation, d (nm)

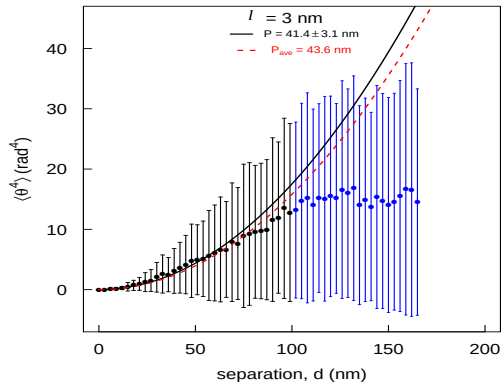
l = 3 nm
P = 41.4±3.1 nm
P_ave = 43.6 nm
⟨θ⁴⟩ (rad⁴)
separation, d (nm)

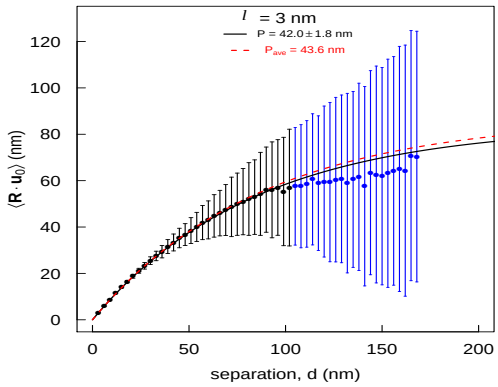
l = 3 nm
P = 42.0±1.8 nm
P_ave = 43.6 nm
⟨R · u₀⟩ (nm)
separation, d (nm)

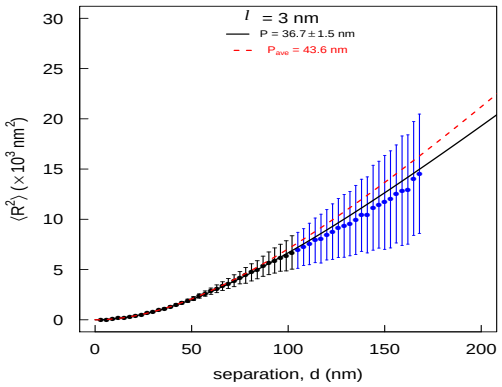
l = 3 nm
P = 36.7±1.5 nm
P_ave = 43.6 nm
⟨R²⟩ (×10³ nm²)
separation, d (nm)

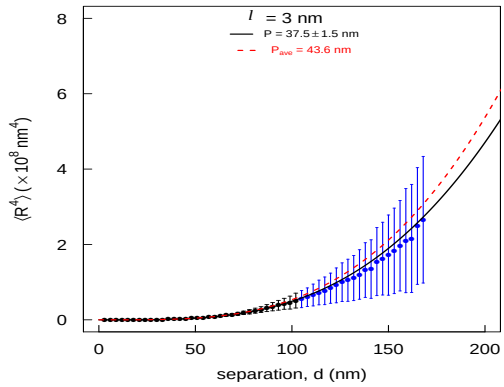
l = 3 nm
P = 37.5±1.5 nm
P_ave = 43.6 nm
⟨R⁴⟩ (×10⁸ nm⁴)
separation, d (nm)

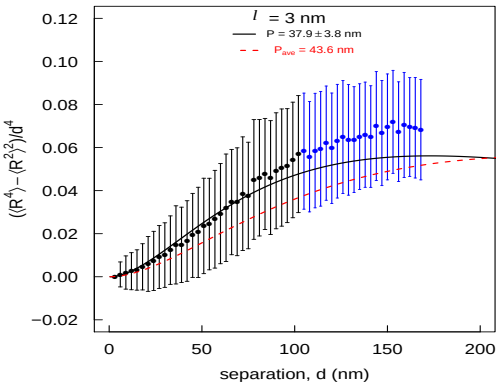
l = 3 nm
P = 37.9±3.8 nm
P_ave = 43.6 nm
(⟨R⁴⟩ − ⟨R²⟩²)/d⁴
separation, d (nm)

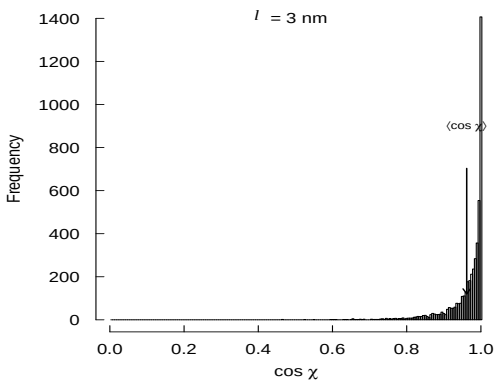
l = 3 nm
⟨cos χ⟩
Frequency
cos χ

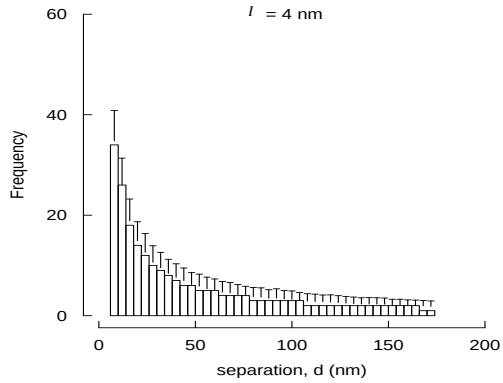
l = 4 nm
Frequency
separation, d (nm)

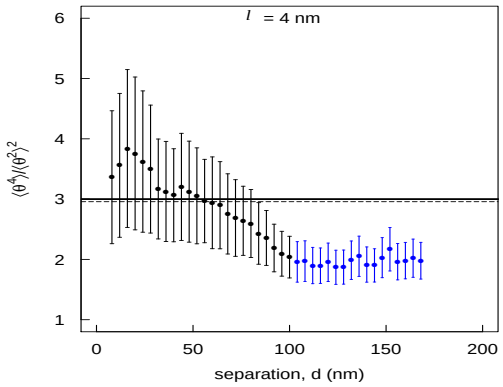
l = 4 nm
⟨θ⁴⟩/⟨θ²⟩²
separation, d (nm)

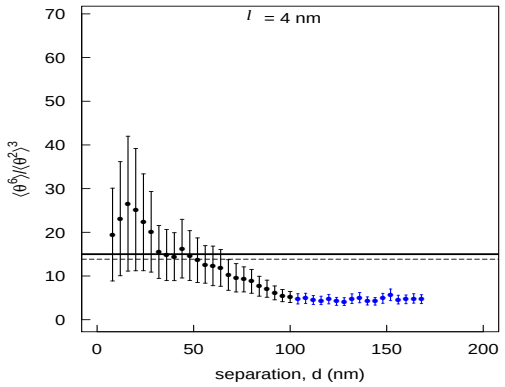
l = 4 nm
⟨θ⁶⟩/⟨θ²⟩³
separation, d (nm)

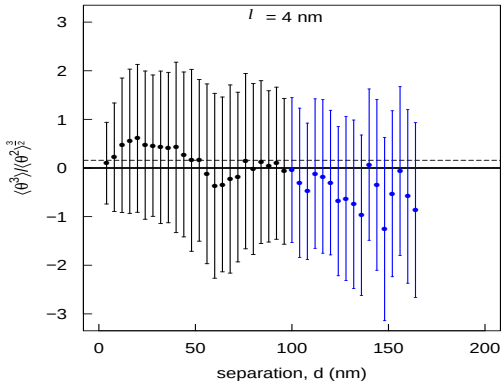
l = 4 nm
⟨θ³⟩/⟨θ²⟩^3/2
separation, d (nm)

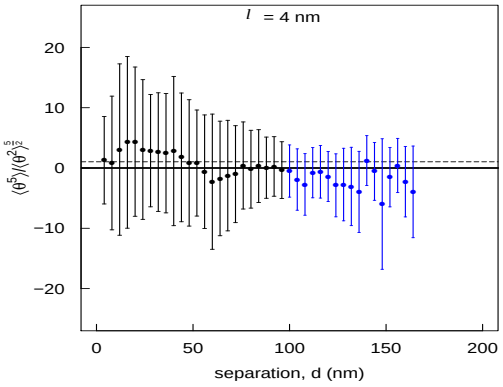
l = 4 nm
⟨θ⁵⟩/⟨θ²⟩^5/2
separation, d (nm)

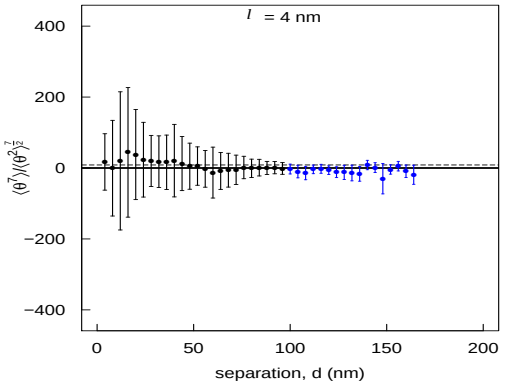
l = 4 nm
⟨θ⁷⟩/⟨θ²⟩^7/2
separation, d (nm)

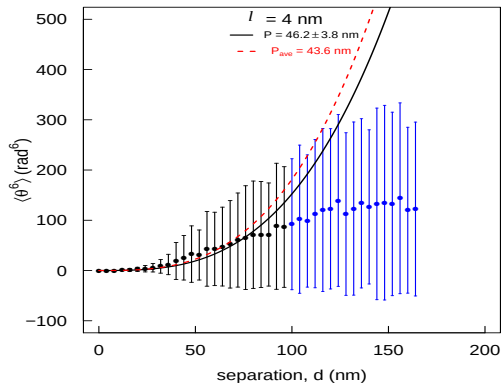
l = 4 nm
P = 46.2±3.8 nm
P_ave = 43.6 nm
⟨θ⁶⟩ (rad⁶)
separation, d (nm)

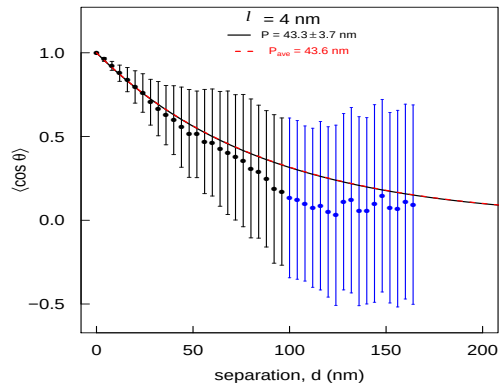
l = 4 nm
P = 43.3±3.7 nm
P_ave = 43.6 nm
⟨cos θ⟩
separation, d (nm)

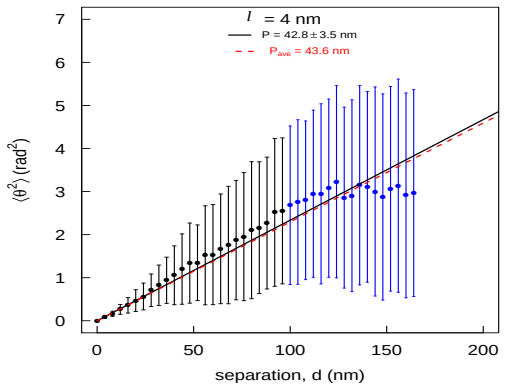
l = 4 nm
P = 42.8±3.5 nm
P_ave = 43.6 nm
⟨θ²⟩ (rad²)
separation, d (nm)

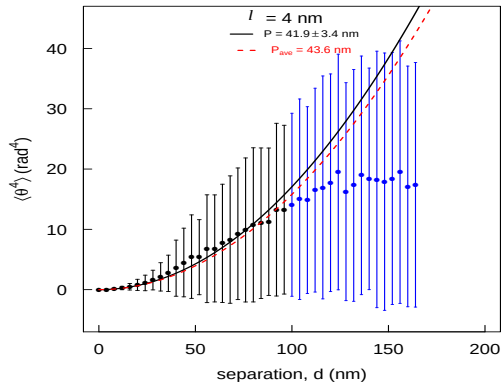
l = 4 nm
P = 41.9±3.4 nm
P_ave = 43.6 nm
⟨θ⁴⟩ (rad⁴)
separation, d (nm)

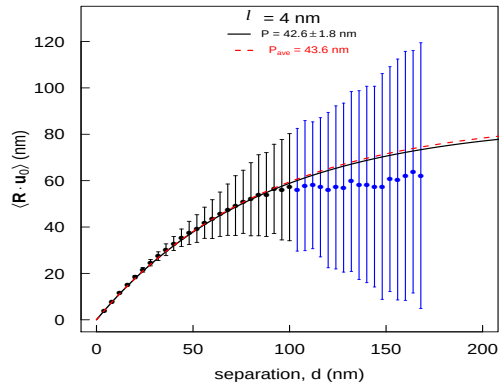
l = 4 nm
P = 42.6±1.8 nm
P_ave = 43.6 nm
⟨R · u₀⟩ (nm)
separation, d (nm)

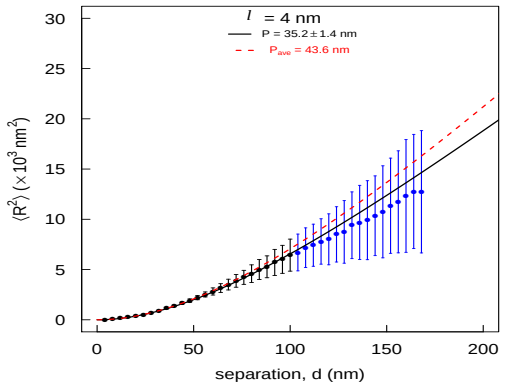
l = 4 nm
P = 35.2±1.4 nm
P_ave = 43.6 nm
⟨R²⟩ (×10³ nm²)
separation, d (nm)

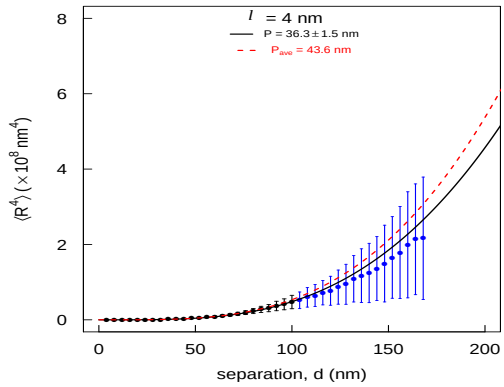
l = 4 nm
P = 36.3±1.5 nm
P_ave = 43.6 nm
⟨R⁴⟩ (×10⁸ nm⁴)
separation, d (nm)

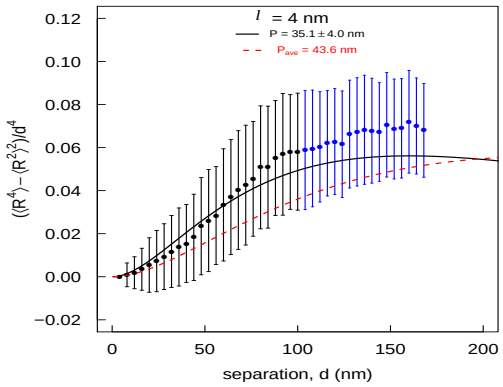
l = 4 nm
P = 35.1±4.0 nm
P_ave = 43.6 nm
⟨(R⁴) − ⟨R²⟩²⟩/d⁴
separation, d (nm)

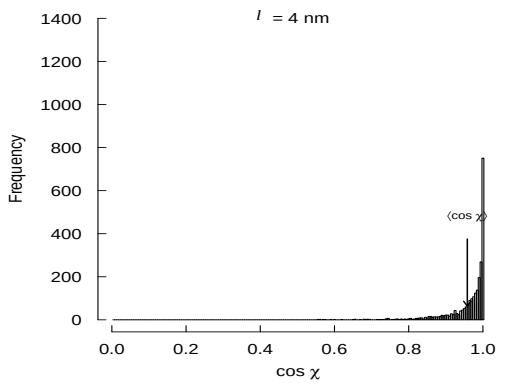
l = 4 nm
Frequency
⟨cos χ⟩
cos χ

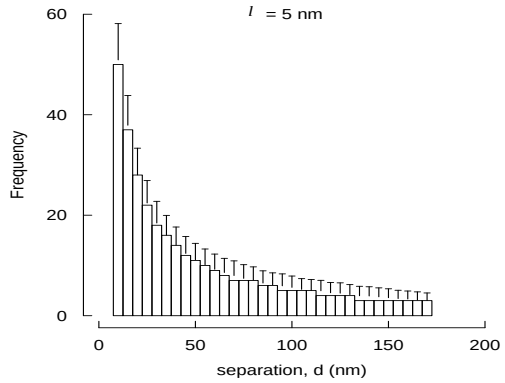
l = 5 nm
Frequency
separation, d (nm)

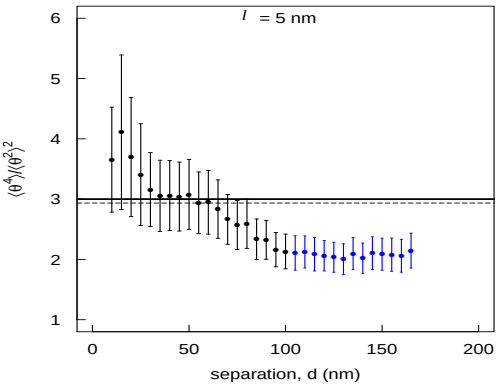
l = 5 nm
⟨θ⁴⟩/⟨θ²⟩²
separation, d (nm)

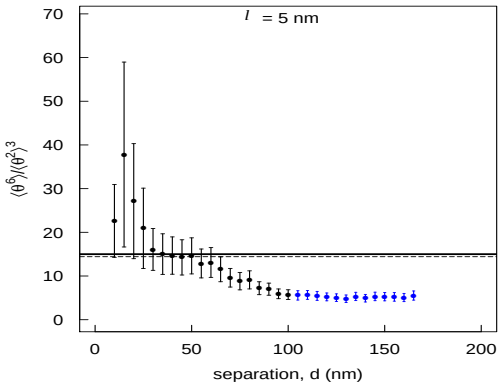
l = 5 nm
⟨θ⁶⟩/⟨θ²⟩³
separation, d (nm)

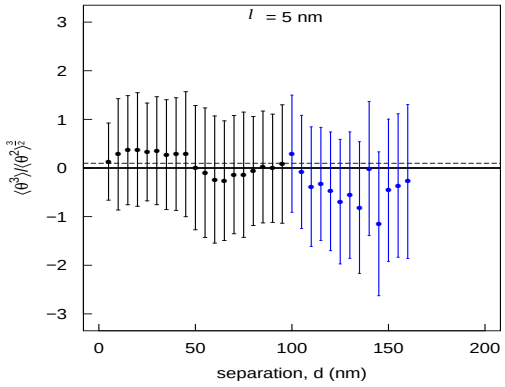
l = 5 nm
⟨θ³⟩/⟨θ²⟩^3/2
separation, d (nm)

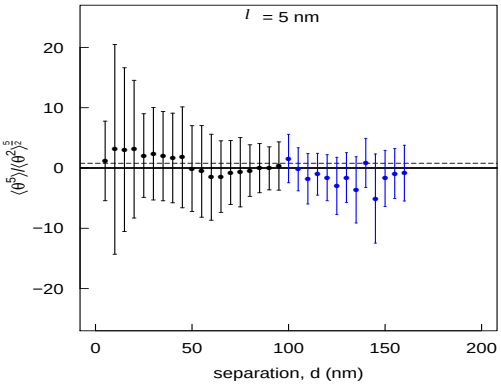
l = 5 nm
⟨θ⁵⟩/⟨θ²⟩^5/2
separation, d (nm)

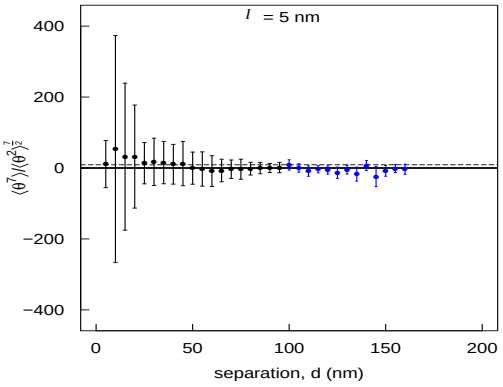
l = 5 nm
⟨θ⁷⟩/⟨θ²⟩^7/2
separation, d (nm)

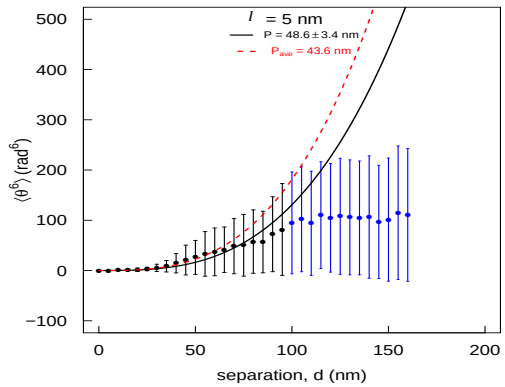
l = 5 nm
P = 48.6±3.4 nm
P_ave = 43.6 nm
⟨θ⁶⟩ (rad⁶)
separation, d (nm)

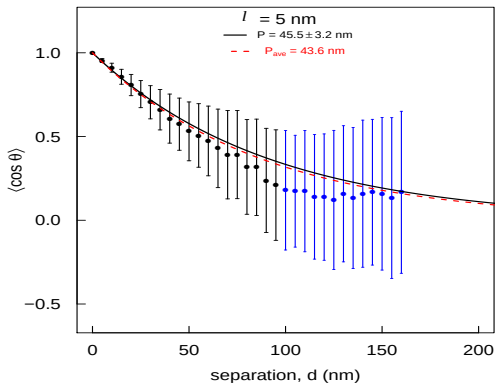
l = 5 nm
P = 45.5±3.2 nm
P_ave = 43.6 nm
⟨cos θ⟩
separation, d (nm)

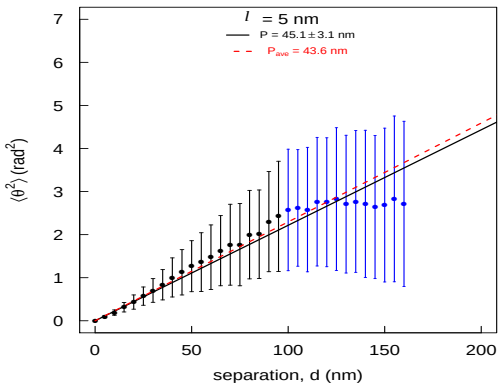
l = 5 nm
P = 45.1±3.1 nm
P_ave = 43.6 nm
⟨θ²⟩ (rad²)
separation, d (nm)

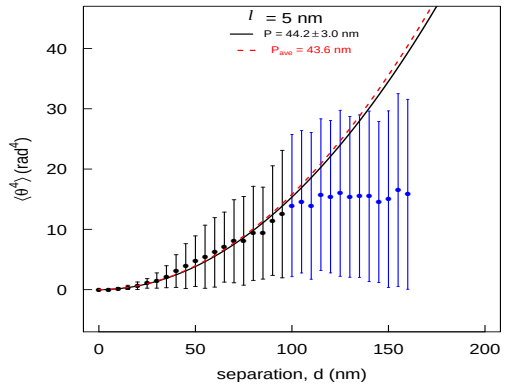
l = 5 nm
P = 44.2±3.0 nm
P_ave = 43.6 nm
⟨θ⁴⟩ (rad⁴)
separation, d (nm)

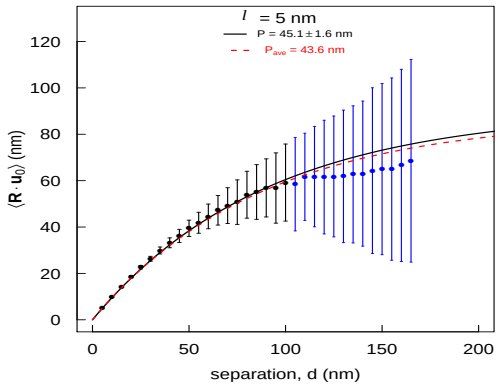
l = 5 nm
P = 45.1±1.6 nm
P_ave = 43.6 nm
⟨R · u₀⟩ (nm)
separation, d (nm)

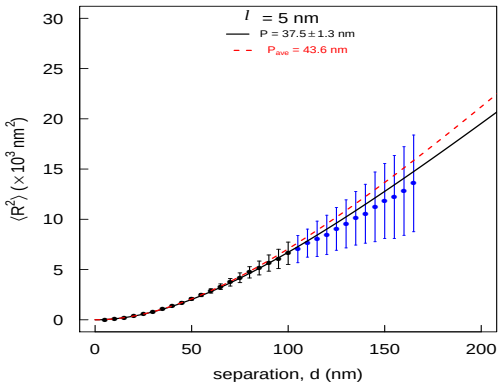
l = 5 nm
P = 37.5±1.3 nm
P_ave = 43.6 nm
⟨R²⟩ (×10³ nm²)
separation, d (nm)

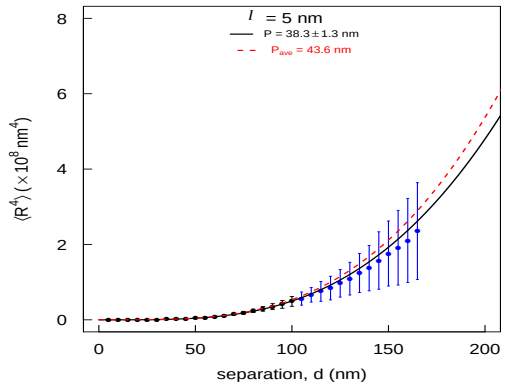
l = 5 nm
P = 38.3±1.3 nm
P_ave = 43.6 nm
⟨R⁴⟩ (×10⁸ nm⁴)
separation, d (nm)

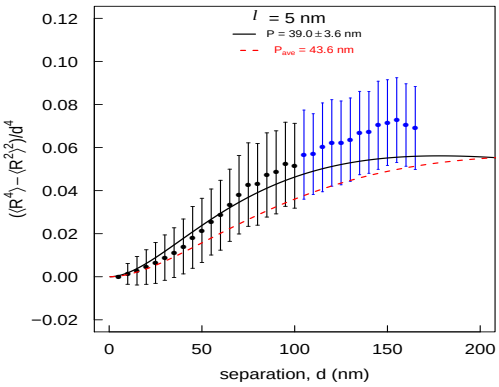
l = 5 nm
P = 39.0±3.6 nm
P_ave = 43.6 nm
⟨(R⁴) − ⟨R²⟩²⟩/d⁴
separation, d (nm)

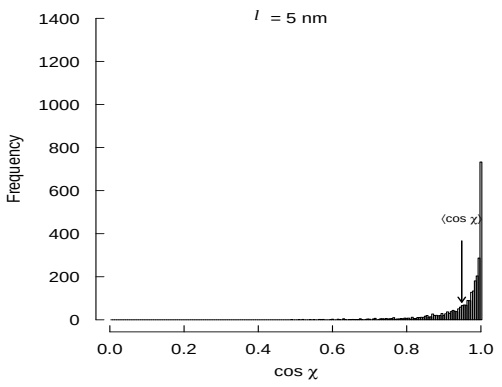
l = 5 nm
Frequency
⟨cos χ⟩
cos χ

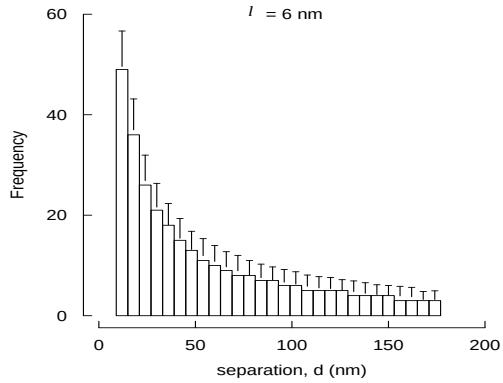
l = 6 nm
Frequency
separation, d (nm)

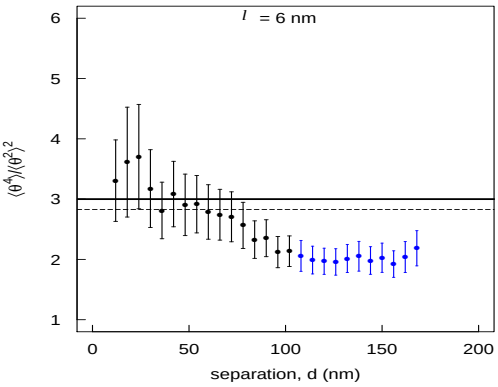
l = 6 nm
⟨θ⁴⟩/⟨θ²⟩²
separation, d (nm)

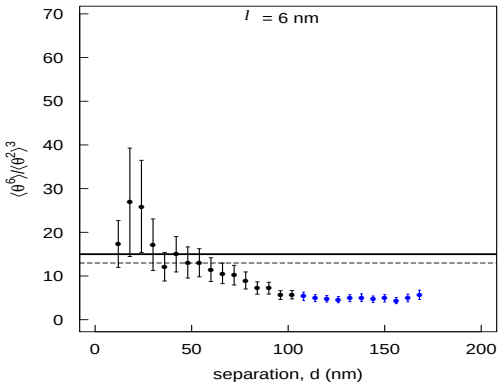
l = 6 nm
⟨θ⁶⟩/⟨θ²⟩³
separation, d (nm)

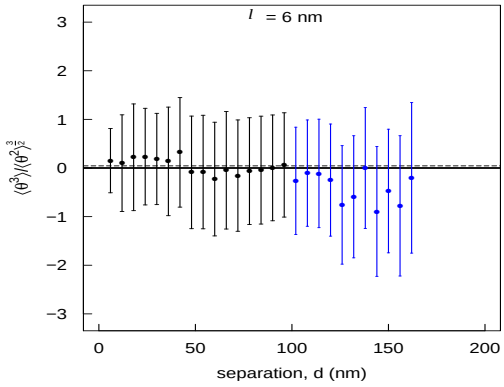
l = 6 nm
⟨θ³⟩/⟨θ²⟩^3/2
separation, d (nm)

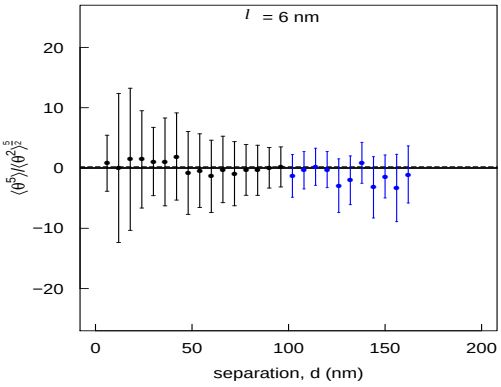
l = 6 nm
⟨θ⁵⟩/⟨θ²⟩^5/2
separation, d (nm)

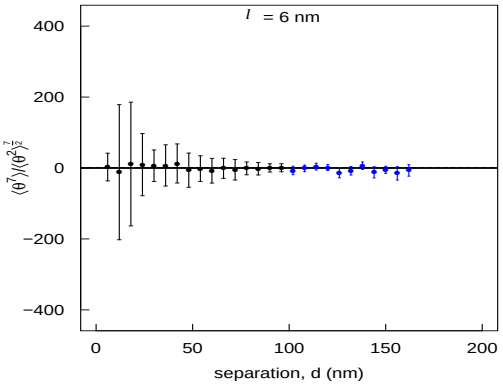
l = 6 nm
⟨θ⁷⟩/⟨θ²⟩^7/2
separation, d (nm)

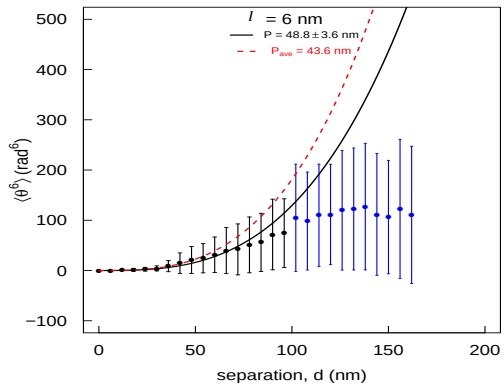
l = 6 nm
P = 48.8±3.6 nm
P_ave = 43.6 nm
⟨θ⁶⟩ (rad⁶)
separation, d (nm)

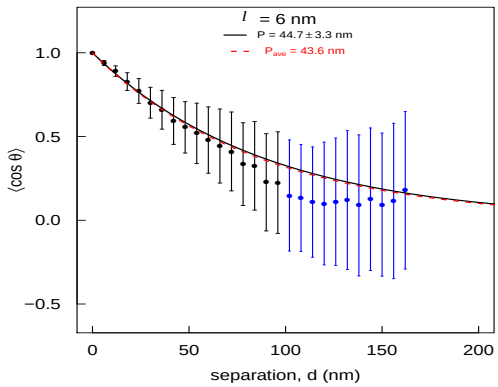
l = 6 nm
P = 44.7±3.3 nm
P_ave = 43.6 nm
⟨cos θ⟩
separation, d (nm)

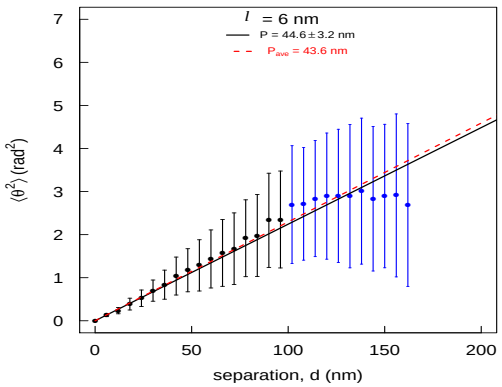
l = 6 nm
P = 44.6±3.2 nm
P_ave = 43.6 nm
⟨θ²⟩ (rad²)
separation, d (nm)

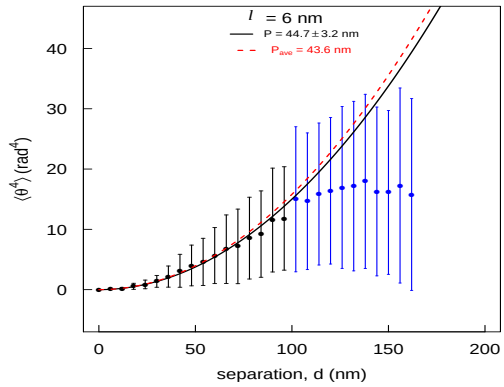
l = 6 nm
P = 44.7±3.2 nm
P_ave = 43.6 nm
⟨θ⁴⟩ (rad⁴)
separation, d (nm)

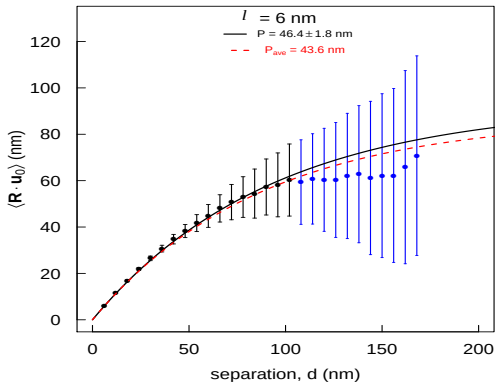
l = 6 nm
P = 46.4±1.8 nm
P_ave = 43.6 nm
⟨R · u₀⟩ (nm)
separation, d (nm)

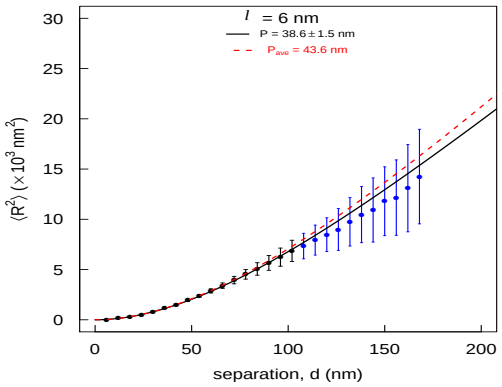
l = 6 nm
P = 38.6±1.5 nm
P_ave = 43.6 nm
⟨R²⟩ (×10³ nm²)
separation, d (nm)

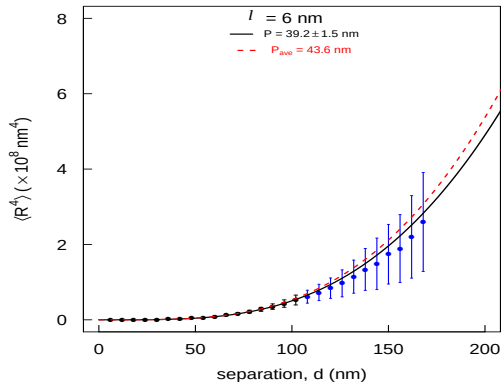
l = 6 nm
P = 39.2±1.5 nm
P_ave = 43.6 nm
⟨R⁴⟩ (×10⁸ nm⁴)
separation, d (nm)

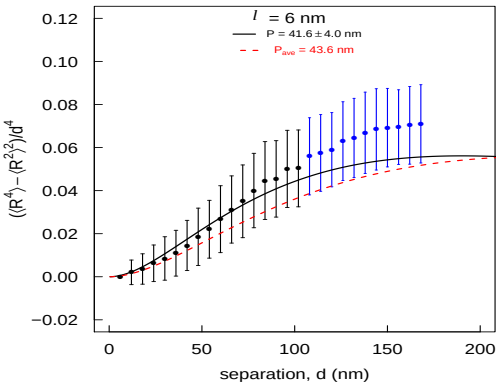
l = 6 nm
P = 41.6±4.0 nm
P_ave = 43.6 nm
⟨(R⁴) − ⟨R²⟩²⟩/d⁴
separation, d (nm)

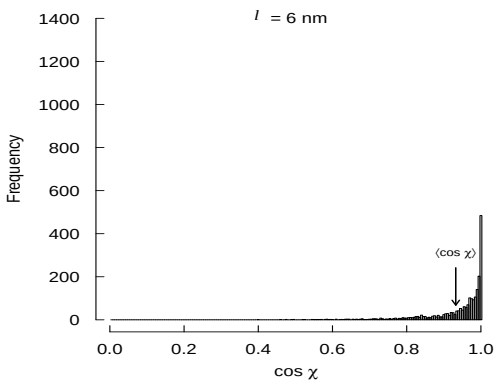
l = 6 nm
Frequency
⟨cos χ⟩
cos χ

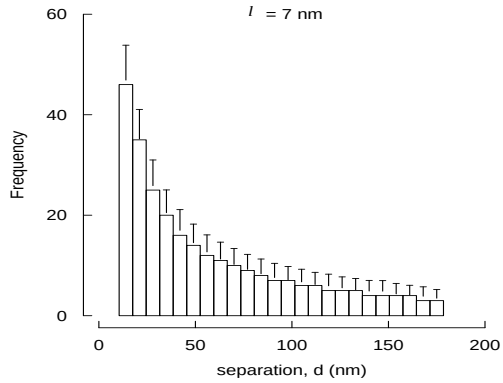
l = 7 nm
Frequency
separation, d (nm)

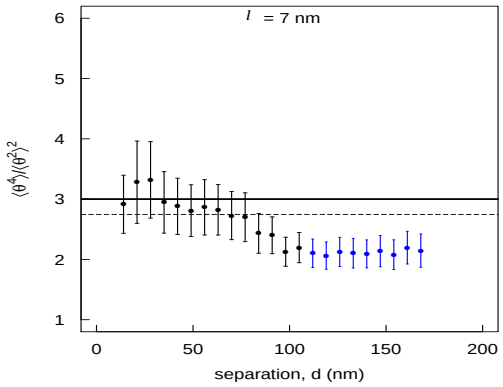
l = 7 nm
⟨θ⁴⟩/⟨θ²⟩²
separation, d (nm)

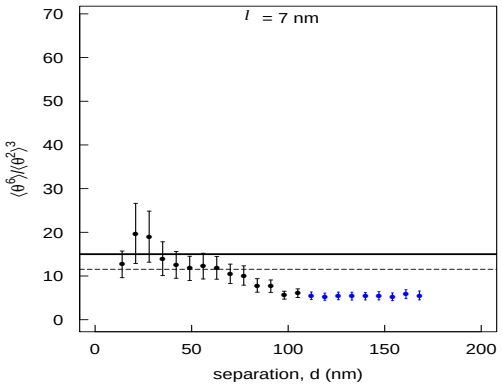
l = 7 nm
⟨θ⁶⟩/⟨θ²⟩³
separation, d (nm)

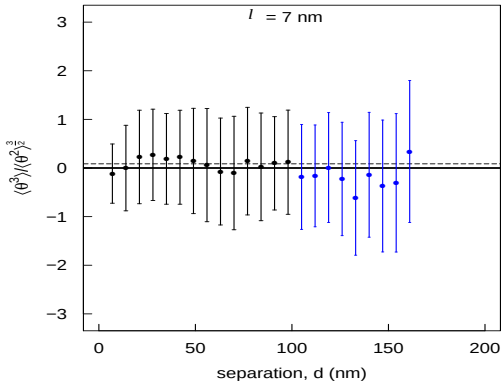
l = 7 nm
⟨θ³⟩/⟨θ²⟩^3/2
separation, d (nm)

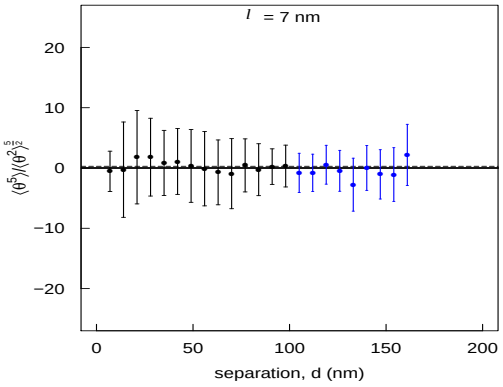
l = 7 nm
⟨θ⁵⟩/⟨θ²⟩^5/2
separation, d (nm)

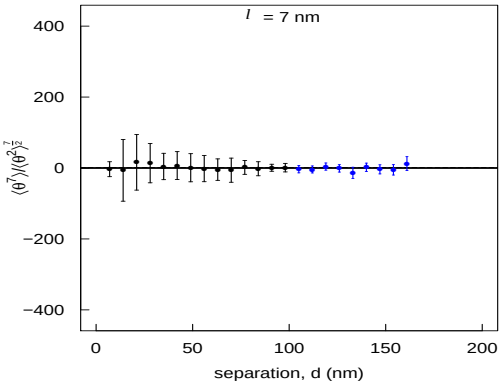
l = 7 nm
⟨θ⁷⟩/⟨θ²⟩^7/2
separation, d (nm)

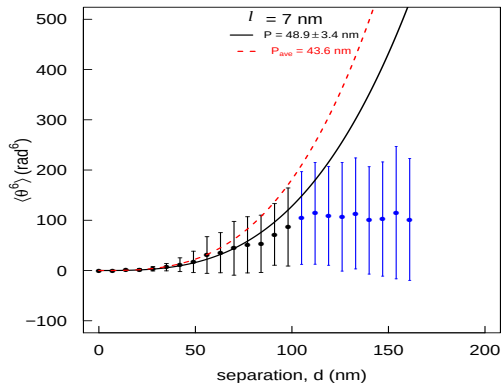
l = 7 nm
P = 48.9±3.4 nm
P_ave = 43.6 nm
⟨θ⁶⟩ (rad⁶)
separation, d (nm)

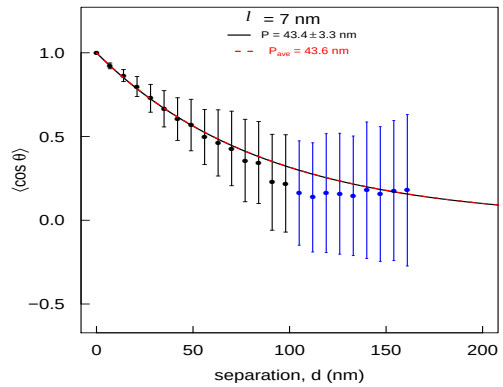
l = 7 nm
P = 43.4±3.3 nm
P_ave = 43.6 nm
⟨cos θ⟩
separation, d (nm)

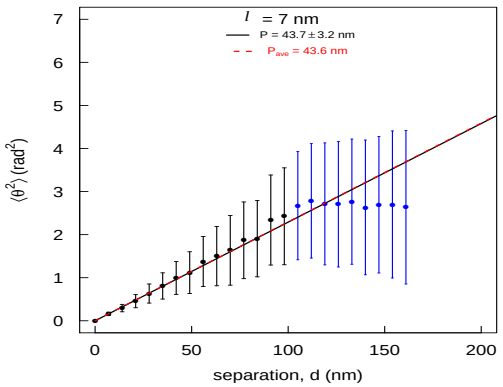
l = 7 nm
P = 43.7±3.2 nm
P_ave = 43.6 nm
⟨θ²⟩ (rad²)
separation, d (nm)

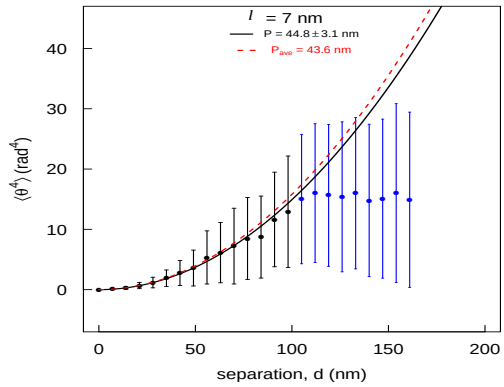
l = 7 nm
P = 44.8±3.1 nm
P_ave = 43.6 nm
⟨θ⁴⟩ (rad⁴)
separation, d (nm)

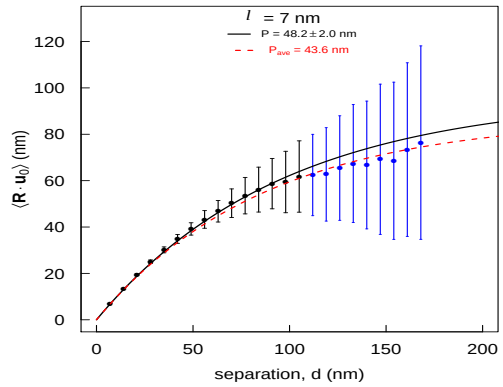
l = 7 nm
P = 48.2±2.0 nm
P_ave = 43.6 nm
⟨R · u₀⟩ (nm)
separation, d (nm)

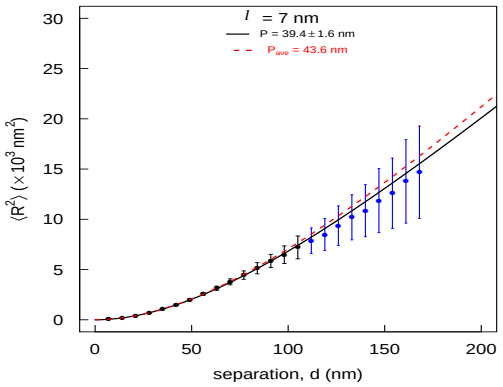
l = 7 nm
P = 39.4±1.6 nm
P_ave = 43.6 nm
⟨R²⟩ (×10³ nm²)
separation, d (nm)

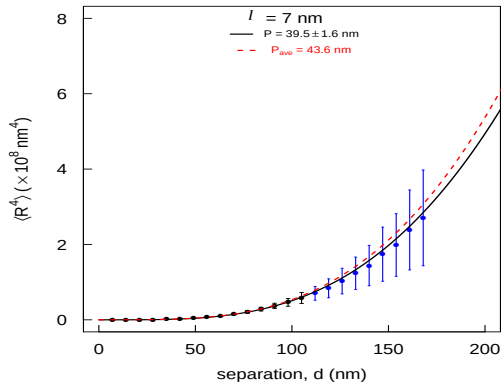
l = 7 nm
P = 39.5±1.6 nm
P_ave = 43.6 nm
⟨R⁴⟩ (×10⁸ nm⁴)
separation, d (nm)

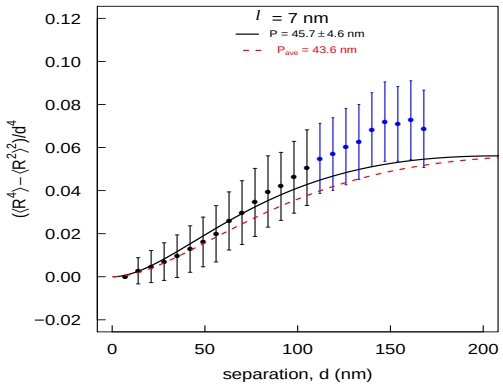
l = 7 nm
P = 45.7±4.6 nm
P_ave = 43.6 nm
(⟨R⁴⟩ − ⟨R²⟩²)/d⁴
separation, d (nm)

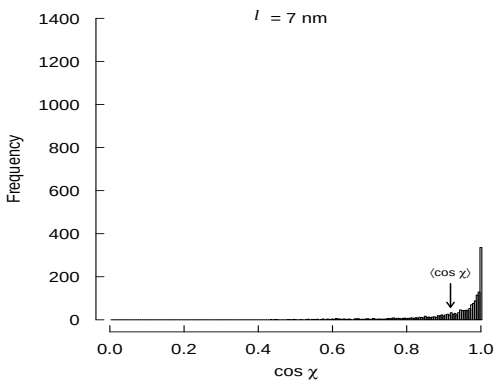
l = 7 nm
Frequency
⟨cos χ⟩
cos χ

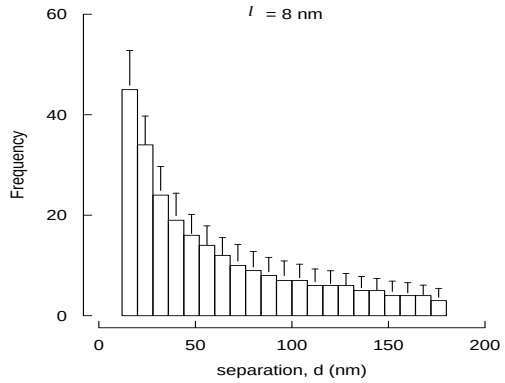
l = 8 nm
Frequency
separation, d (nm)

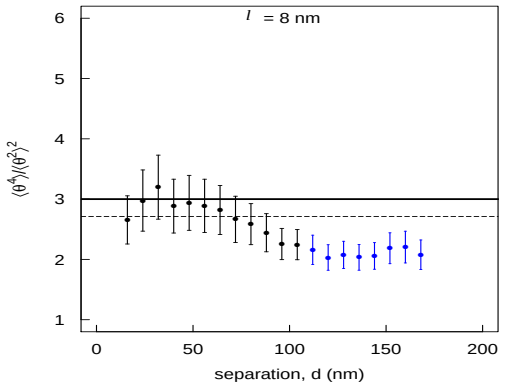
l = 8 nm
⟨θ⁴⟩/⟨θ²⟩²
separation, d (nm)

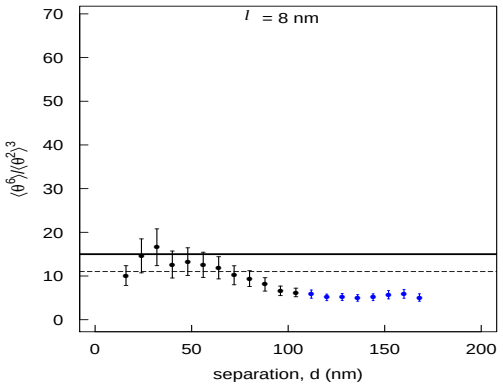
l = 8 nm
⟨θ⁶⟩/⟨θ²⟩³
separation, d (nm)

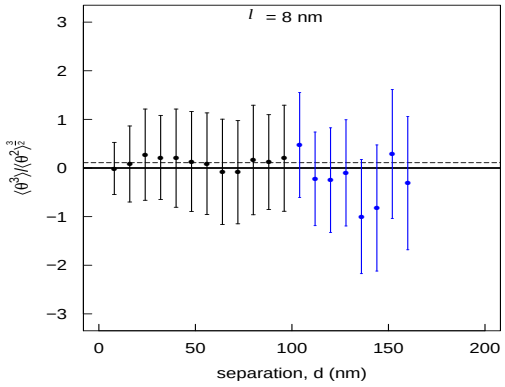
l = 8 nm
⟨θ³⟩/⟨θ²⟩^3/2
separation, d (nm)

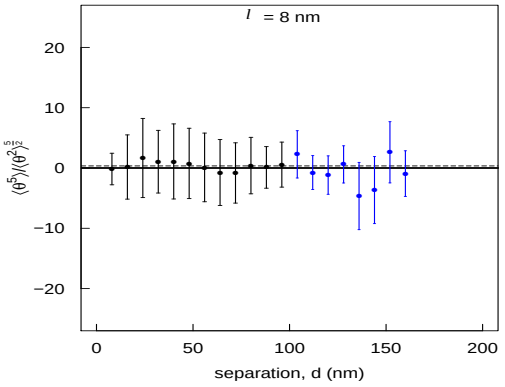
l = 8 nm
⟨θ⁵⟩/⟨θ²⟩^5/2
separation, d (nm)

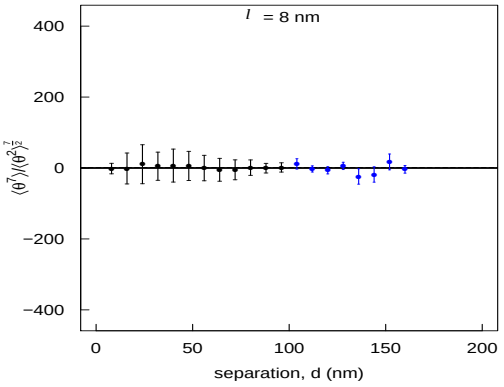
l = 8 nm
⟨θ⁷⟩/⟨θ²⟩^7/2
separation, d (nm)

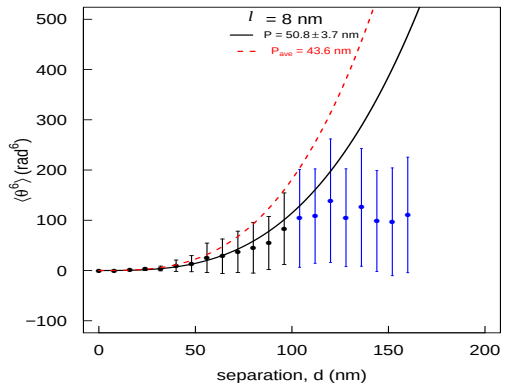
l = 8 nm
P = 50.8±3.7 nm
P_ave = 43.6 nm
⟨θ⁶⟩ (rad⁶)
separation, d (nm)

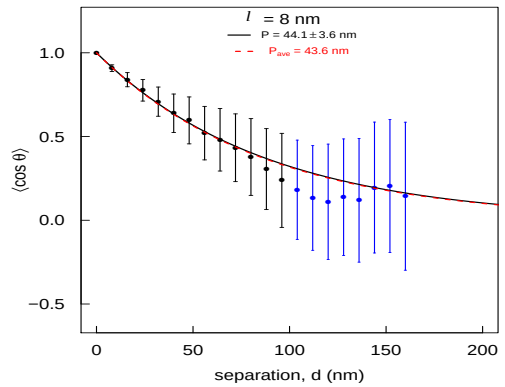
l = 8 nm
P = 44.1±3.6 nm
P_ave = 43.6 nm
⟨cos θ⟩
separation, d (nm)

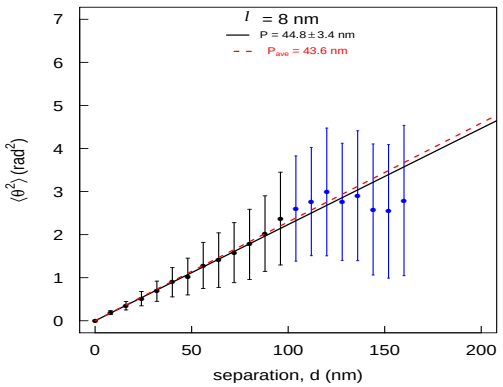
l = 8 nm
P = 44.8±3.4 nm
P_ave = 43.6 nm
⟨θ²⟩ (rad²)
separation, d (nm)

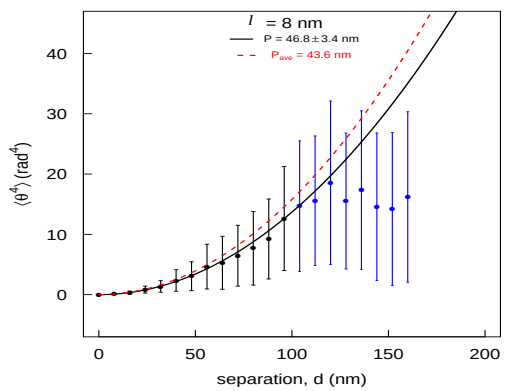
l = 8 nm
P = 46.8±3.4 nm
P_ave = 43.6 nm
⟨θ⁴⟩ (rad⁴)
separation, d (nm)

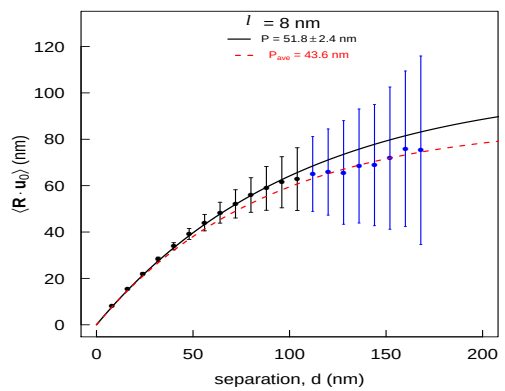
l = 8 nm
P = 51.8±2.4 nm
P_ave = 43.6 nm
⟨R · u₀⟩ (nm)
separation, d (nm)

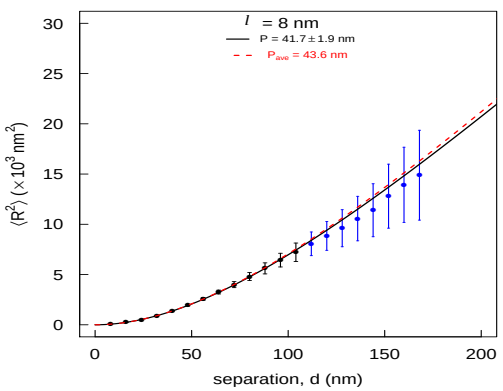
l = 8 nm
P = 41.7±1.9 nm
P_ave = 43.6 nm
⟨R²⟩ (×10³ nm²)
separation, d (nm)

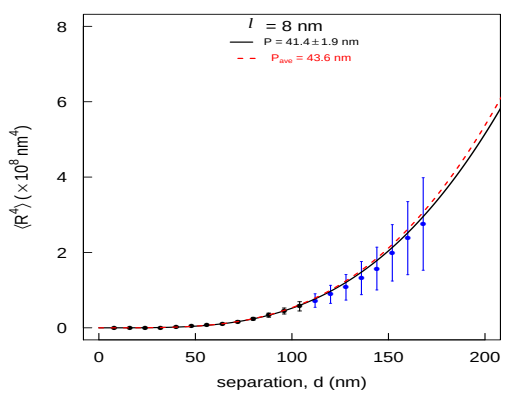
l = 8 nm
P = 41.4±1.9 nm
P_ave = 43.6 nm
⟨R⁴⟩ (×10⁸ nm⁴)
separation, d (nm)

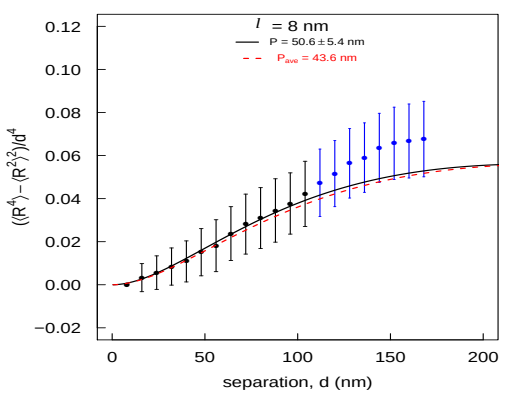
l = 8 nm
P = 50.6±5.4 nm
P_ave = 43.6 nm
⟨(R⁴) − ⟨R²⟩²⟩/d⁴
separation, d (nm)

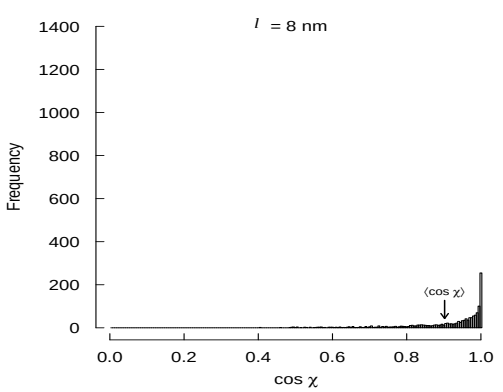
l = 8 nm
Frequency
⟨cos χ⟩
cos χ

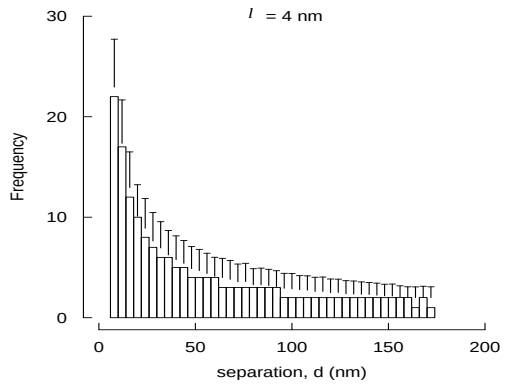
l = 4 nm
Frequency
separation, d (nm)

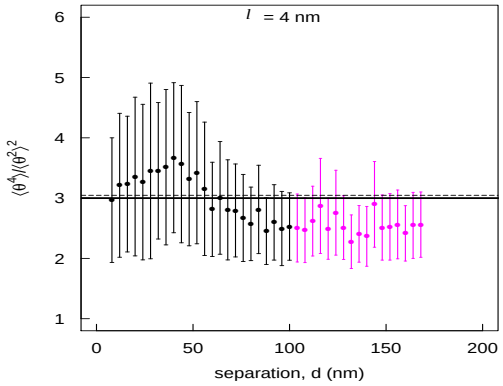
l = 4 nm
⟨θ⁴⟩/⟨θ²⟩²
separation, d (nm)

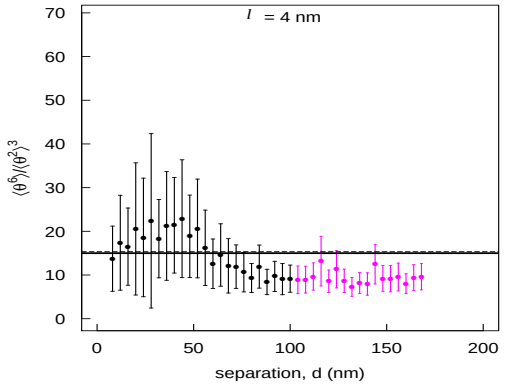
l = 4 nm
⟨θ⁶⟩/⟨θ²⟩³
separation, d (nm)

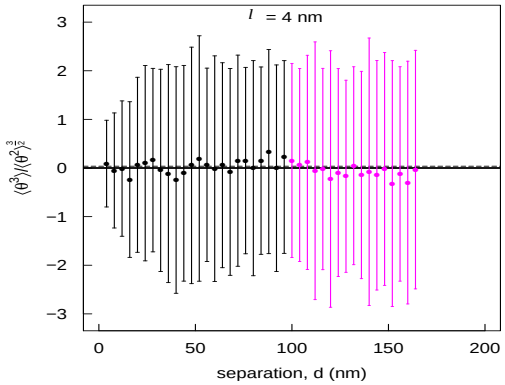
l = 4 nm
⟨θ³⟩/⟨θ²⟩^3/2
separation, d (nm)

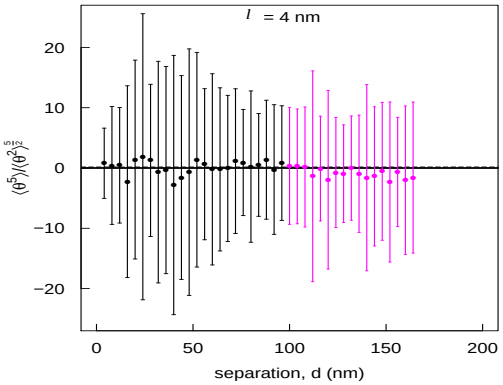
l = 4 nm
⟨θ⁵⟩/⟨θ²⟩^5/2
separation, d (nm)

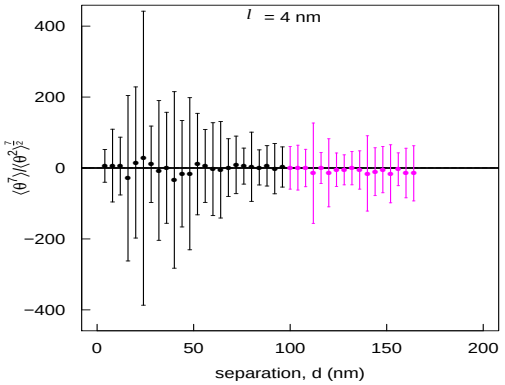
l = 4 nm
⟨θ⁷⟩/⟨θ²⟩^7/2
separation, d (nm)

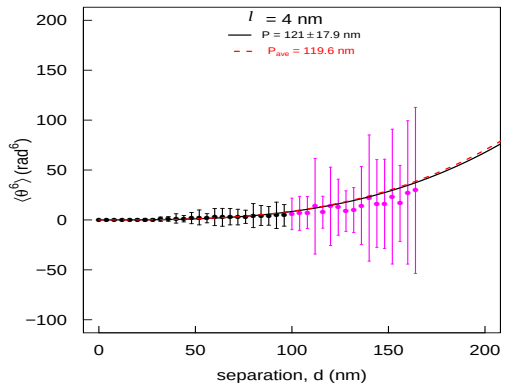
l = 4 nm
P = 121 ± 17.9 nm
P_ave = 119.6 nm
⟨θ⁶⟩ (rad⁶)
separation, d (nm)

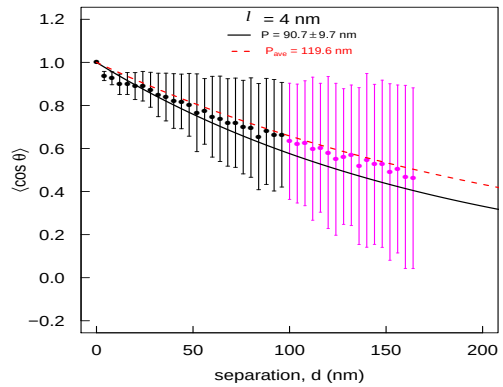
l = 4 nm
P = 90.7 ± 9.7 nm
P_ave = 119.6 nm
⟨cos θ⟩
separation, d (nm)

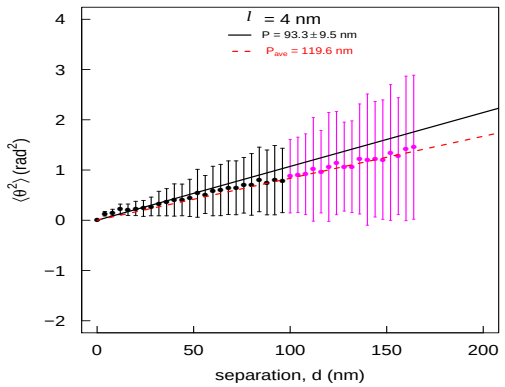
l = 4 nm
P = 93.3 ± 9.5 nm
P_ave = 119.6 nm
⟨θ²⟩ (rad²)
separation, d (nm)

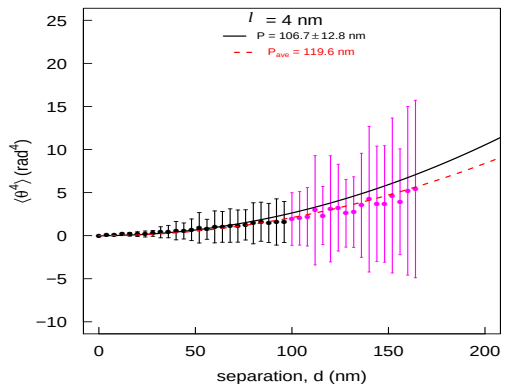
l = 4 nm
P = 106.7 ± 12.8 nm
P_ave = 119.6 nm
⟨θ⁴⟩ (rad⁴)
separation, d (nm)

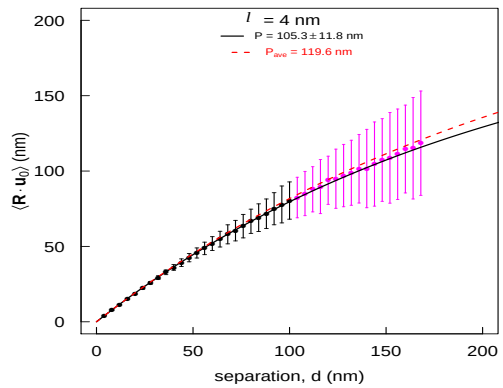
l = 4 nm
P = 105.3 ± 11.8 nm
P_ave = 119.6 nm
⟨R · u₀⟩ (nm)
separation, d (nm)

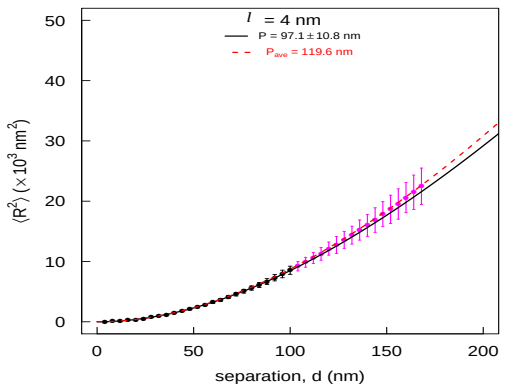
l = 4 nm
P = 97.1 ± 10.8 nm
P_ave = 119.6 nm
⟨R²⟩ (×10³ nm²)
separation, d (nm)

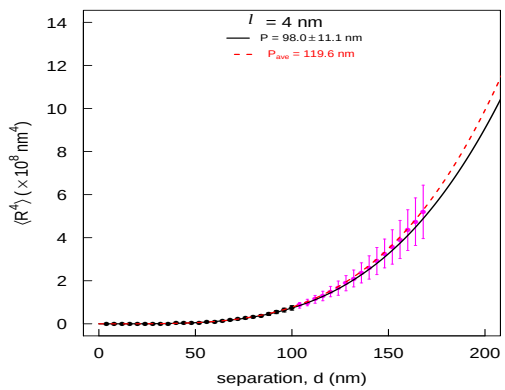
l = 4 nm
P = 98.0 ± 11.1 nm
P_ave = 119.6 nm
⟨R⁴⟩ (×10⁸ nm⁴)
separation, d (nm)

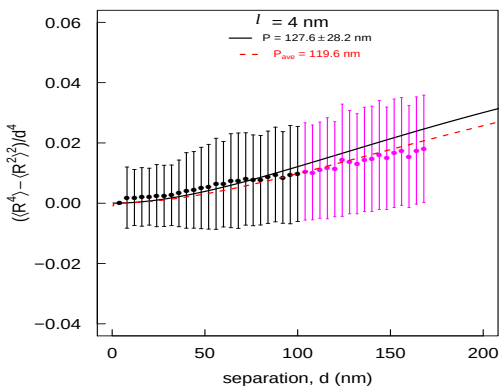
l = 4 nm
P = 127.6 ± 28.2 nm
P_ave = 119.6 nm
(⟨R⁴⟩ − ⟨R²⟩²)/d⁴
separation, d (nm)

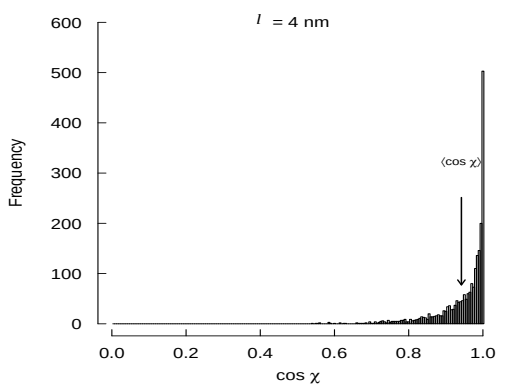
l = 4 nm
Frequency
⟨cos χ⟩
cos χ

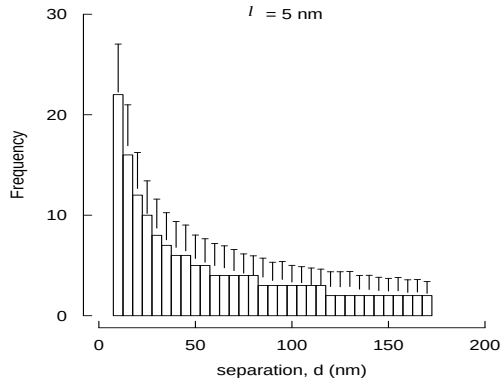
l = 5 nm
Frequency
separation, d (nm)

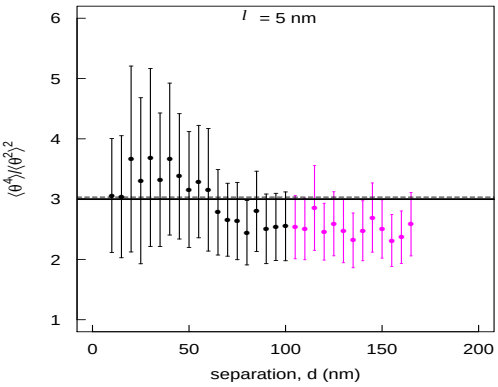
l = 5 nm
⟨θ⁴⟩/⟨θ²⟩²
separation, d (nm)

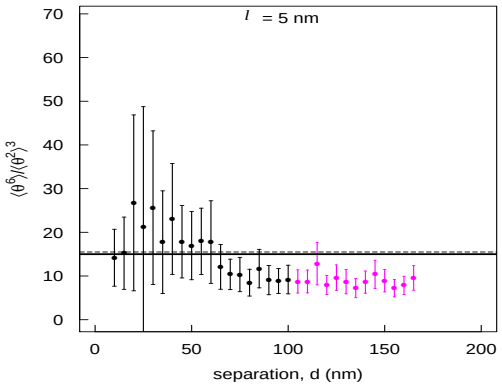
l = 5 nm
⟨θ⁶⟩/⟨θ²⟩³
separation, d (nm)

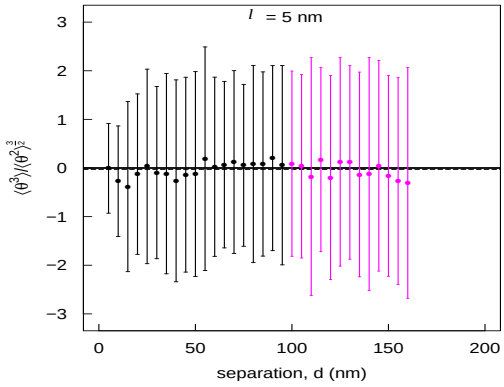
l = 5 nm
⟨θ³⟩/⟨θ²⟩^3/2
separation, d (nm)

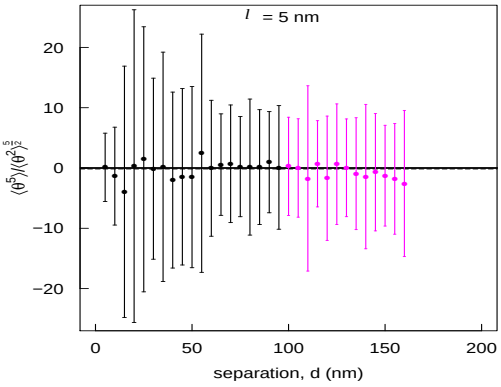
l = 5 nm
⟨θ⁵⟩/⟨θ²⟩^5/2
separation, d (nm)

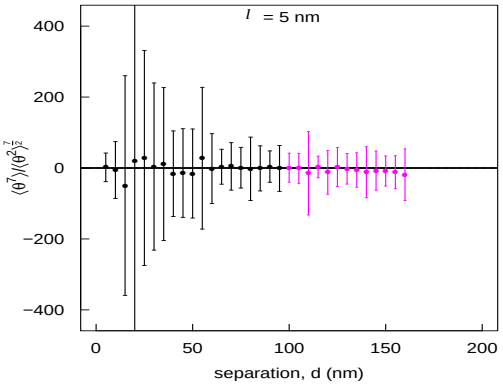
l = 5 nm
⟨θ⁷⟩/⟨θ²⟩^7/2
separation, d (nm)

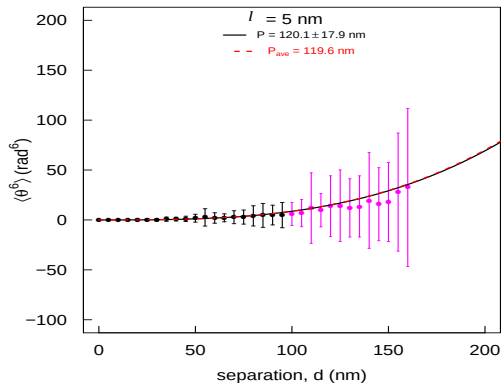
l = 5 nm
P = 120.1±17.9 nm
P_ave = 119.6 nm
⟨θ⁶⟩ (rad⁶)
separation, d (nm)

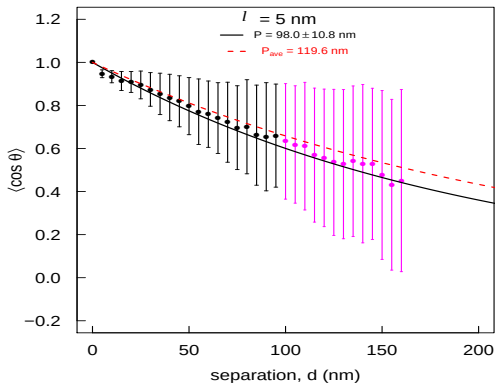
l = 5 nm
P = 98.0±10.8 nm
P_ave = 119.6 nm
⟨cos θ⟩
separation, d (nm)

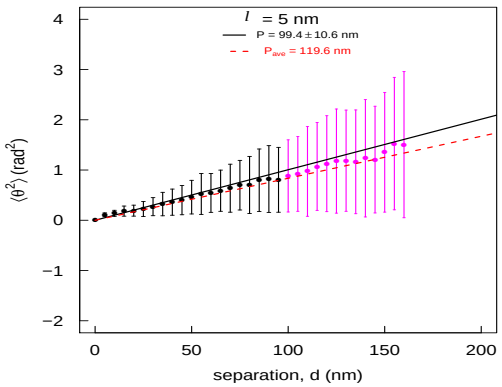
l = 5 nm
P = 99.4±10.6 nm
P_ave = 119.6 nm
⟨θ²⟩ (rad²)
separation, d (nm)

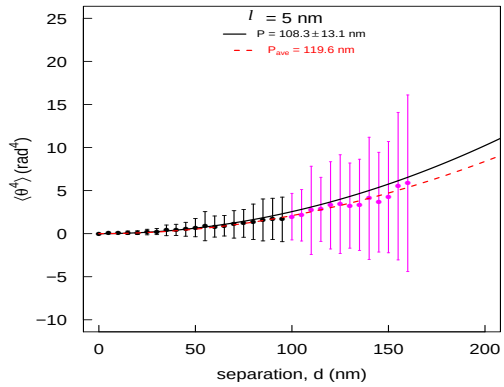
l = 5 nm
P = 108.3±13.1 nm
P_ave = 119.6 nm
⟨θ⁴⟩ (rad⁴)
separation, d (nm)

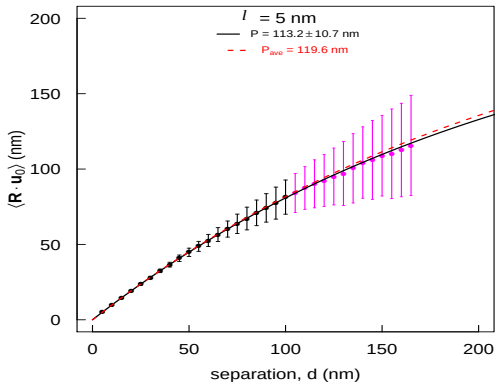
l = 5 nm
P = 113.2±10.7 nm
P_ave = 119.6 nm
⟨R · u₀⟩ (nm)
separation, d (nm)

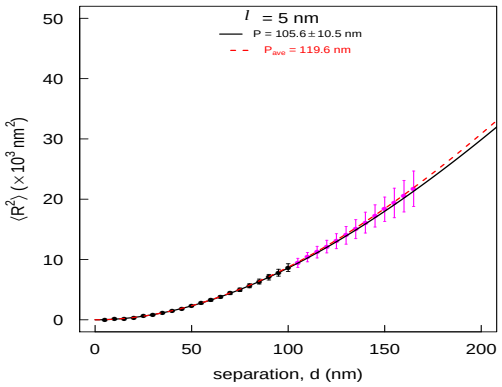
l = 5 nm
P = 105.6±10.5 nm
P_ave = 119.6 nm
⟨R²⟩ (×10³ nm²)
separation, d (nm)

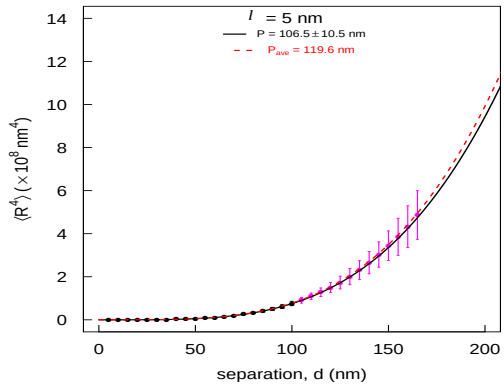
l = 5 nm
P = 106.5±10.5 nm
P_ave = 119.6 nm
⟨R⁴⟩ (×10⁸ nm⁴)
separation, d (nm)

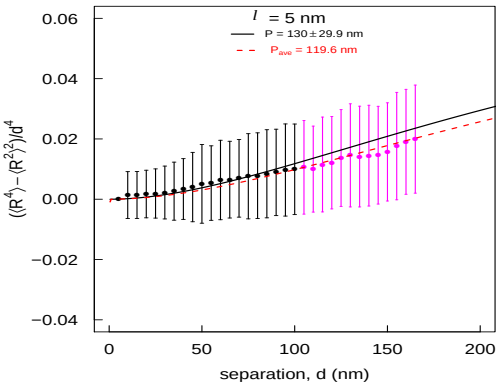
l = 5 nm
P = 130±29.9 nm
P_ave = 119.6 nm
⟨(R⁴) − ⟨R²⟩²⟩/d⁴
separation, d (nm)

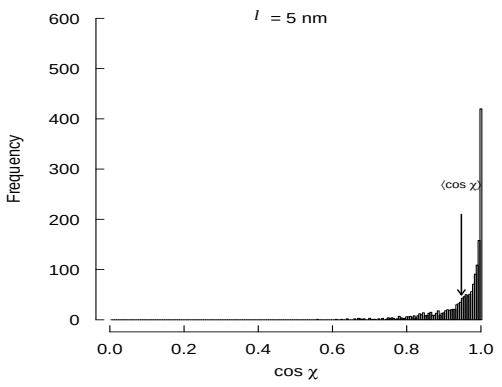
l = 5 nm
Frequency
⟨cos χ⟩
cos χ

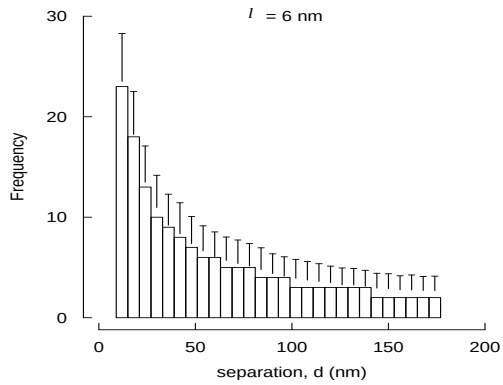
l = 6 nm
Frequency
separation, d (nm)

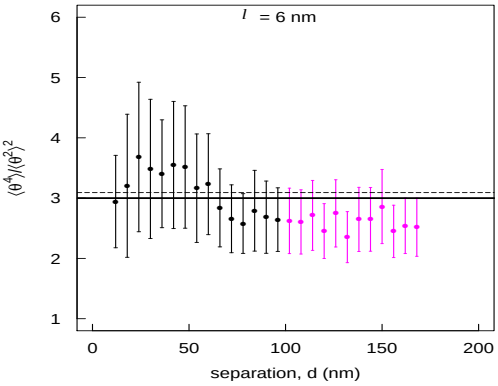
l = 6 nm
⟨θ⁴⟩/⟨θ²⟩²
separation, d (nm)

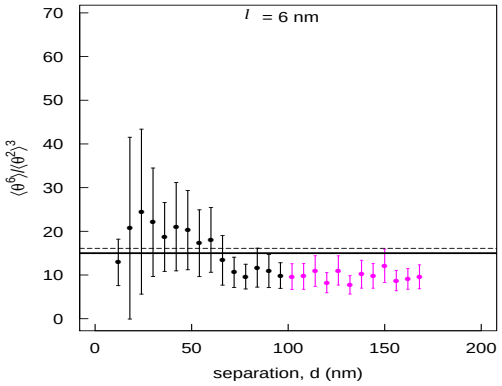
l = 6 nm
⟨θ⁶⟩/⟨θ²⟩³
separation, d (nm)

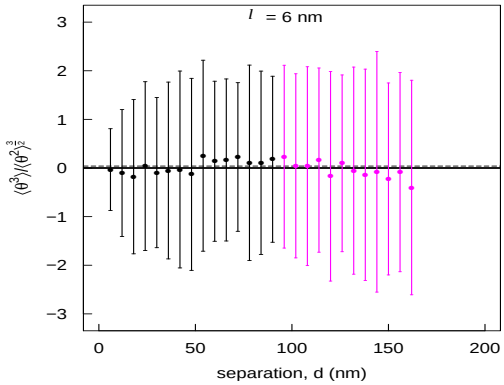
l = 6 nm
⟨θ³⟩/⟨θ²⟩^3/2
separation, d (nm)

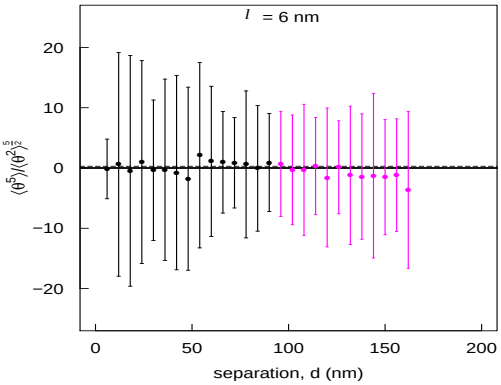
l = 6 nm
⟨θ⁵⟩/⟨θ²⟩^5/2
separation, d (nm)

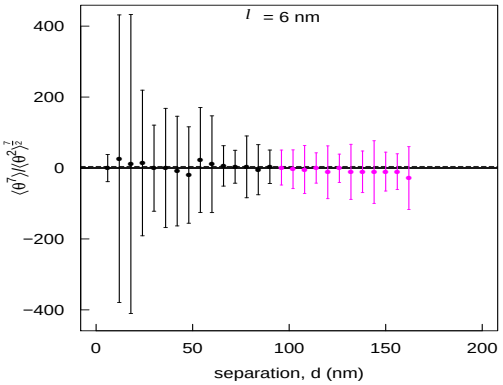
l = 6 nm
⟨θ⁷⟩/⟨θ²⟩^7/2
separation, d (nm)

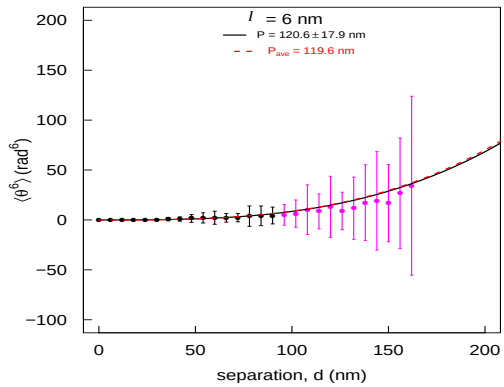
l = 6 nm
P = 120.6±17.9 nm
P_ave = 119.6 nm
⟨θ⁶⟩ (rad⁶)
separation, d (nm)

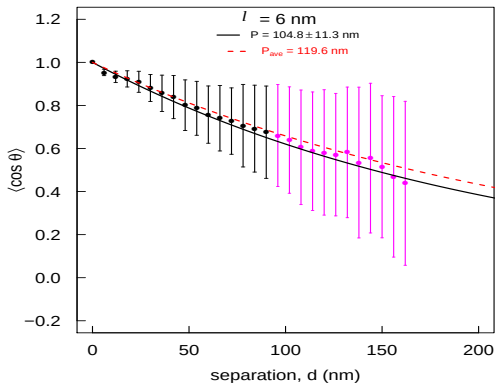
l = 6 nm
P = 104.8±11.3 nm
P_ave = 119.6 nm
⟨cos θ⟩
separation, d (nm)

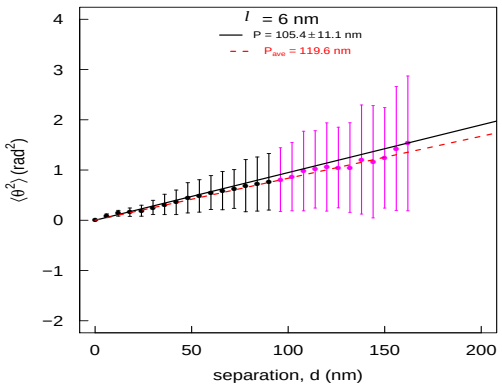
l = 6 nm
P = 105.4±11.1 nm
P_ave = 119.6 nm
⟨θ²⟩ (rad²)
separation, d (nm)

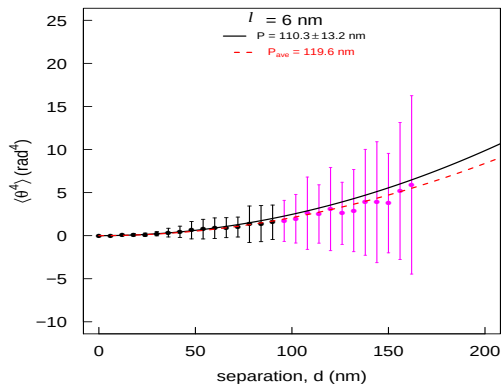
l = 6 nm
P = 110.3±13.2 nm
P_ave = 119.6 nm
⟨θ⁴⟩ (rad⁴)
separation, d (nm)

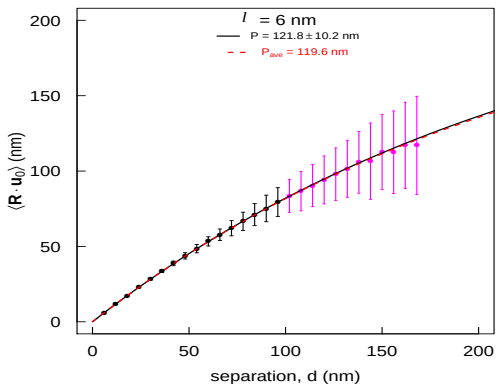
l = 6 nm
P = 121.8±10.2 nm
P_ave = 119.6 nm
⟨R · u₀⟩ (nm)
separation, d (nm)

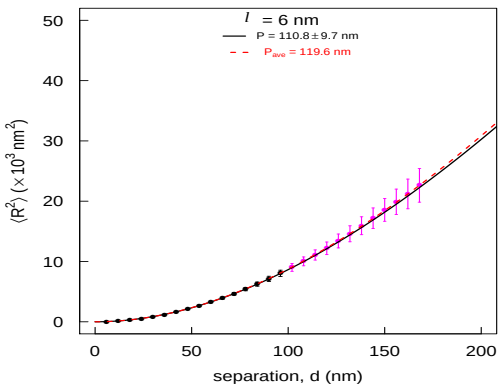
l = 6 nm
P = 110.8±9.7 nm
P_ave = 119.6 nm
⟨R²⟩ (×10³ nm²)
separation, d (nm)

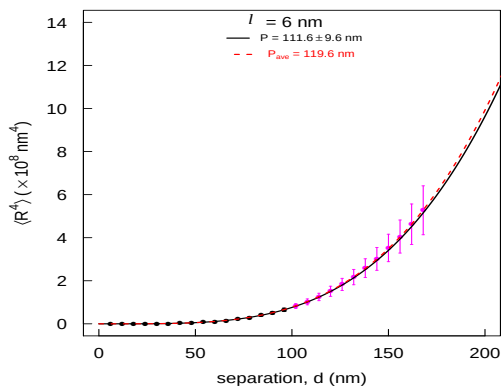
l = 6 nm
P = 111.6±9.6 nm
P_ave = 119.6 nm
⟨R⁴⟩ (×10⁸ nm⁴)
separation, d (nm)

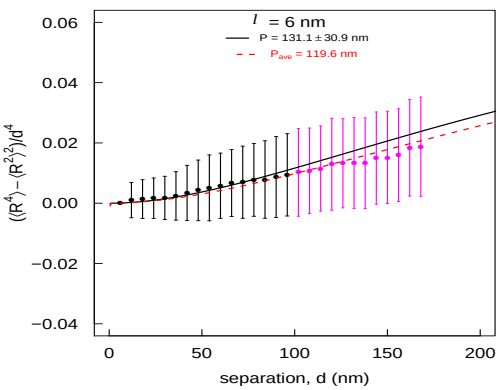
l = 6 nm
P = 131.1±30.9 nm
P_ave = 119.6 nm
⟨(R⁴) − ⟨R²⟩²⟩/d⁴
separation, d (nm)

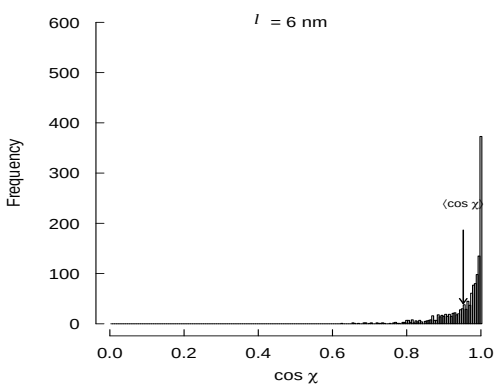
l = 6 nm
Frequency
⟨cos χ⟩
cos χ

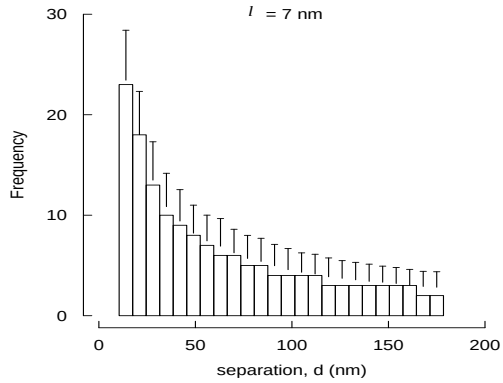
l = 7 nm
Frequency
separation, d (nm)

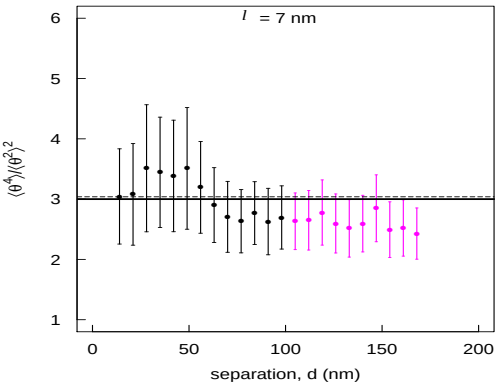
l = 7 nm
⟨θ⁴⟩/⟨θ²⟩²
separation, d (nm)

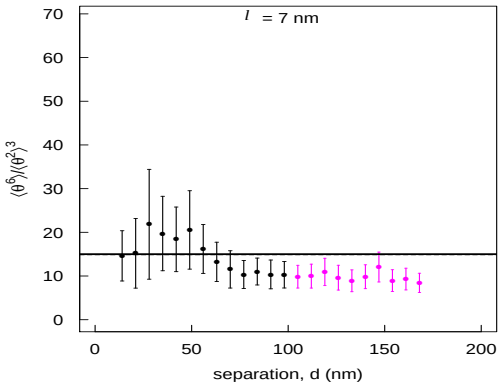
l = 7 nm
⟨θ⁶⟩/⟨θ²⟩³
separation, d (nm)

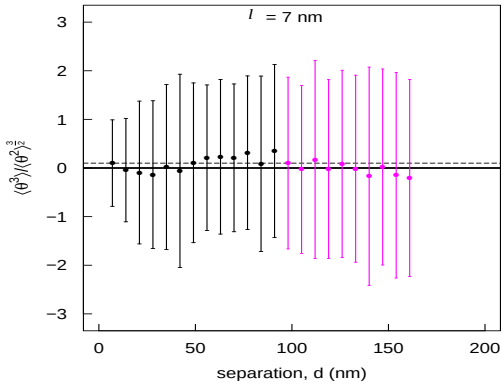
l = 7 nm
⟨θ³⟩/⟨θ²⟩^3/2
separation, d (nm)

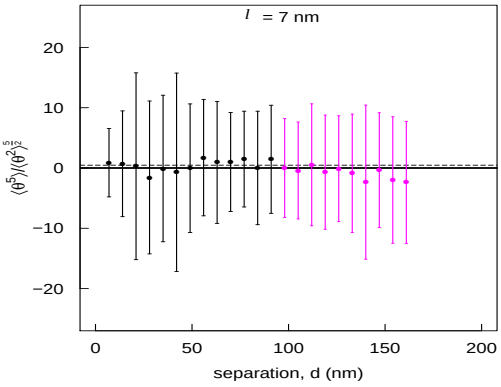
l = 7 nm
⟨θ⁵⟩/⟨θ²⟩^5/2
separation, d (nm)

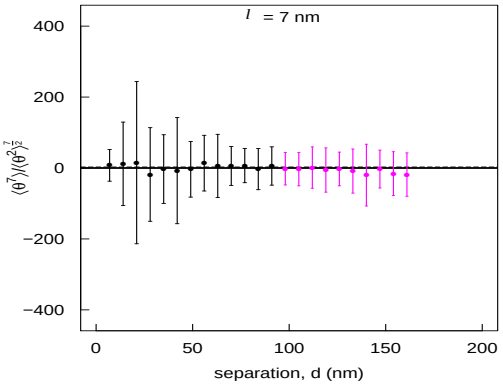
l = 7 nm
⟨θ⁷⟩/⟨θ²⟩^7/2
separation, d (nm)

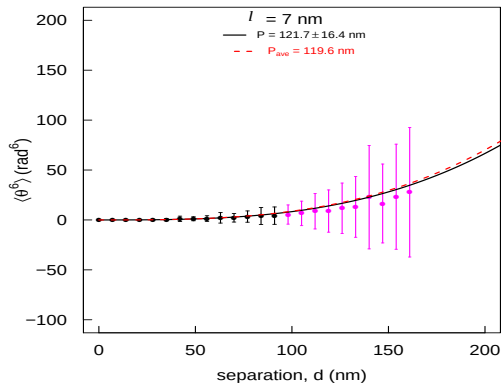
l = 7 nm
P = 121.7±16.4 nm
P_ave = 119.6 nm
⟨θ⁶⟩ (rad⁶)
separation, d (nm)

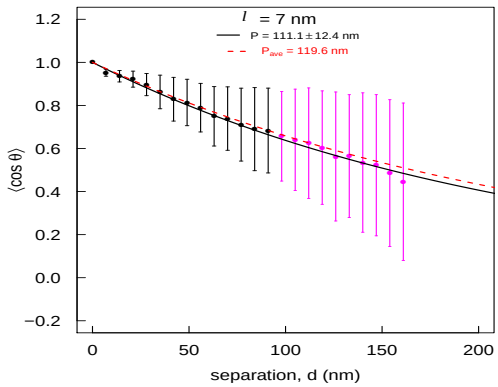
l = 7 nm
P = 111.1±12.4 nm
P_ave = 119.6 nm
⟨cos θ⟩
separation, d (nm)

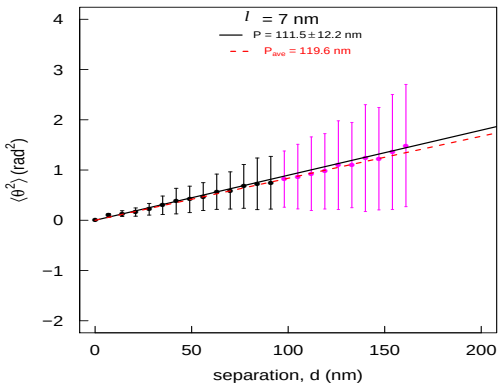
l = 7 nm
P = 111.5±12.2 nm
P_ave = 119.6 nm
⟨θ²⟩ (rad²)
separation, d (nm)

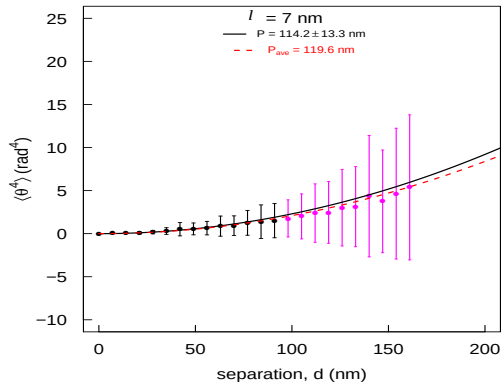
l = 7 nm
P = 114.2±13.3 nm
P_ave = 119.6 nm
⟨θ⁴⟩ (rad⁴)
separation, d (nm)

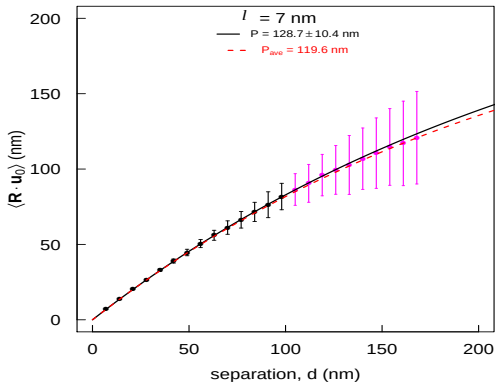
l = 7 nm
P = 128.7±10.4 nm
P_ave = 119.6 nm
⟨R · u₀⟩ (nm)
separation, d (nm)

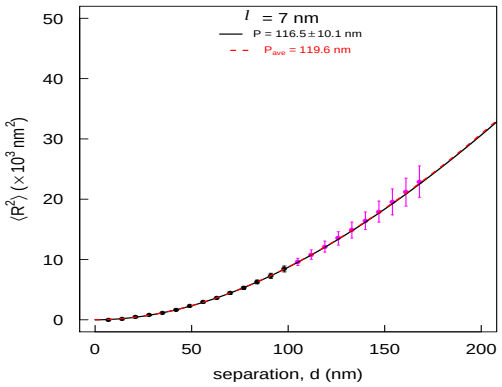
l = 7 nm
P = 116.5±10.1 nm
P_ave = 119.6 nm
⟨R²⟩ (×10³ nm²)
separation, d (nm)

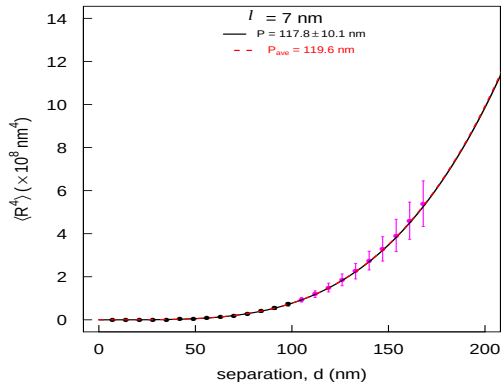
l = 7 nm
P = 117.8±10.1 nm
P_ave = 119.6 nm
⟨R⁴⟩ (×10⁸ nm⁴)
separation, d (nm)

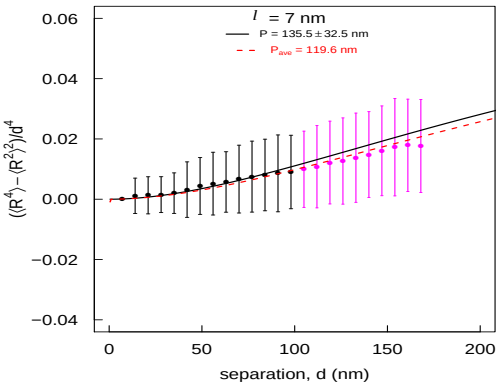
l = 7 nm
P = 135.5±32.5 nm
P_ave = 119.6 nm
⟨R⁴⟩−⟨R²⟩²)/d⁴
separation, d (nm)

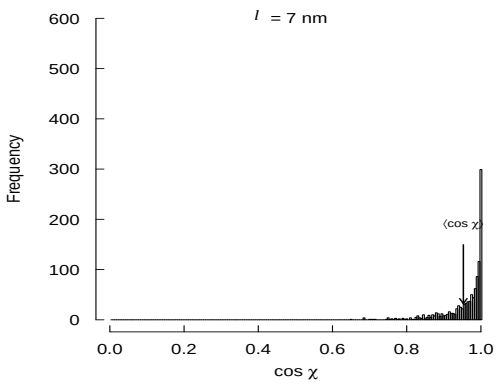
l = 7 nm
Frequency
⟨cos χ⟩
cos χ

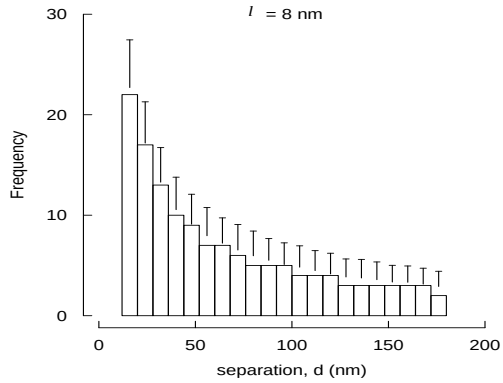
l = 8 nm
Frequency
separation, d (nm)

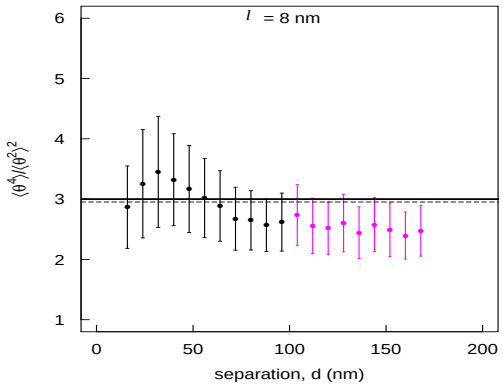
l = 8 nm
⟨θ⁴⟩/⟨θ²⟩²
separation, d (nm)

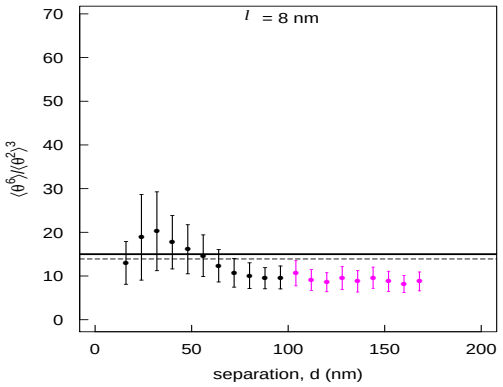
l = 8 nm
⟨θ⁶⟩/⟨θ²⟩³
separation, d (nm)

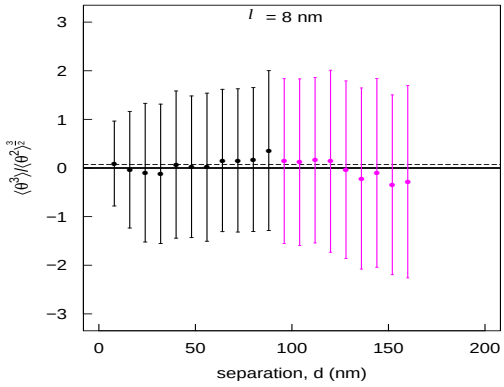
l = 8 nm
⟨θ³⟩/⟨θ²⟩^3/2
separation, d (nm)

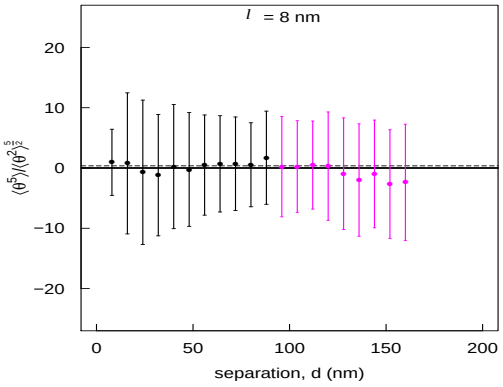
l = 8 nm
⟨θ⁵⟩/⟨θ²⟩^5/2
separation, d (nm)

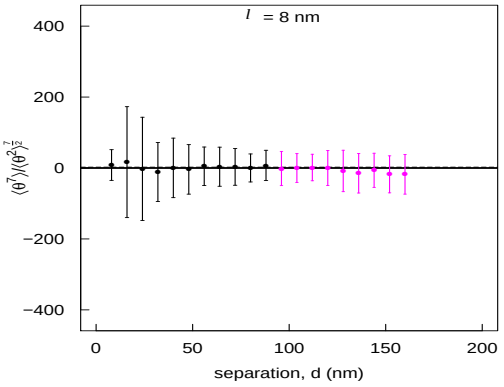
l = 8 nm
⟨θ⁷⟩/⟨θ²⟩^7/2
separation, d (nm)

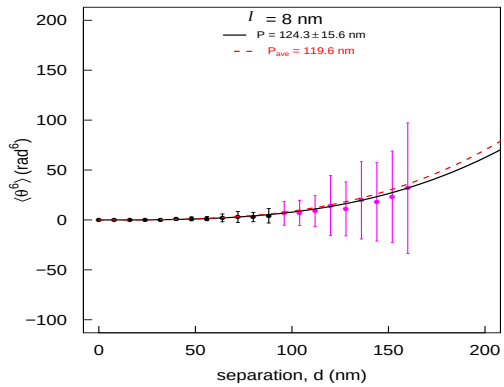
l = 8 nm
P = 124.3 ± 15.6 nm
P_ave = 119.6 nm
⟨θ⁶⟩ (rad⁶)
separation, d (nm)

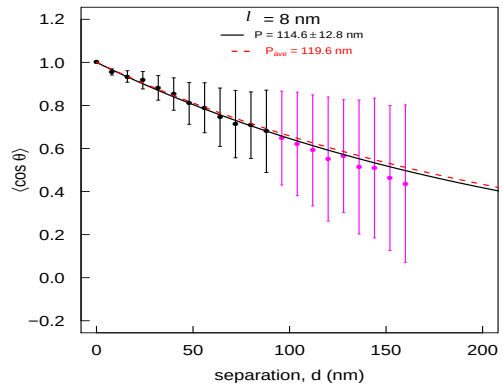
l = 8 nm
P = 114.6 ± 12.8 nm
P_ave = 119.6 nm
⟨cos θ⟩
separation, d (nm)

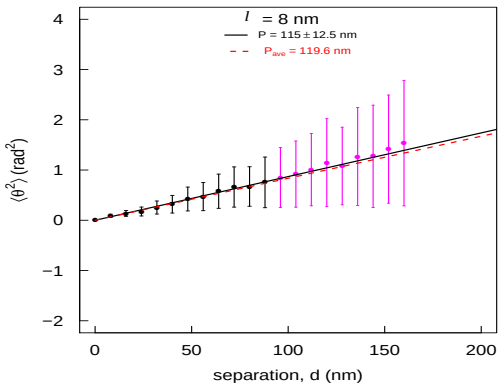
l = 8 nm
P = 115 ± 12.5 nm
P_ave = 119.6 nm
⟨θ²⟩ (rad²)
separation, d (nm)

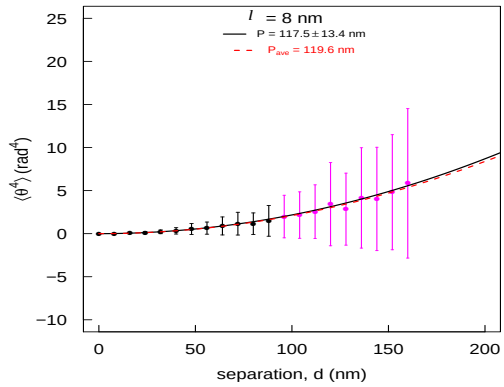
l = 8 nm
P = 117.5 ± 13.4 nm
P_ave = 119.6 nm
⟨θ⁴⟩ (rad⁴)
separation, d (nm)

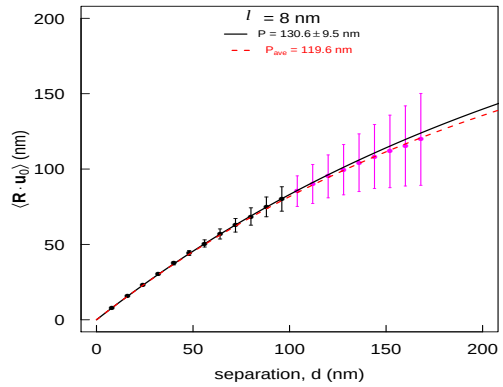
l = 8 nm
P = 130.6 ± 9.5 nm
P_ave = 119.6 nm
⟨R · u₀⟩ (nm)
separation, d (nm)

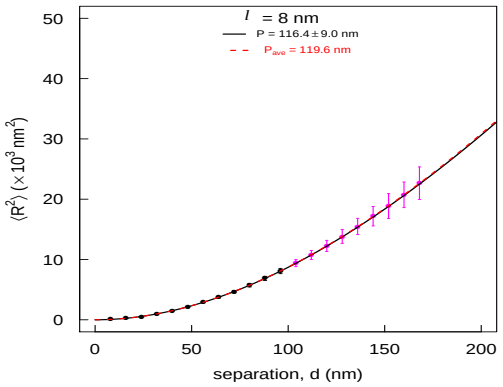
l = 8 nm
P = 116.4 ± 9.0 nm
P_ave = 119.6 nm
⟨R²⟩ (×10³ nm²)
separation, d (nm)

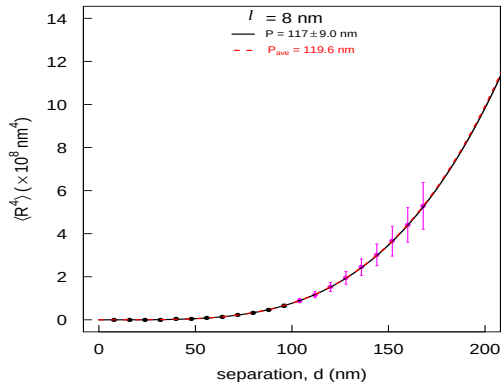
l = 8 nm
P = 117 ± 9.0 nm
P_ave = 119.6 nm
⟨R⁴⟩ (×10⁸ nm⁴)
separation, d (nm)

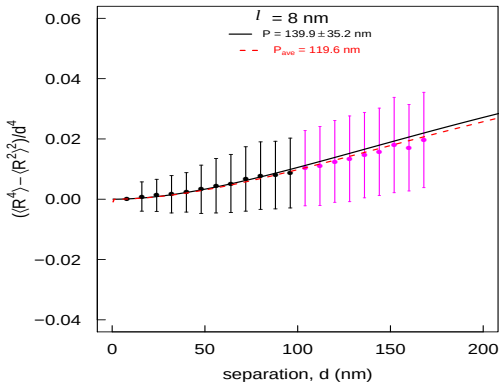
l = 8 nm
P = 139.9 ± 35.2 nm
P_ave = 119.6 nm
(⟨R⁴⟩ − ⟨R²⟩²)/d⁴
separation, d (nm)

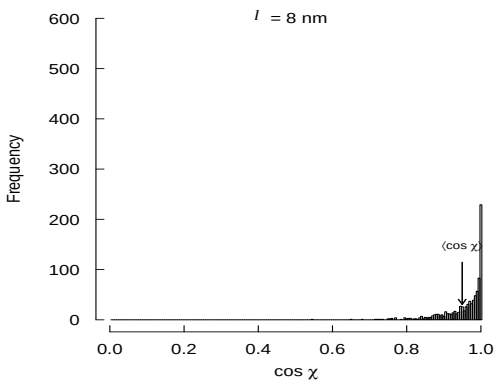
l = 8 nm
Frequency
⟨cos χ⟩
cos χ

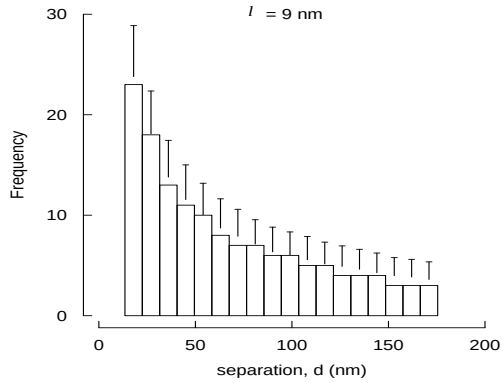
l = 9 nm
Frequency
separation, d (nm)

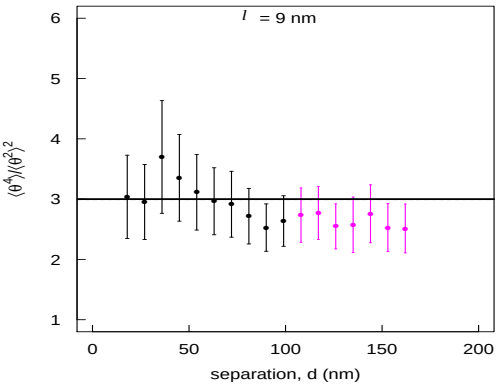
l = 9 nm
⟨θ⁴⟩/⟨θ²⟩²
separation, d (nm)

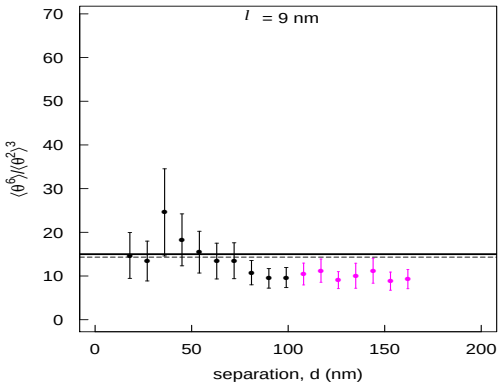
l = 9 nm
⟨θ⁶⟩/⟨θ²⟩³
separation, d (nm)

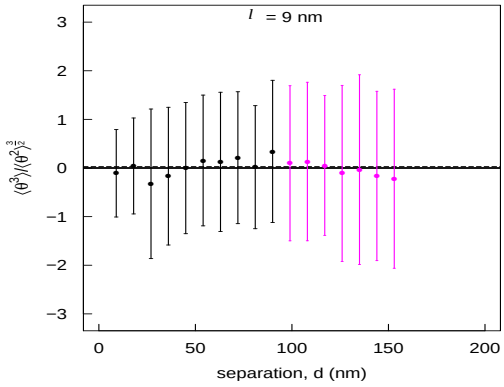
l = 9 nm
⟨θ³⟩/⟨θ²⟩^3/2
separation, d (nm)

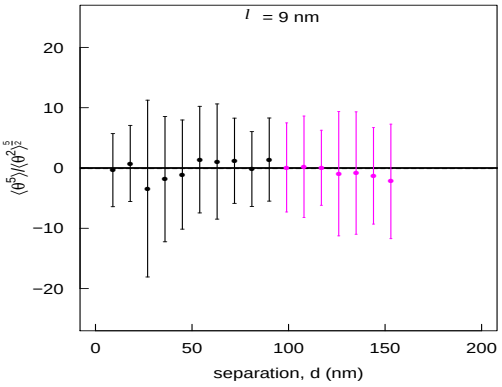
l = 9 nm
⟨θ⁵⟩/⟨θ²⟩^5/2
separation, d (nm)

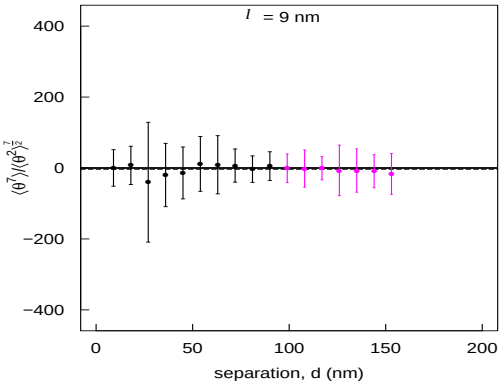
l = 9 nm
⟨θ⁷⟩/⟨θ²⟩^7/2
separation, d (nm)

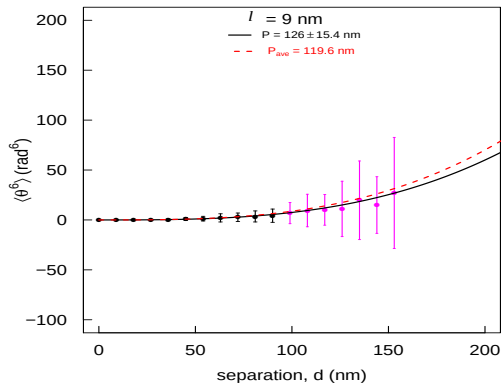
l = 9 nm
P = 126 ± 15.4 nm
P_ave = 119.6 nm
⟨θ⁶⟩ (rad⁶)
separation, d (nm)

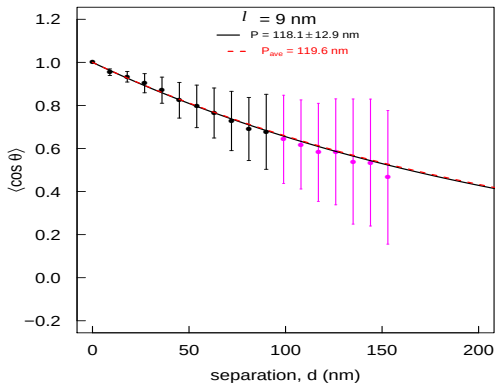
l = 9 nm
P = 118.1 ± 12.9 nm
P_ave = 119.6 nm
⟨cos θ⟩
separation, d (nm)

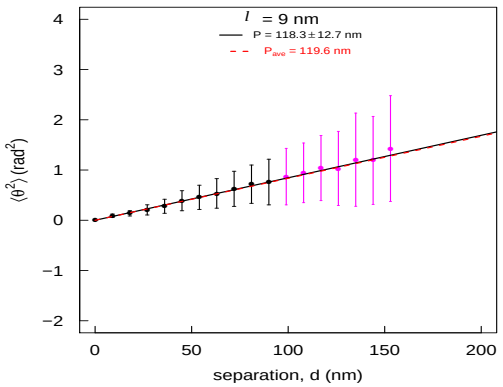
l = 9 nm
P = 118.3 ± 12.7 nm
P_ave = 119.6 nm
⟨θ²⟩ (rad²)
separation, d (nm)

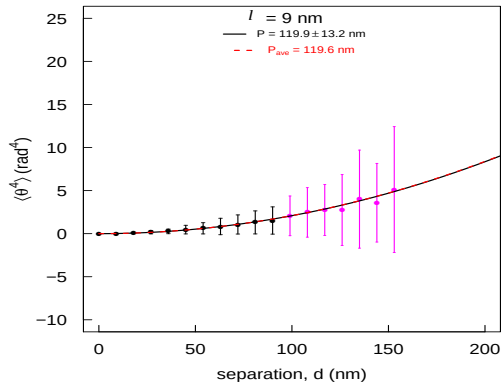
l = 9 nm
P = 119.9 ± 13.2 nm
P_ave = 119.6 nm
⟨θ⁴⟩ (rad⁴)
separation, d (nm)

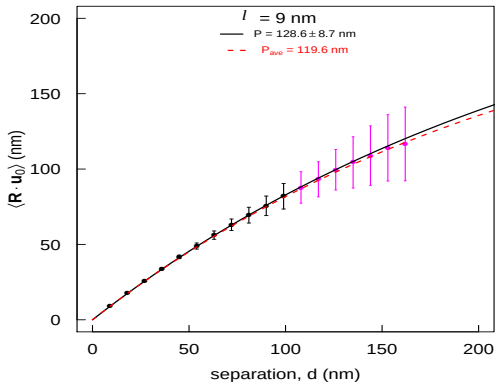
l = 9 nm
P = 128.6 ± 8.7 nm
P_ave = 119.6 nm
⟨R · u₀⟩ (nm)
separation, d (nm)

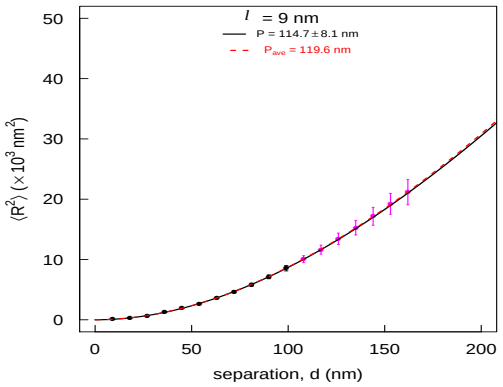
l = 9 nm
P = 114.7 ± 8.1 nm
P_ave = 119.6 nm
⟨R²⟩ (×10³ nm²)
separation, d (nm)

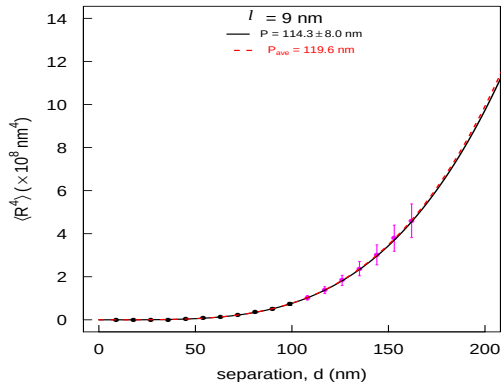
l = 9 nm
P = 114.3 ± 8.0 nm
P_ave = 119.6 nm
⟨R⁴⟩ (×10⁸ nm⁴)
separation, d (nm)

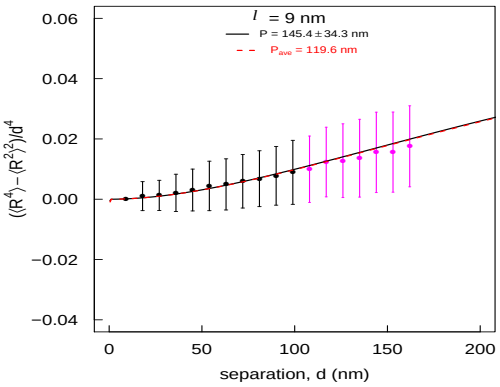
l = 9 nm
P = 145.4 ± 34.3 nm
P_ave = 119.6 nm
⟨R⁴⟩ − ⟨R²⟩²)/d⁴
separation, d (nm)

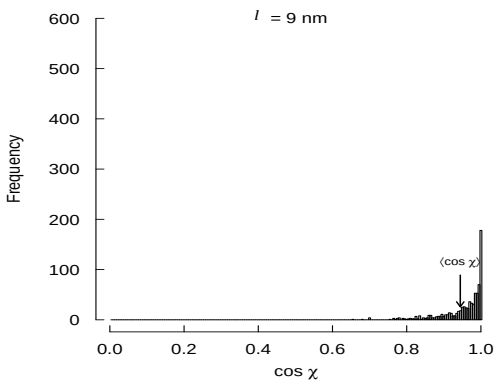
l = 9 nm
Frequency
⟨cos χ⟩
cos χ

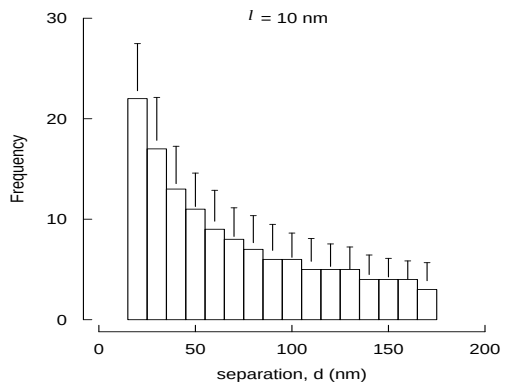
l = 10 nm
Frequency
separation, d (nm)

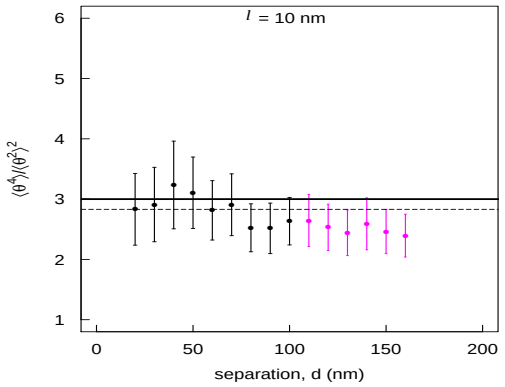
l = 10 nm
⟨θ⁴⟩/⟨θ²⟩²
separation, d (nm)

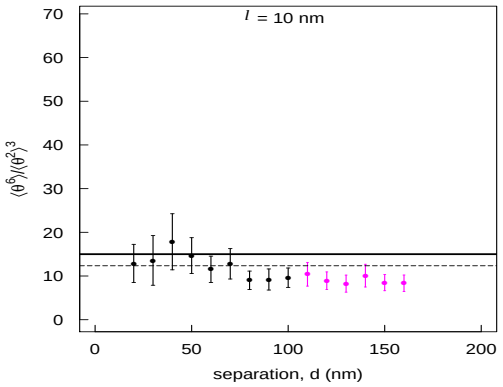
l = 10 nm
⟨θ⁶⟩/⟨θ²⟩³
separation, d (nm)

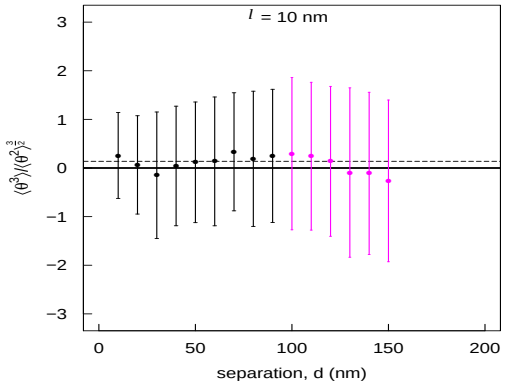
l = 10 nm
⟨θ³⟩/⟨θ²⟩^3/2
separation, d (nm)

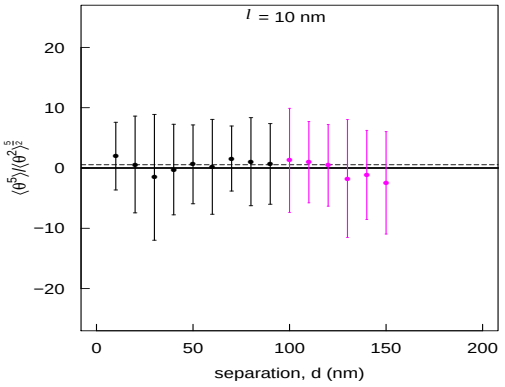
l = 10 nm
⟨θ⁵⟩/⟨θ²⟩^5/2
separation, d (nm)

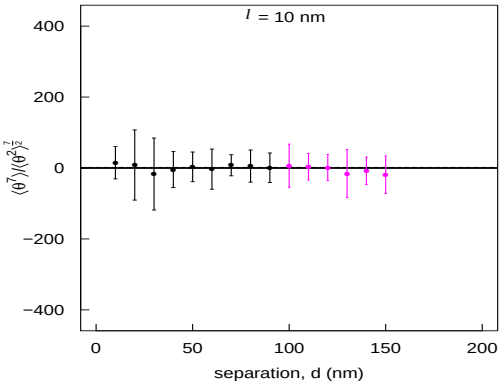
l = 10 nm
⟨θ⁷⟩/⟨θ²⟩^7/2
separation, d (nm)

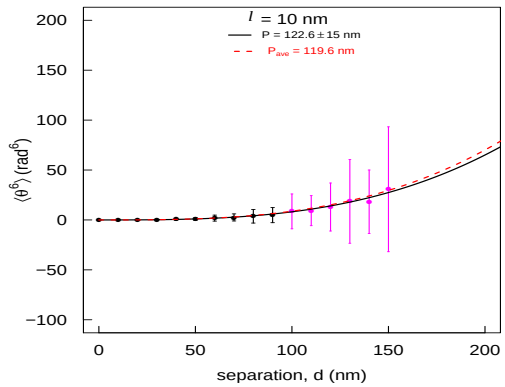
l = 10 nm
P = 122.6±15 nm
P_ave = 119.6 nm
⟨θ⁶⟩ (rad⁶)
separation, d (nm)

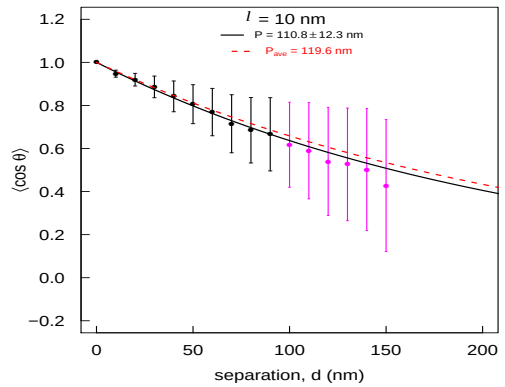
l = 10 nm
P = 110.8±12.3 nm
P_ave = 119.6 nm
⟨cos θ⟩
separation, d (nm)

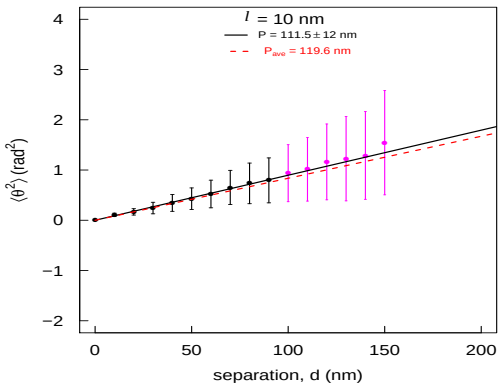
l = 10 nm
P = 111.5±12 nm
P_ave = 119.6 nm
⟨θ²⟩ (rad²)
separation, d (nm)

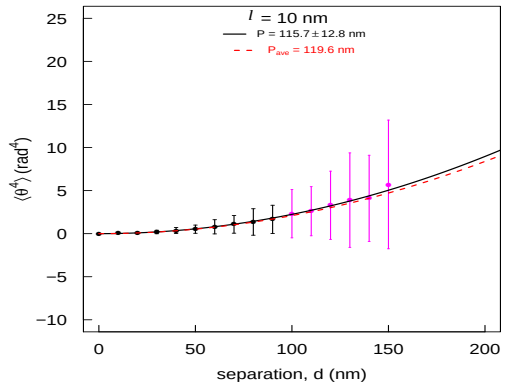
l = 10 nm
P = 115.7±12.8 nm
P_ave = 119.6 nm
⟨θ⁴⟩ (rad⁴)
separation, d (nm)

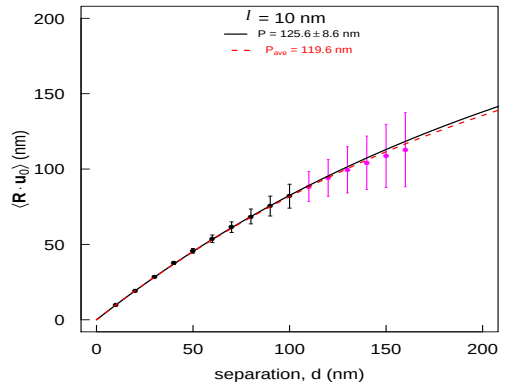
l = 10 nm
P = 125.6±8.6 nm
P_ave = 119.6 nm
⟨R · u₀⟩ (nm)
separation, d (nm)

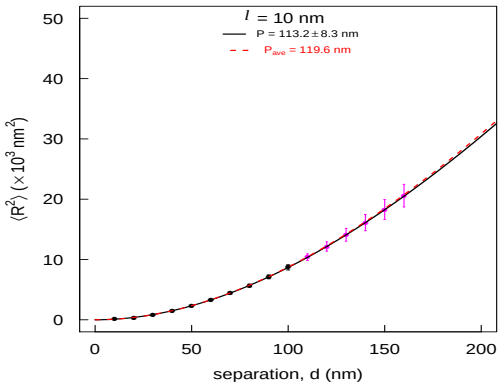
l = 10 nm
P = 113.2±8.3 nm
P_ave = 119.6 nm
⟨R²⟩ (×10³ nm²)
separation, d (nm)

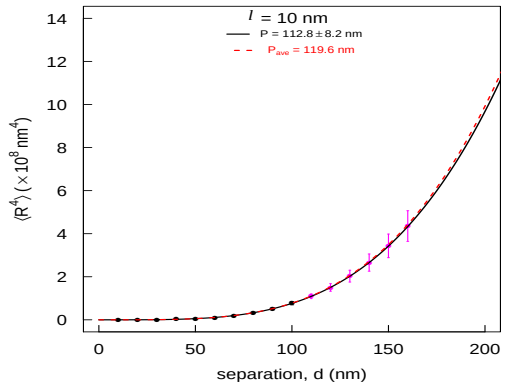
l = 10 nm
P = 112.8±8.2 nm
P_ave = 119.6 nm
⟨R⁴⟩ (×10⁸ nm⁴)
separation, d (nm)

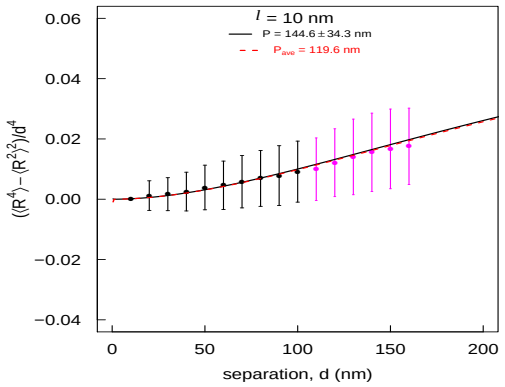
l = 10 nm
P = 144.6±34.3 nm
P_ave = 119.6 nm
(⟨R⁴⟩−⟨R²⟩²)/d⁴
separation, d (nm)

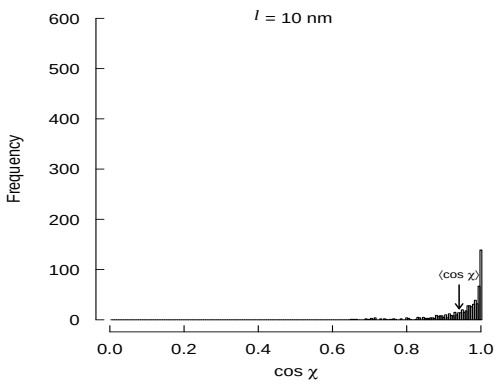
l = 10 nm
Frequency
⟨cos χ⟩
cos χ

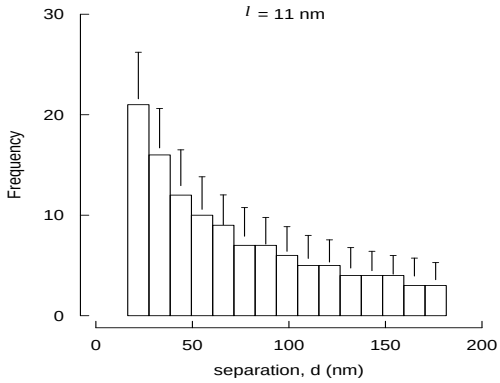
l = 11 nm
Frequency
separation, d (nm)

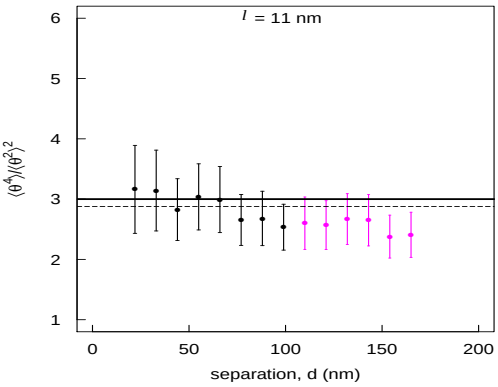
l = 11 nm
⟨θ⁴⟩/⟨θ²⟩²
separation, d (nm)

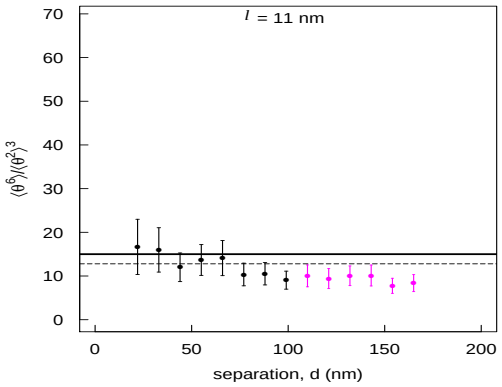
l = 11 nm
⟨θ⁶⟩/⟨θ²⟩³
separation, d (nm)

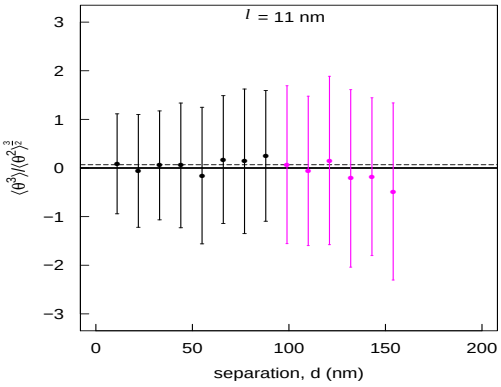
l = 11 nm
⟨θ³⟩/⟨θ²⟩^3/2
separation, d (nm)

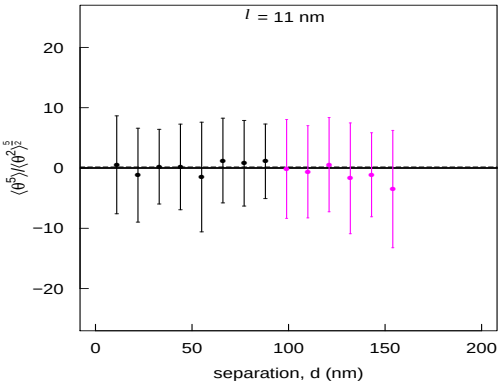
l = 11 nm
⟨θ⁵⟩/⟨θ²⟩^5/2
separation, d (nm)

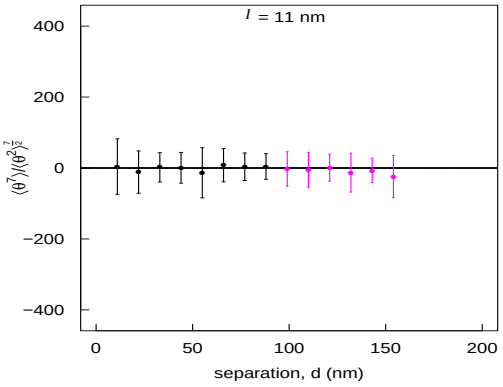
l = 11 nm
⟨θ⁷⟩/⟨θ²⟩^7/2
separation, d (nm)

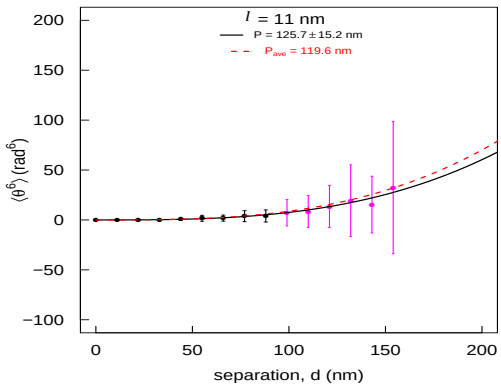
l = 11 nm
P = 125.7±15.2 nm
P_ave = 119.6 nm
⟨θ⁶⟩ (rad⁶)
separation, d (nm)

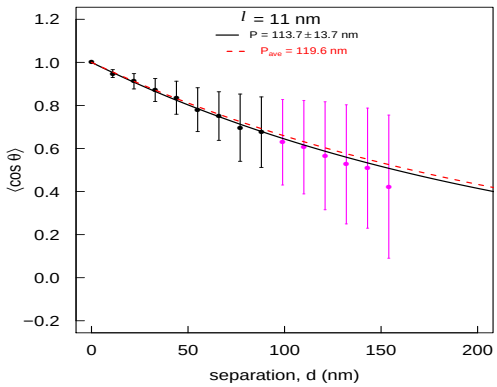
l = 11 nm
P = 113.7±13.7 nm
P_ave = 119.6 nm
⟨cos θ⟩
separation, d (nm)

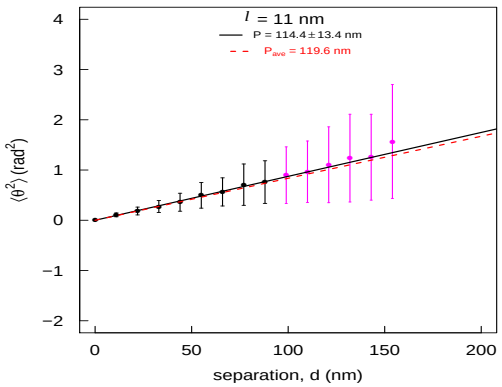
l = 11 nm
P = 114.4±13.4 nm
P_ave = 119.6 nm
⟨θ²⟩ (rad²)
separation, d (nm)

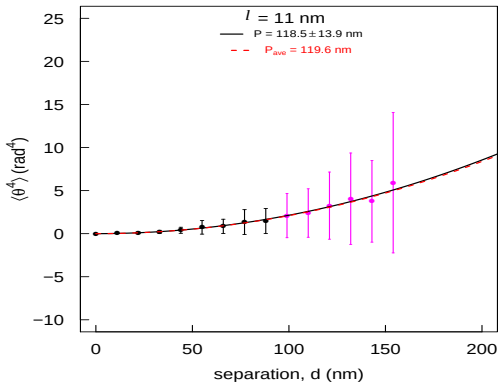
l = 11 nm
P = 118.5±13.9 nm
P_ave = 119.6 nm
⟨θ⁴⟩ (rad⁴)
separation, d (nm)

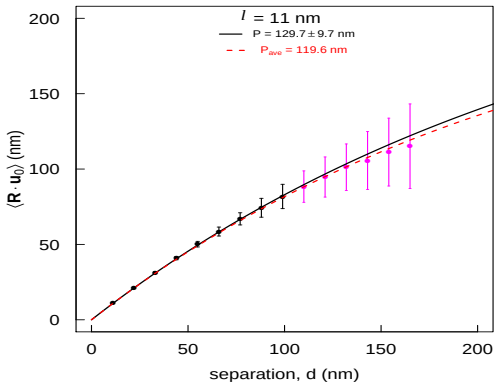
l = 11 nm
P = 129.7±9.7 nm
P_ave = 119.6 nm
⟨R · u₀⟩ (nm)
separation, d (nm)

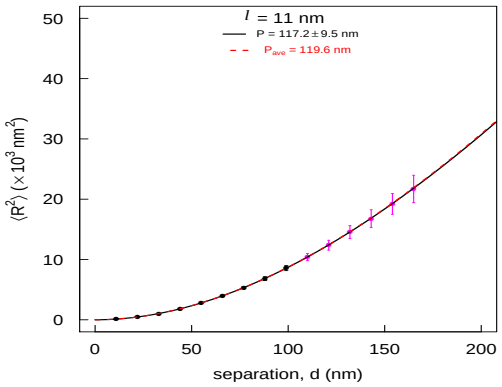
l = 11 nm
P = 117.2±9.5 nm
P_ave = 119.6 nm
⟨R²⟩ (×10³ nm²)
separation, d (nm)

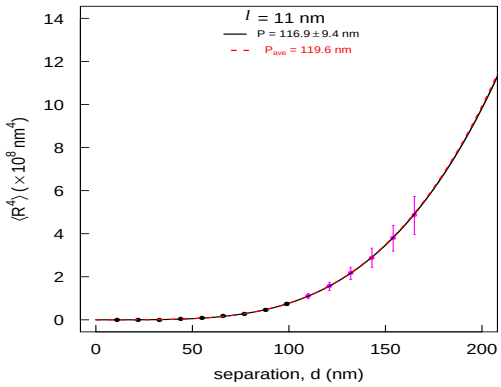
l = 11 nm
P = 116.9±9.4 nm
P_ave = 119.6 nm
⟨R⁴⟩ (×10⁸ nm⁴)
separation, d (nm)

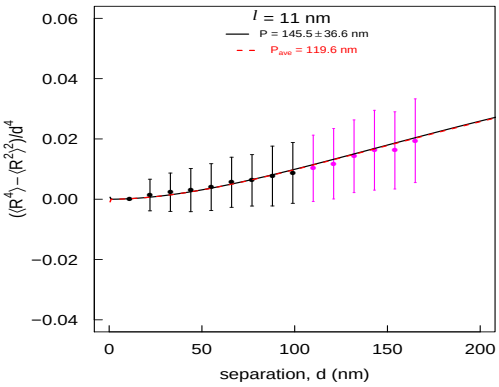
l = 11 nm
P = 145.5±36.6 nm
P_ave = 119.6 nm
(⟨R⁴⟩−⟨R²⟩²)/d⁴
separation, d (nm)

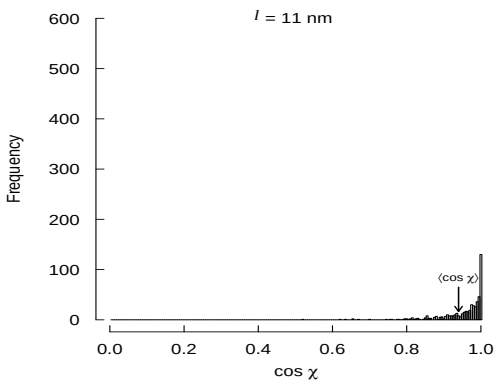
l = 11 nm
Frequency
⟨cos χ⟩
cos χ

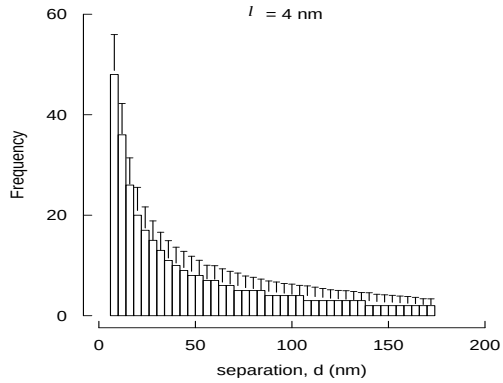
l = 4 nm
Frequency
separation, d (nm)

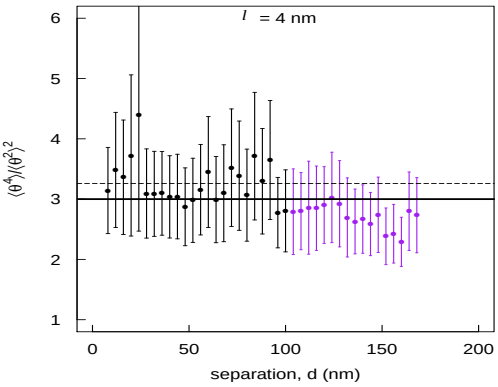
l = 4 nm
⟨θ⁴⟩/⟨θ²⟩²
separation, d (nm)

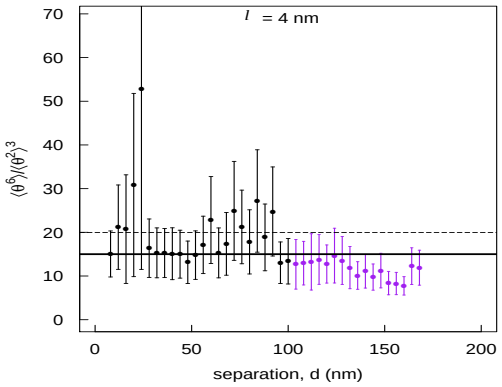
l = 4 nm
⟨θ⁶⟩/⟨θ²⟩³
separation, d (nm)

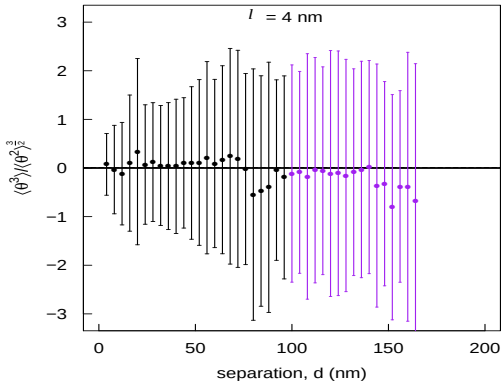
l = 4 nm
⟨θ³⟩/⟨θ²⟩^3/2
separation, d (nm)

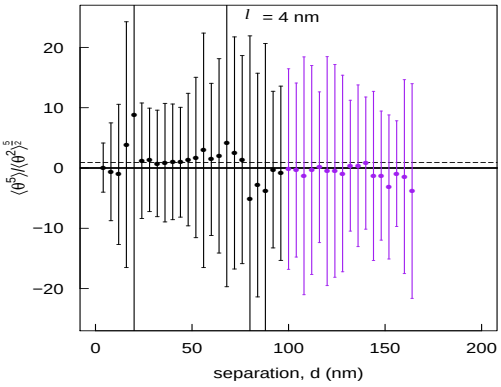
l = 4 nm
⟨θ⁵⟩/⟨θ²⟩^5/2
separation, d (nm)

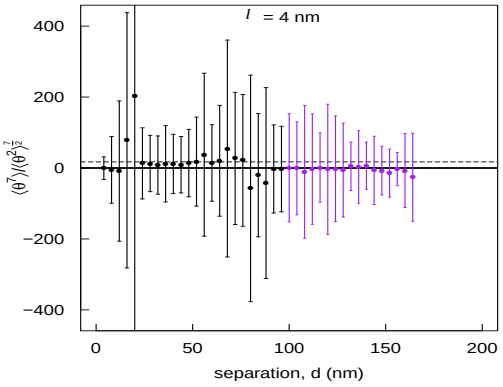
l = 4 nm
⟨θ⁷⟩/⟨θ²⟩^7/2
separation, d (nm)

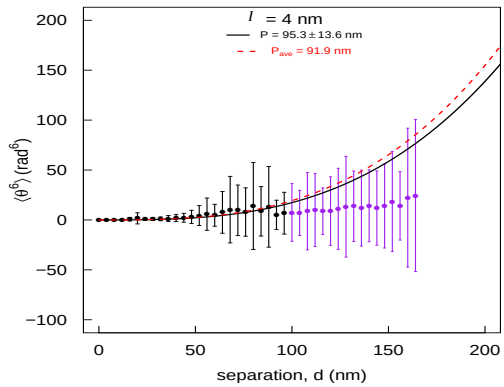
l = 4 nm
P = 95.3±13.6 nm
P_ave = 91.9 nm
⟨θ⁶⟩ (rad⁶)
separation, d (nm)

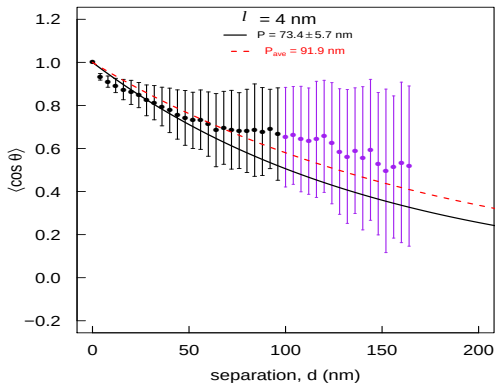
l = 4 nm
P = 73.4±5.7 nm
P_ave = 91.9 nm
⟨cos θ⟩
separation, d (nm)

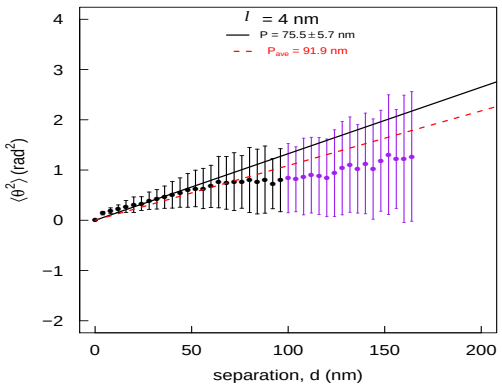
l = 4 nm
P = 75.5±5.7 nm
P_ave = 91.9 nm
⟨θ²⟩ (rad²)
separation, d (nm)

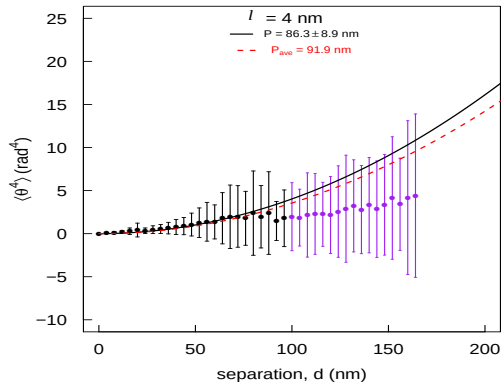
l = 4 nm
P = 86.3±8.9 nm
P_ave = 91.9 nm
⟨θ⁴⟩ (rad⁴)
separation, d (nm)

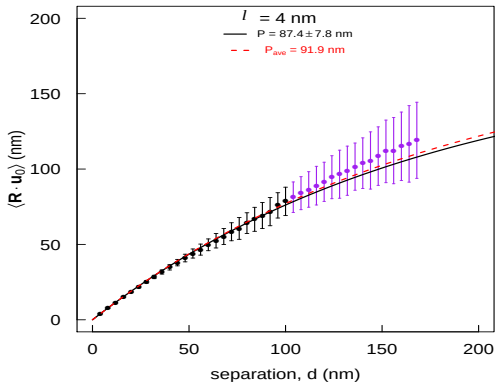
l = 4 nm
P = 87.4±7.8 nm
P_ave = 91.9 nm
⟨R · u₀⟩ (nm)
separation, d (nm)

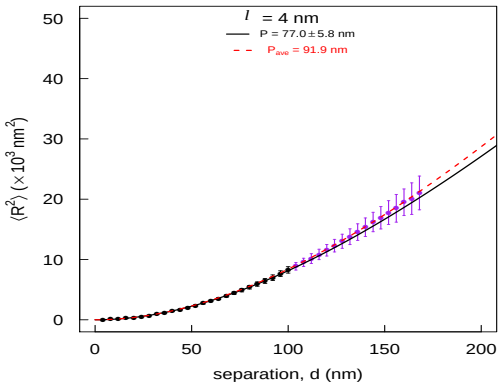
l = 4 nm
P = 77.0±5.8 nm
P_ave = 91.9 nm
⟨R²⟩ (×10³ nm²)
separation, d (nm)

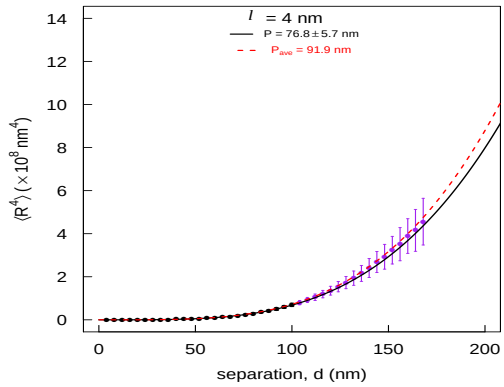
l = 4 nm
P = 76.8±5.7 nm
P_ave = 91.9 nm
⟨R⁴⟩ (×10⁸ nm⁴)
separation, d (nm)

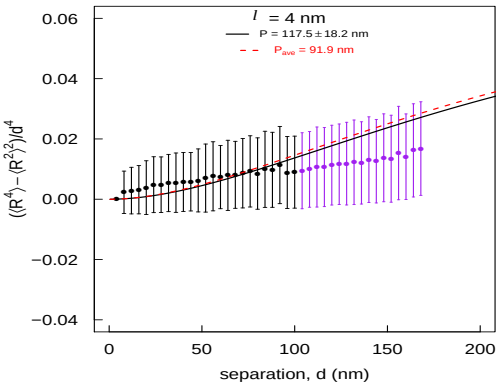
l = 4 nm
P = 117.5±18.2 nm
P_ave = 91.9 nm
(⟨R⁴⟩−⟨R²⟩²)/d⁴
separation, d (nm)

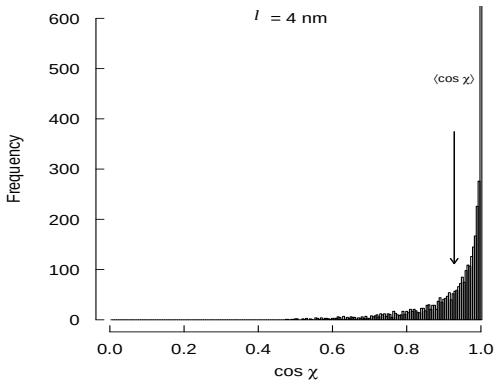
l = 4 nm
⟨cos χ⟩
Frequency
cos χ

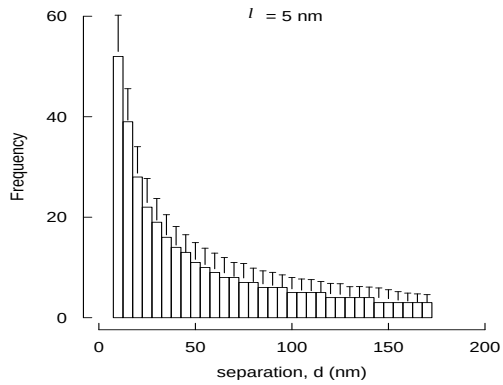
l = 5 nm
Frequency
separation, d (nm)

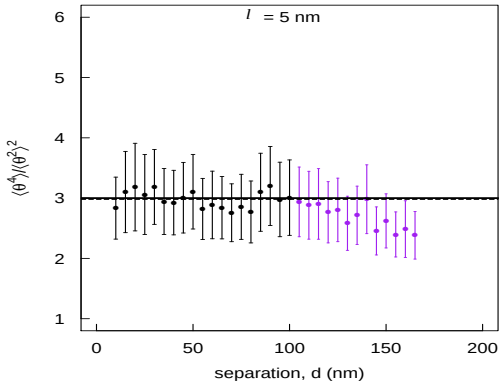
l = 5 nm
⟨θ⁴⟩/⟨θ²⟩²
separation, d (nm)

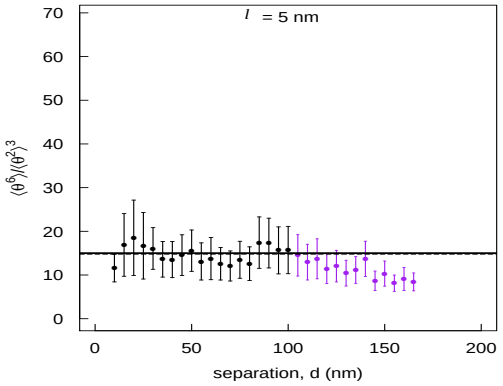
l = 5 nm
⟨θ⁶⟩/⟨θ²⟩³
separation, d (nm)

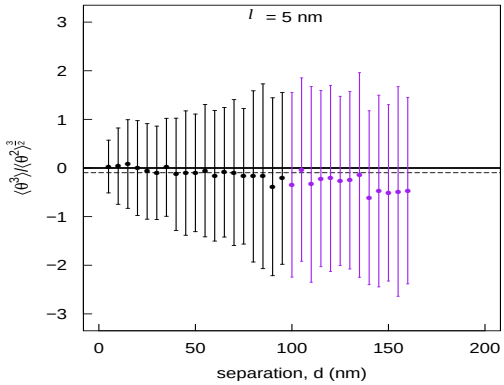
l = 5 nm
⟨θ³⟩/⟨θ²⟩^3/2
separation, d (nm)

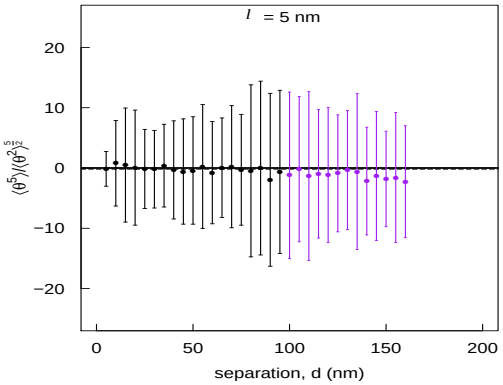
l = 5 nm
⟨θ⁵⟩/⟨θ²⟩^5/2
separation, d (nm)

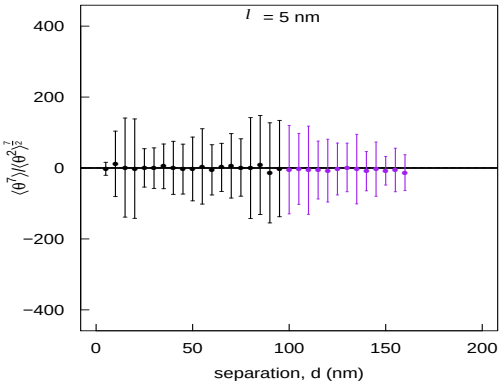
l = 5 nm
⟨θ⁷⟩/⟨θ²⟩^7/2
separation, d (nm)

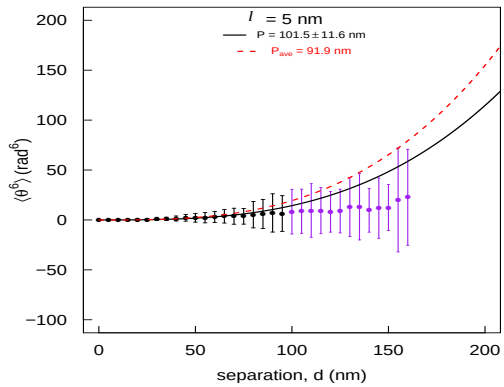
l = 5 nm
P = 101.5±11.6 nm
P_ave = 91.9 nm
⟨θ⁶⟩ (rad⁶)
separation, d (nm)

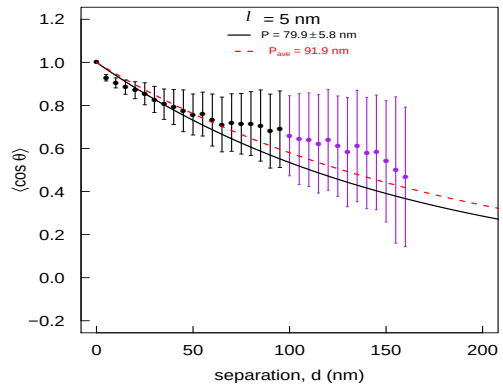
l = 5 nm
P = 79.9±5.8 nm
P_ave = 91.9 nm
⟨cos θ⟩
separation, d (nm)

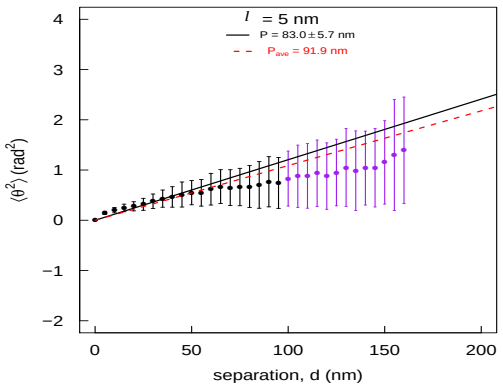
l = 5 nm
P = 83.0±5.7 nm
P_ave = 91.9 nm
⟨θ²⟩ (rad²)
separation, d (nm)

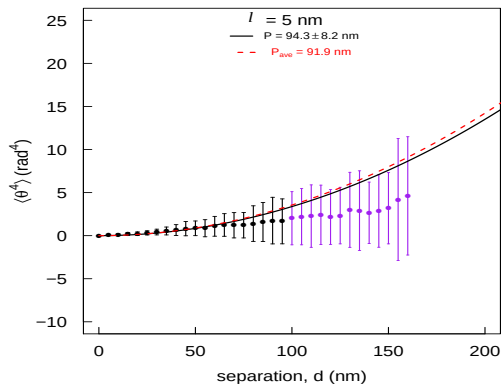
l = 5 nm
P = 94.3±8.2 nm
P_ave = 91.9 nm
⟨θ⁴⟩ (rad⁴)
separation, d (nm)

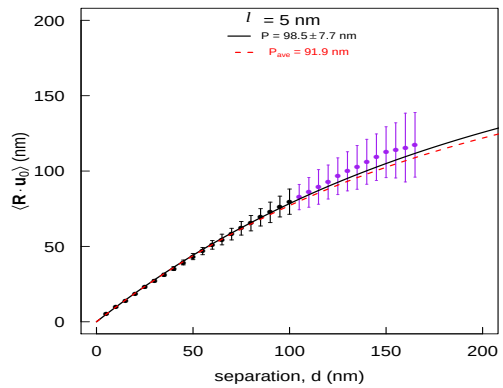
l = 5 nm
P = 98.5±7.7 nm
P_ave = 91.9 nm
⟨R · u₀⟩ (nm)
separation, d (nm)

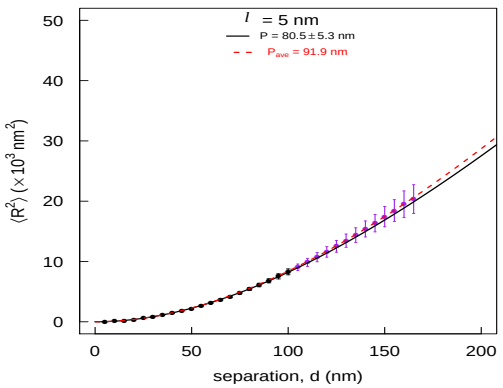
l = 5 nm
P = 80.5±5.3 nm
P_ave = 91.9 nm
⟨R²⟩ (×10³ nm²)
separation, d (nm)

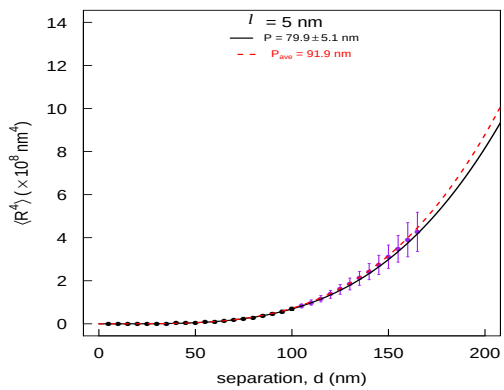
l = 5 nm
P = 79.9±5.1 nm
P_ave = 91.9 nm
⟨R⁴⟩ (×10⁸ nm⁴)
separation, d (nm)

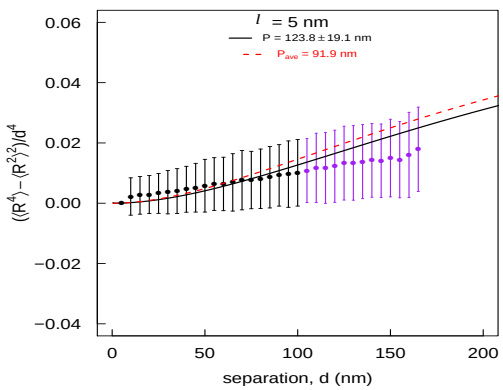
l = 5 nm
P = 123.8±19.1 nm
P_ave = 91.9 nm
⟨(R⁴) − ⟨R²⟩²⟩/d⁴
separation, d (nm)

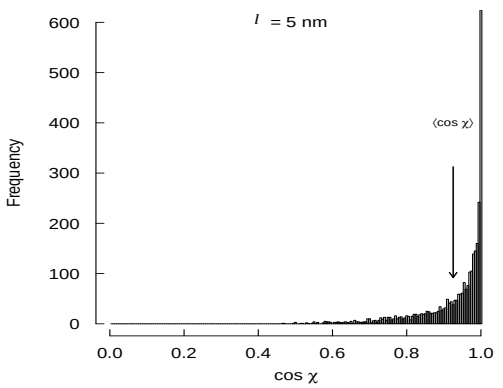
l = 5 nm
⟨cos χ⟩
Frequency
cos χ

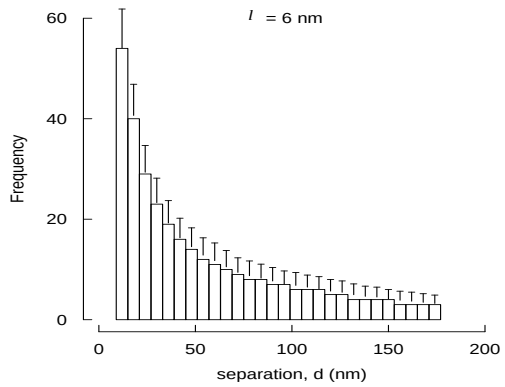
l = 6 nm
Frequency
separation, d (nm)

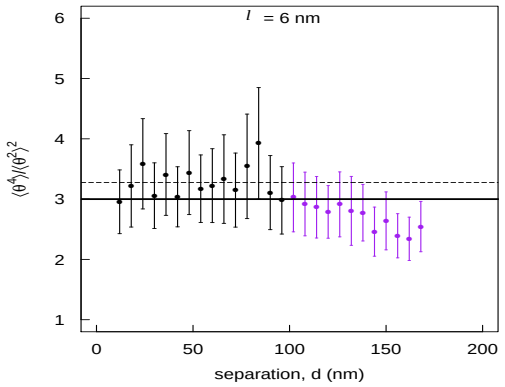
l = 6 nm
⟨θ⁴⟩/⟨θ²⟩²
separation, d (nm)

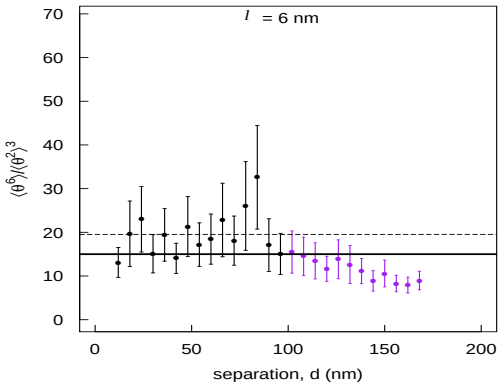
l = 6 nm
⟨θ⁶⟩/⟨θ²⟩³
separation, d (nm)

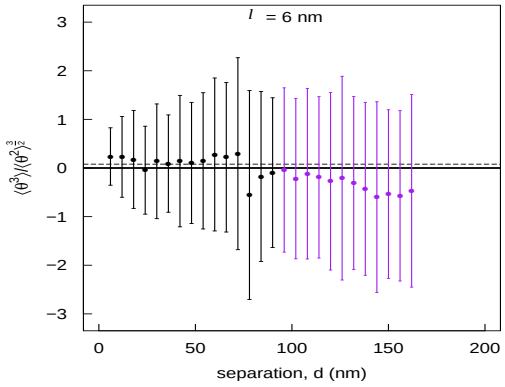
l = 6 nm
⟨θ³⟩/⟨θ²⟩^3/2
separation, d (nm)

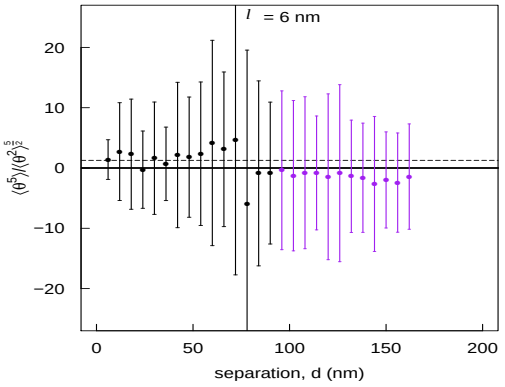
l = 6 nm
⟨θ⁵⟩/⟨θ²⟩^5/2
separation, d (nm)

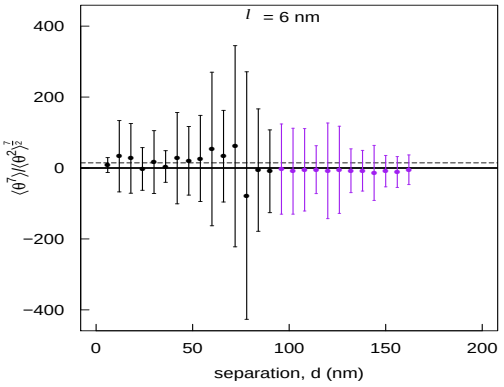
l = 6 nm
⟨θ⁷⟩/⟨θ²⟩^7/2
separation, d (nm)

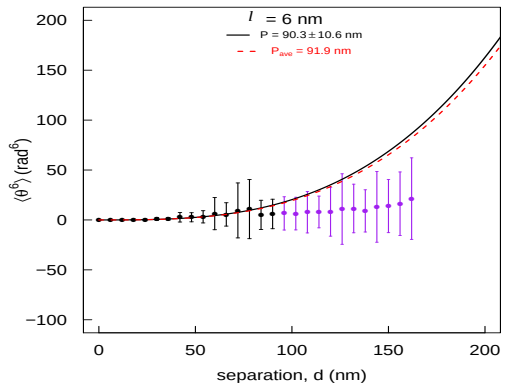
l = 6 nm
P = 90.3±10.6 nm
P_ave = 91.9 nm
⟨θ⁶⟩ (rad⁶)
separation, d (nm)

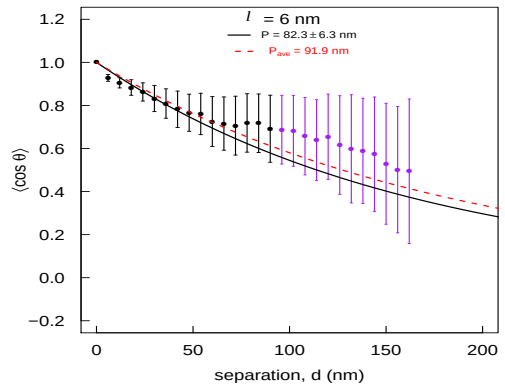
l = 6 nm
P = 82.3±6.3 nm
P_ave = 91.9 nm
⟨cos θ⟩
separation, d (nm)

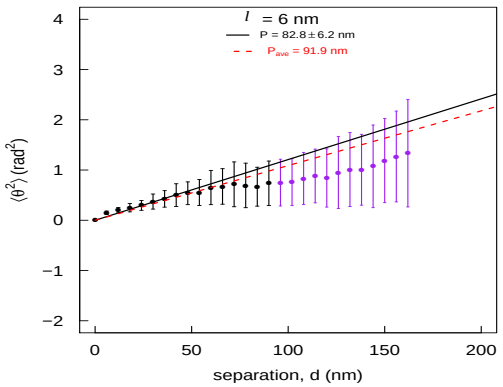
l = 6 nm
P = 82.8±6.2 nm
P_ave = 91.9 nm
⟨θ²⟩ (rad²)
separation, d (nm)

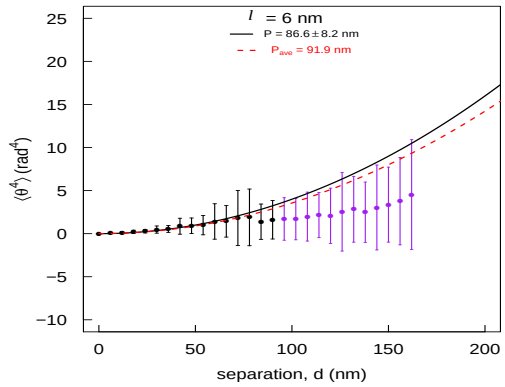
l = 6 nm
P = 86.6±8.2 nm
P_ave = 91.9 nm
⟨θ⁴⟩ (rad⁴)
separation, d (nm)

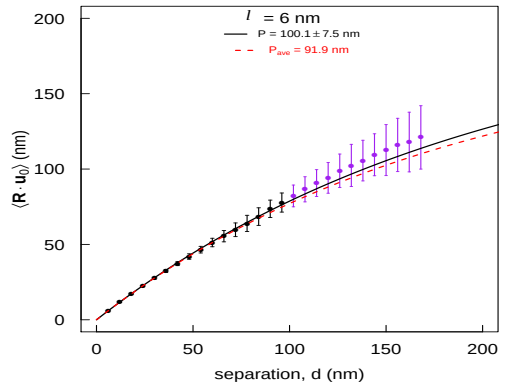
l = 6 nm
P = 100.1±7.5 nm
P_ave = 91.9 nm
⟨R · u₀⟩ (nm)
separation, d (nm)

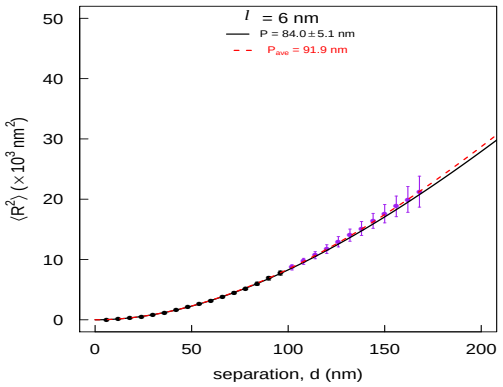
l = 6 nm
P = 84.0±5.1 nm
P_ave = 91.9 nm
⟨R²⟩ (×10³ nm²)
separation, d (nm)

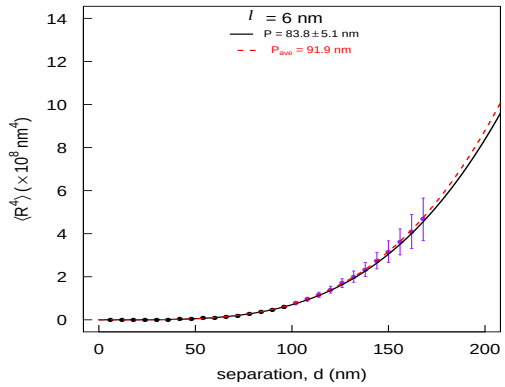
l = 6 nm
P = 83.8±5.1 nm
P_ave = 91.9 nm
⟨R⁴⟩ (×10⁸ nm⁴)
separation, d (nm)

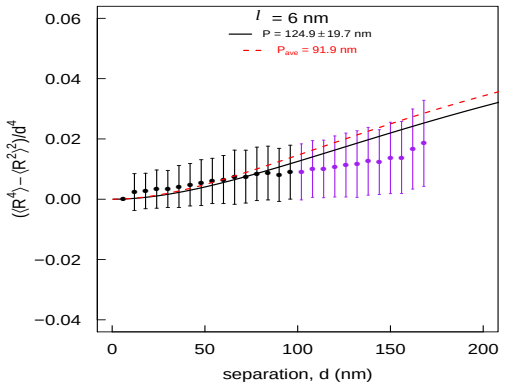
l = 6 nm
P = 124.9±19.7 nm
P_ave = 91.9 nm
⟨⟨R⁴⟩ − ⟨R²⟩²⟩/d⁴
separation, d (nm)

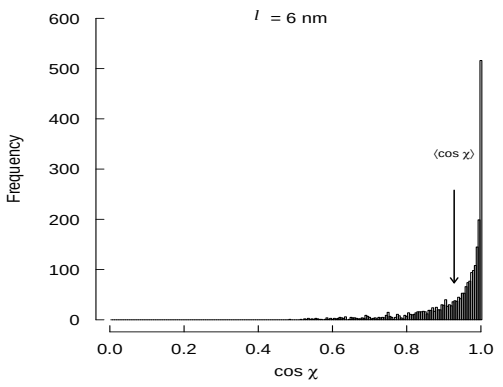
l = 6 nm
⟨cos χ⟩
Frequency
cos χ

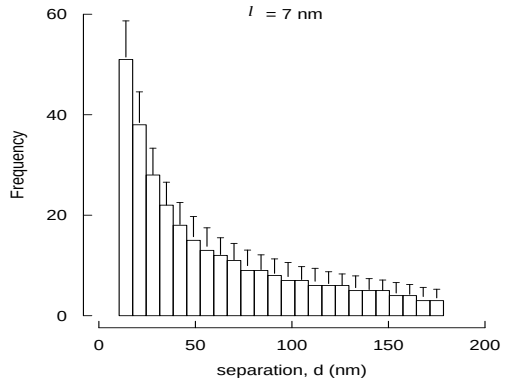
l = 7 nm
Frequency
separation, d (nm)

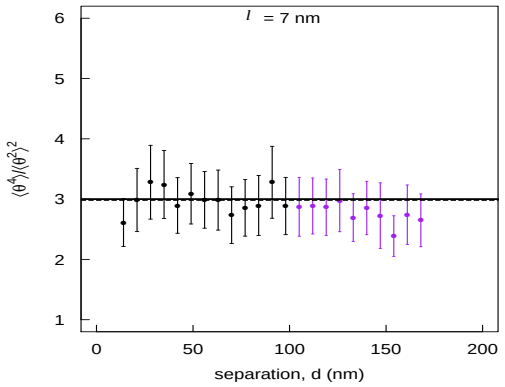
l = 7 nm
⟨θ⁴⟩/⟨θ²⟩²
separation, d (nm)

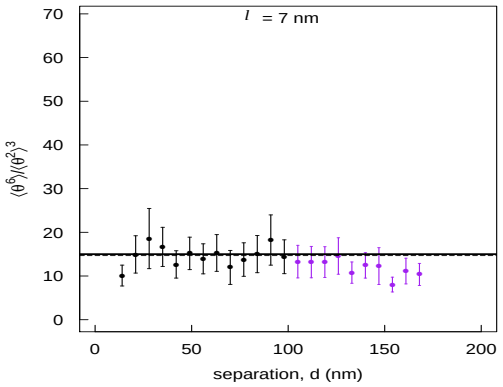
l = 7 nm
⟨θ⁶⟩/⟨θ²⟩³
separation, d (nm)

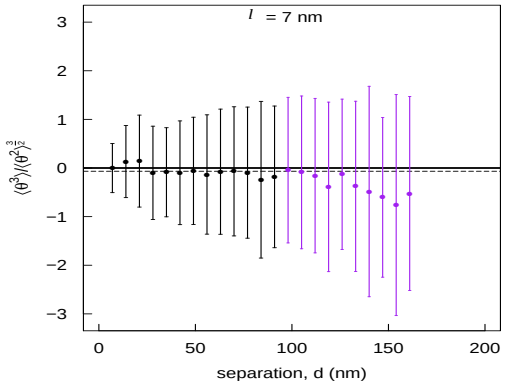
l = 7 nm
⟨θ³⟩/⟨θ²⟩^3/2
separation, d (nm)

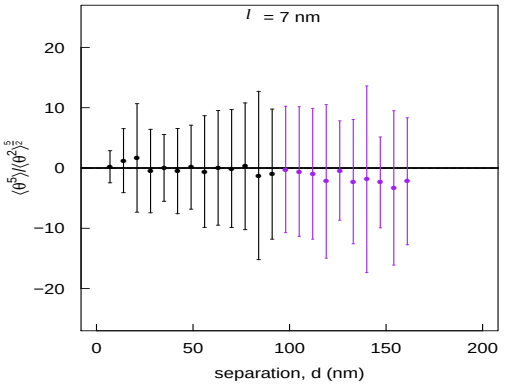
l = 7 nm
⟨θ⁵⟩/⟨θ²⟩^5/2
separation, d (nm)

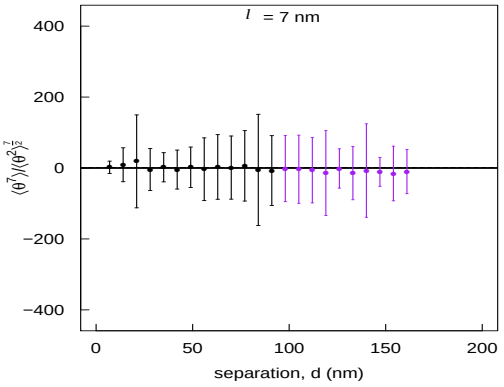
l = 7 nm
⟨θ⁷⟩/⟨θ²⟩^7/2
separation, d (nm)

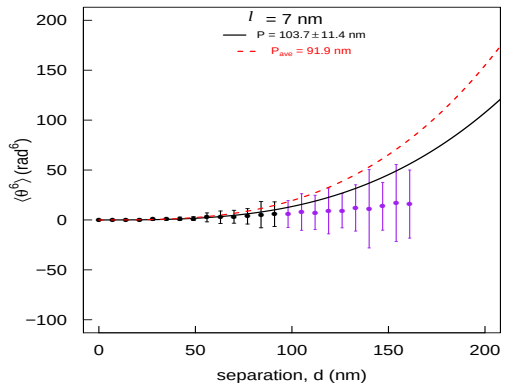
l = 7 nm
P = 103.7±11.4 nm
P_ave = 91.9 nm
⟨θ⁶⟩ (rad⁶)
separation, d (nm)

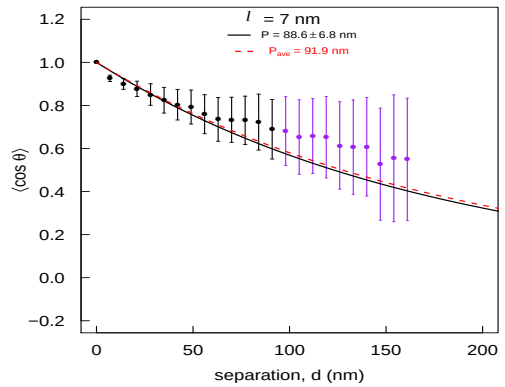
l = 7 nm
P = 88.6±6.8 nm
P_ave = 91.9 nm
⟨cos θ⟩
separation, d (nm)

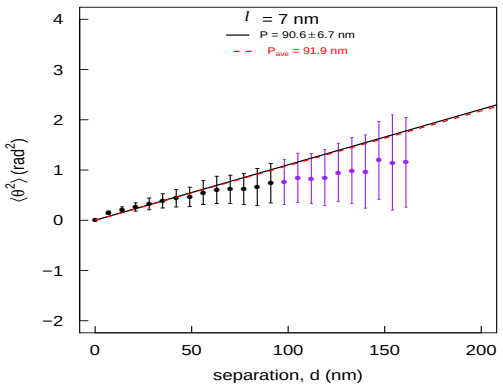
l = 7 nm
P = 90.6±6.7 nm
P_ave = 91.9 nm
⟨θ²⟩ (rad²)
separation, d (nm)

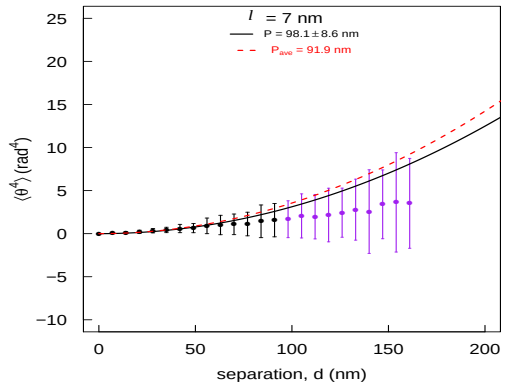
l = 7 nm
P = 98.1±8.6 nm
P_ave = 91.9 nm
⟨θ⁴⟩ (rad⁴)
separation, d (nm)

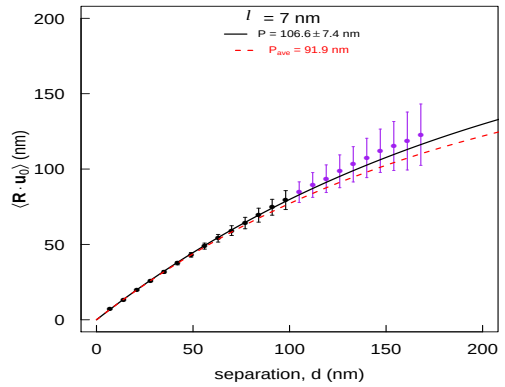
l = 7 nm
P = 106.6±7.4 nm
P_ave = 91.9 nm
⟨R · u₀⟩ (nm)
separation, d (nm)

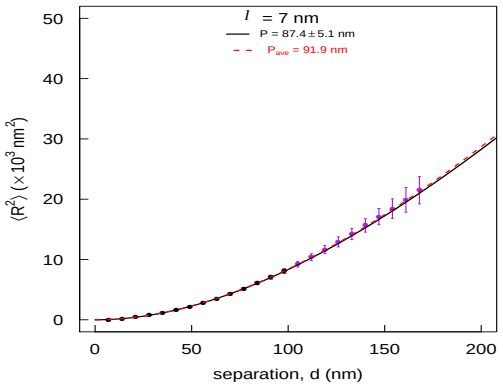
l = 7 nm
P = 87.4±5.1 nm
P_ave = 91.9 nm
⟨R²⟩ (×10³ nm²)
separation, d (nm)

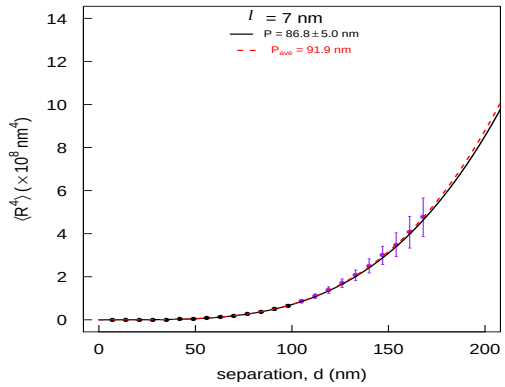
l = 7 nm
P = 86.8±5.0 nm
P_ave = 91.9 nm
⟨R⁴⟩ (×10⁸ nm⁴)
separation, d (nm)

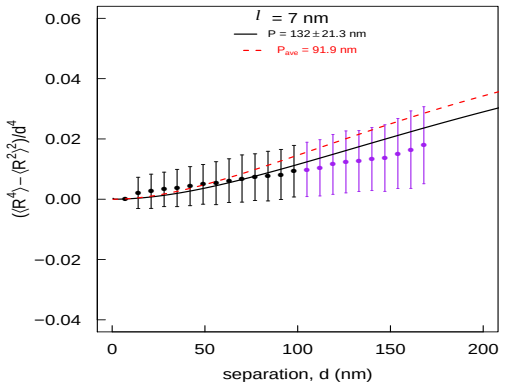
l = 7 nm
P = 132±21.3 nm
P_ave = 91.9 nm
(⟨R⁴⟩−⟨R²⟩²)/d⁴
separation, d (nm)

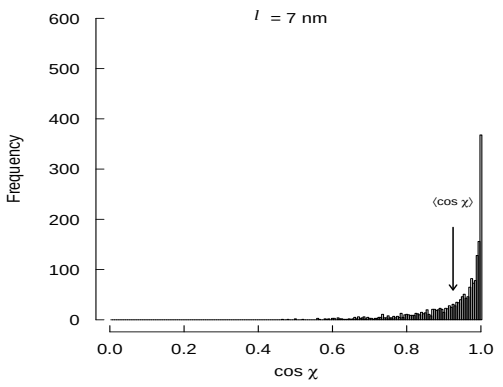
l = 7 nm
Frequency
⟨cos χ⟩
cos χ

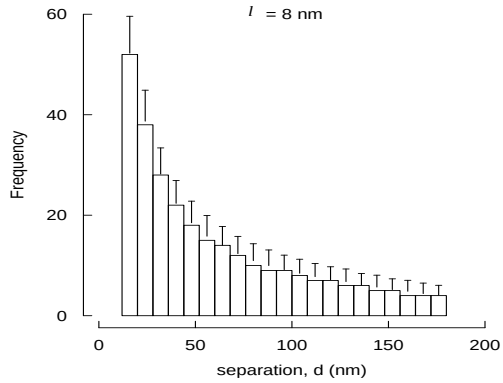
l = 8 nm
Frequency
separation, d (nm)

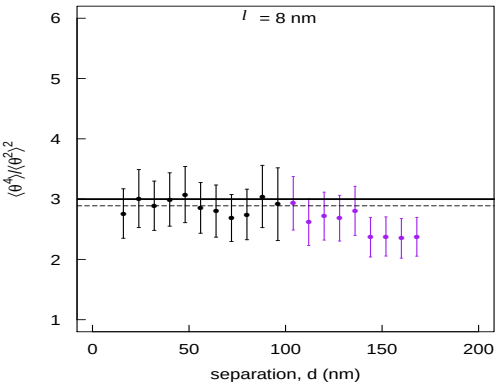
l = 8 nm
⟨θ⁴⟩/⟨θ²⟩²
separation, d (nm)

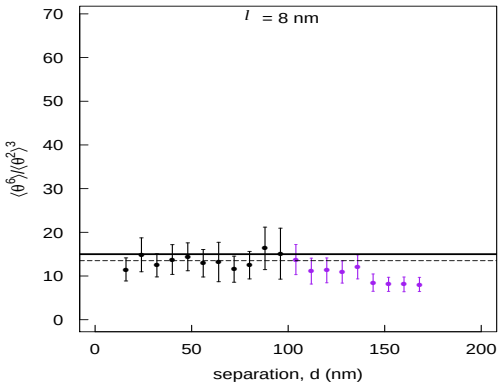
l = 8 nm
⟨θ⁶⟩/⟨θ²⟩³
separation, d (nm)

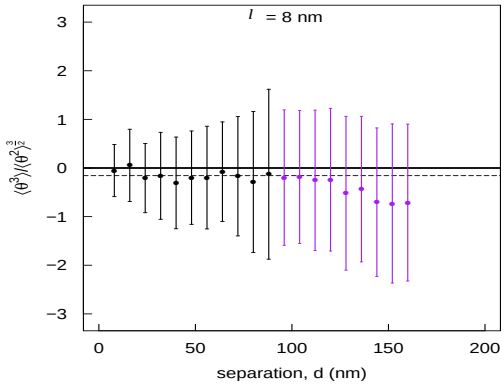
l = 8 nm
⟨θ³⟩/⟨θ²⟩^3/2
separation, d (nm)

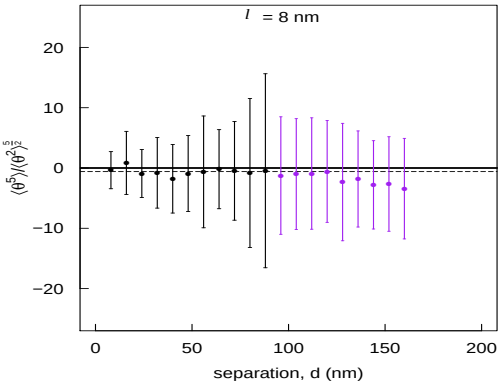
l = 8 nm
⟨θ⁵⟩/⟨θ²⟩^5/2
separation, d (nm)

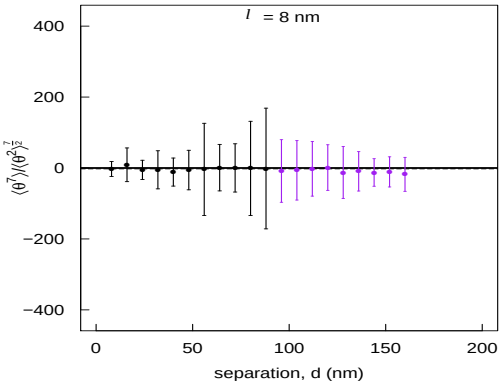
l = 8 nm
⟨θ⁷⟩/⟨θ²⟩^7/2
separation, d (nm)

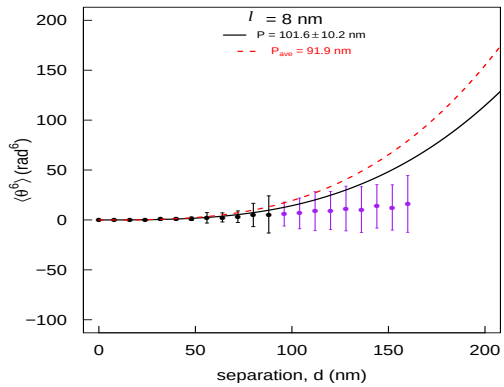
l = 8 nm
P = 101.6 ± 10.2 nm
P_ave = 91.9 nm
⟨θ⁶⟩ (rad⁶)
separation, d (nm)

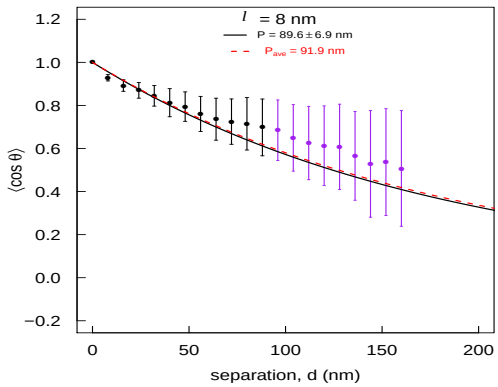
l = 8 nm
P = 89.6 ± 6.9 nm
P_ave = 91.9 nm
⟨cos θ⟩
separation, d (nm)

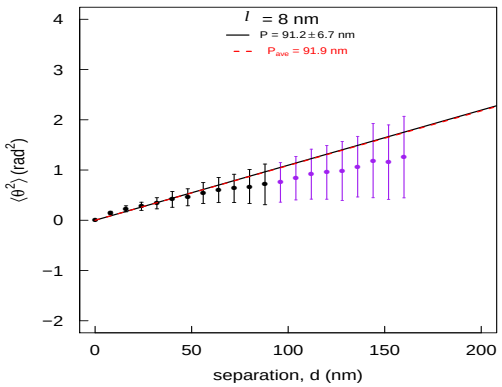
l = 8 nm
P = 91.2 ± 6.7 nm
P_ave = 91.9 nm
⟨θ²⟩ (rad²)
separation, d (nm)

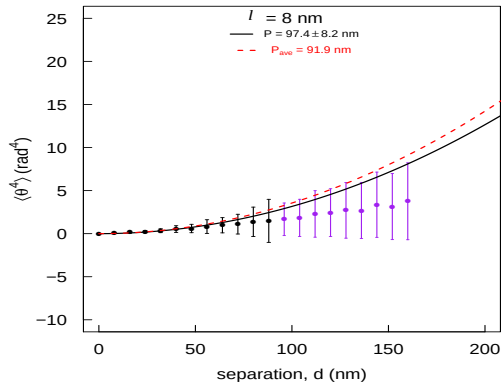
l = 8 nm
P = 97.4 ± 8.2 nm
P_ave = 91.9 nm
⟨θ⁴⟩ (rad⁴)
separation, d (nm)

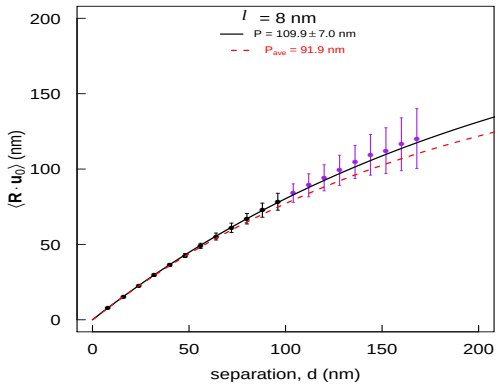
l = 8 nm
P = 109.9 ± 7.0 nm
P_ave = 91.9 nm
⟨R · u₀⟩ (nm)
separation, d (nm)

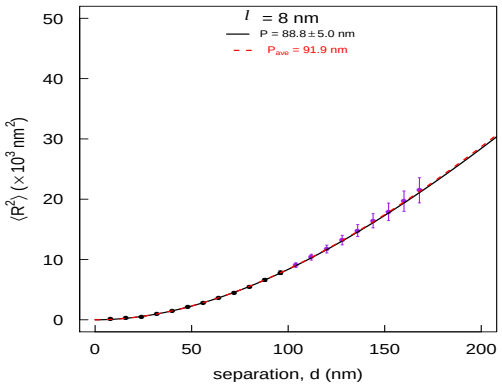
l = 8 nm
P = 88.8 ± 5.0 nm
P_ave = 91.9 nm
⟨R²⟩ (×10³ nm²)
separation, d (nm)

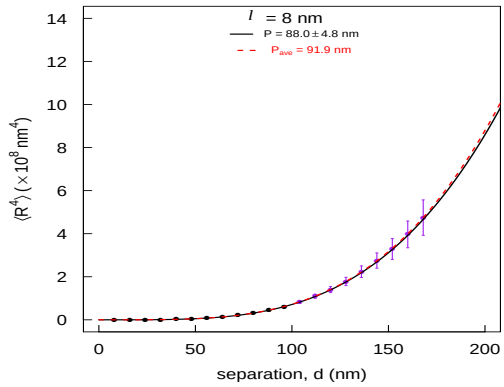
l = 8 nm
P = 88.0 ± 4.8 nm
P_ave = 91.9 nm
⟨R⁴⟩ (×10⁸ nm⁴)
separation, d (nm)

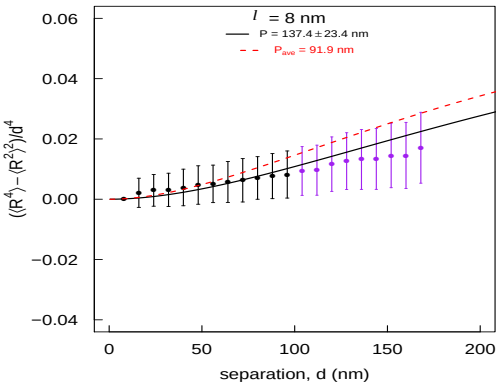
l = 8 nm
P = 137.4 ± 23.4 nm
P_ave = 91.9 nm
⟨⟨R⁴⟩ − ⟨R²⟩²⟩/d⁴
separation, d (nm)

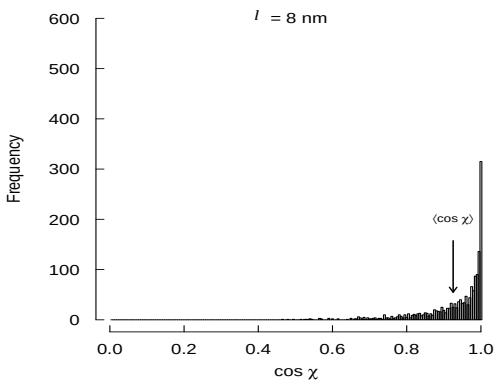
l = 8 nm
Frequency
⟨cos χ⟩
cos χ

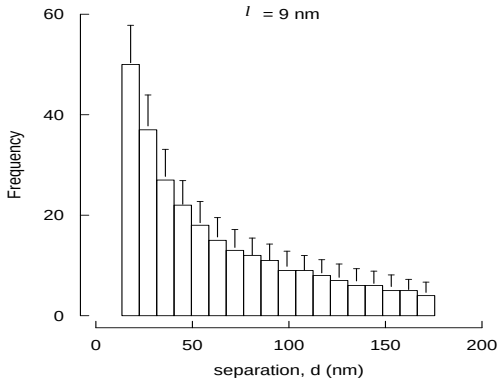
l = 9 nm
Frequency
separation, d (nm)

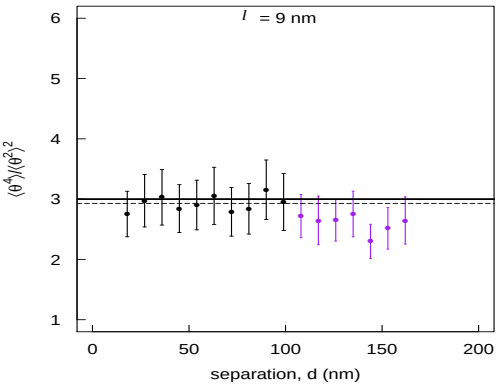
l = 9 nm
⟨θ⁴⟩/⟨θ²⟩²
separation, d (nm)

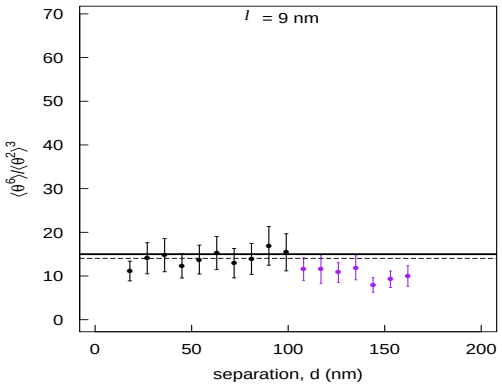
l = 9 nm
⟨θ⁶⟩/⟨θ²⟩³
separation, d (nm)

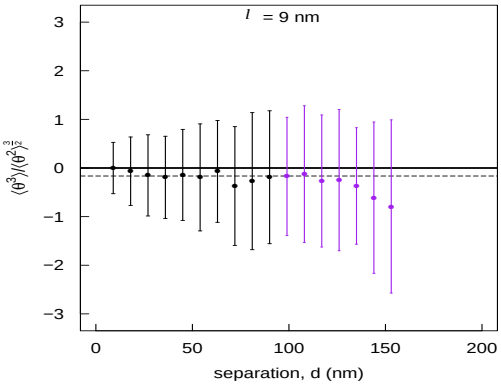
l = 9 nm
⟨θ³⟩/⟨θ²⟩^3/2
separation, d (nm)

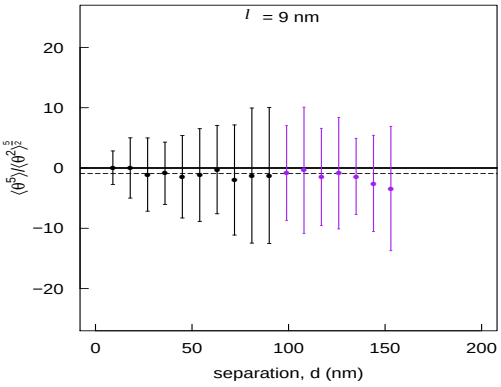
l = 9 nm
⟨θ⁵⟩/⟨θ²⟩^5/2
separation, d (nm)

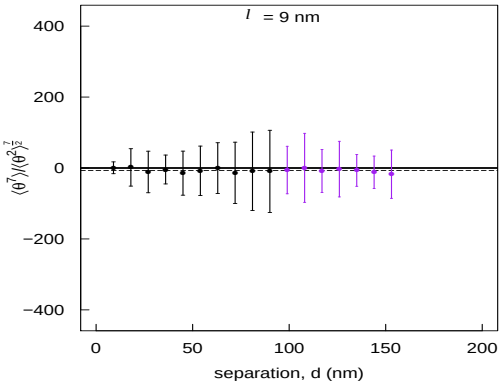
l = 9 nm
⟨θ⁷⟩/⟨θ²⟩^7/2
separation, d (nm)

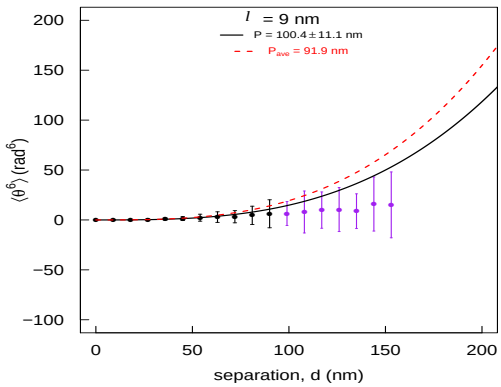
l = 9 nm
P = 100.4±11.1 nm
P_ave = 91.9 nm
⟨θ⁶⟩ (rad⁶)
separation, d (nm)

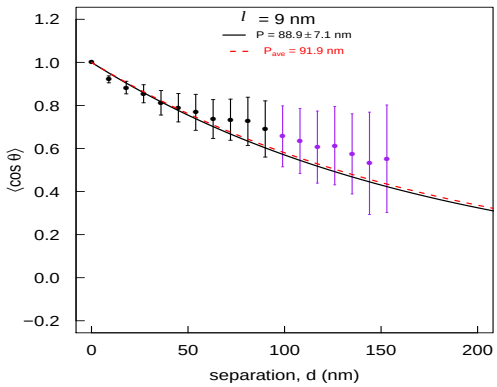
l = 9 nm
P = 88.9±7.1 nm
P_ave = 91.9 nm
⟨cos θ⟩
separation, d (nm)

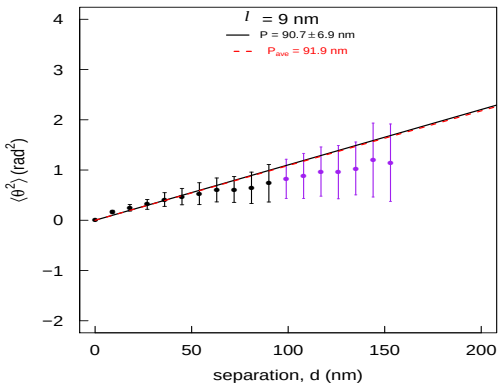
l = 9 nm
P = 90.7±6.9 nm
P_ave = 91.9 nm
⟨θ²⟩ (rad²)
separation, d (nm)

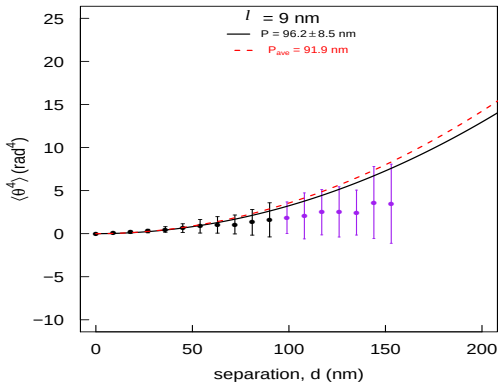
l = 9 nm
P = 96.2±8.5 nm
P_ave = 91.9 nm
⟨θ⁴⟩ (rad⁴)
separation, d (nm)

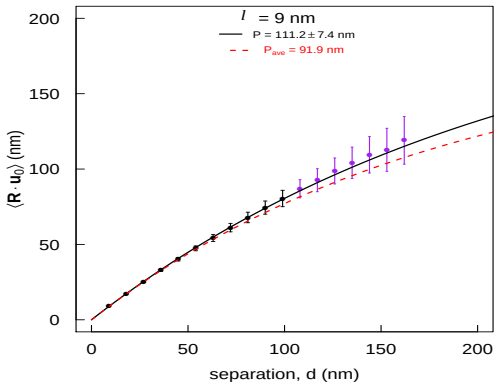
l = 9 nm
P = 111.2±7.4 nm
P_ave = 91.9 nm
⟨R · u₀⟩ (nm)
separation, d (nm)

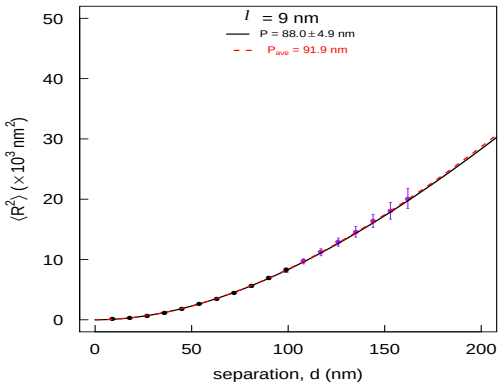
l = 9 nm
P = 88.0±4.9 nm
P_ave = 91.9 nm
⟨R²⟩ (×10³ nm²)
separation, d (nm)

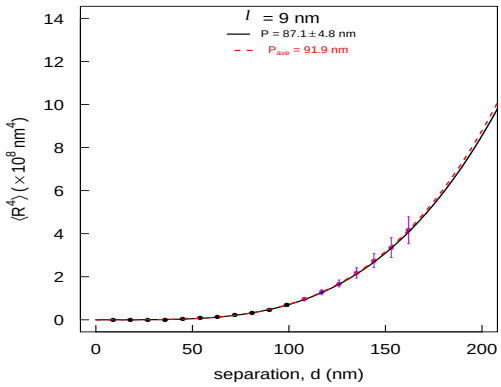
l = 9 nm
P = 87.1±4.8 nm
P_ave = 91.9 nm
⟨R⁴⟩ (×10⁸ nm⁴)
separation, d (nm)

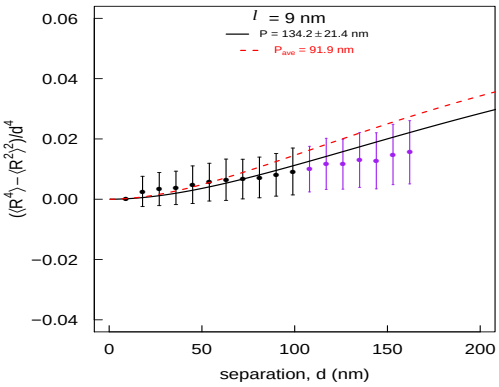
l = 9 nm
P = 134.2±21.4 nm
P_ave = 91.9 nm
⟨R⁴⟩−⟨R²⟩²)/d⁴
separation, d (nm)

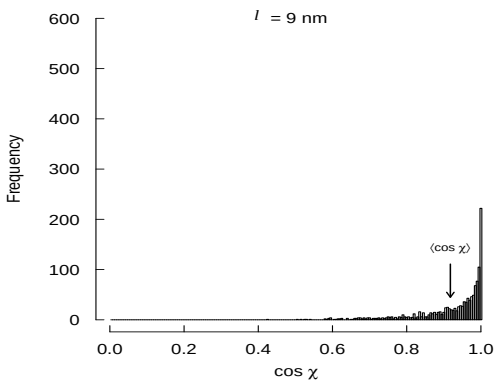
l = 9 nm
Frequency
⟨cos χ⟩
cos χ

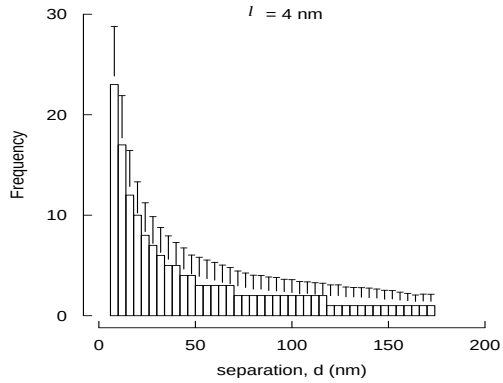
l = 4 nm
Frequency
separation, d (nm)

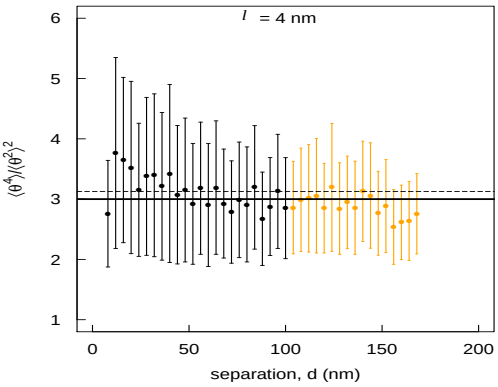
l = 4 nm
⟨θ⁴⟩/⟨θ²⟩²
separation, d (nm)

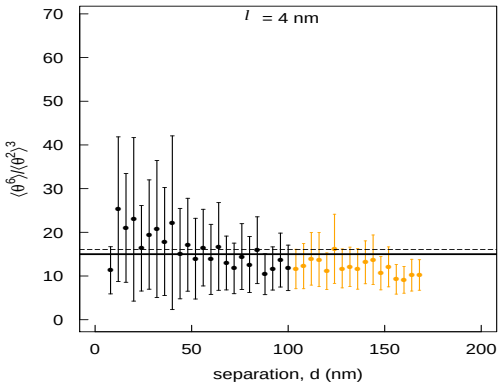
l = 4 nm
⟨θ⁶⟩/⟨θ²⟩³
separation, d (nm)

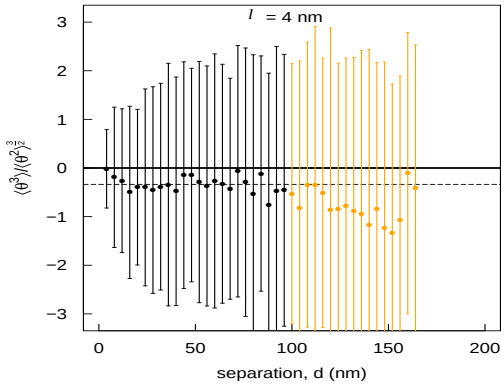
l = 4 nm
⟨θ³⟩/⟨θ²⟩^3/2
separation, d (nm)

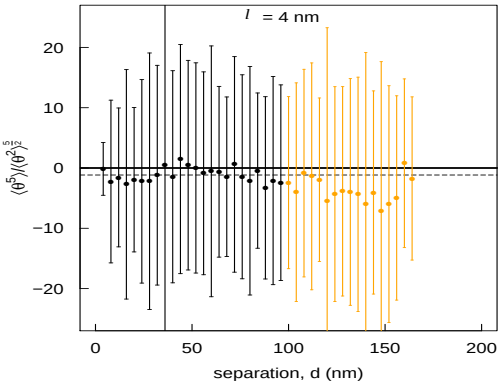
l = 4 nm
⟨θ⁵⟩/⟨θ²⟩^5/2
separation, d (nm)

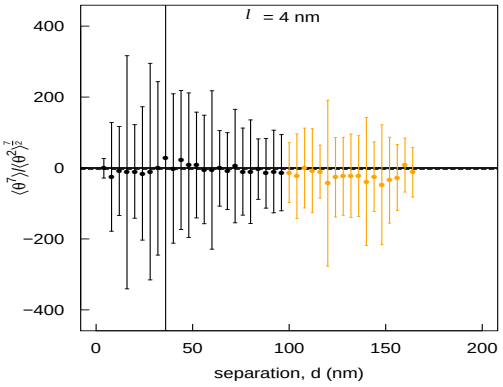
l = 4 nm
⟨θ⁷⟩/⟨θ²⟩^7/2
separation, d (nm)

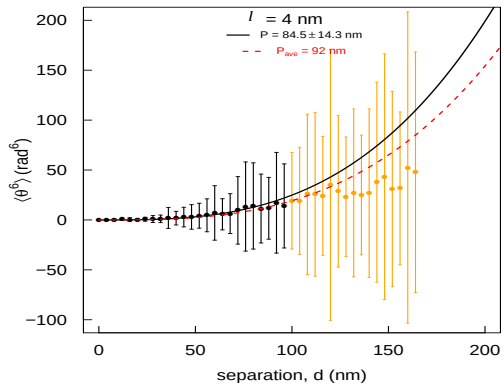
l = 4 nm
P = 84.5±14.3 nm
P_ave = 92 nm
⟨θ⁶⟩ (rad⁶)
separation, d (nm)

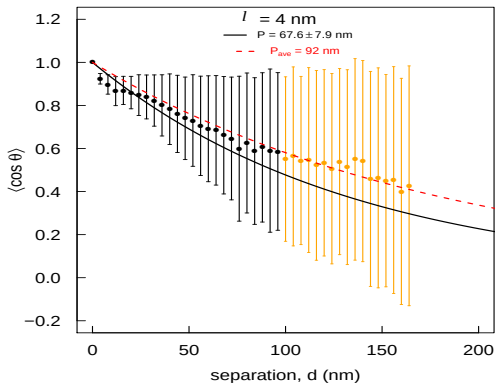
l = 4 nm
P = 67.6±7.9 nm
P_ave = 92 nm
⟨cos θ⟩
separation, d (nm)

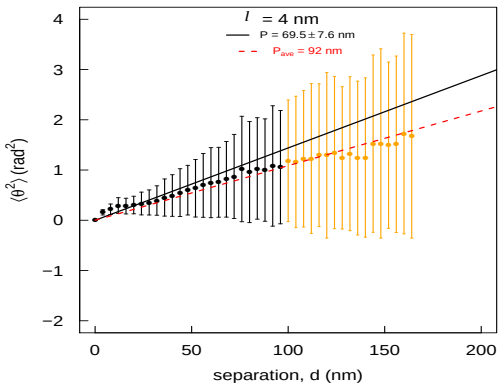
l = 4 nm
P = 69.5±7.6 nm
P_ave = 92 nm
⟨θ²⟩ (rad²)
separation, d (nm)

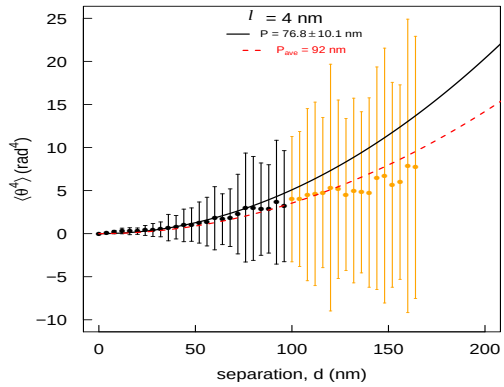
l = 4 nm
P = 76.8±10.1 nm
P_ave = 92 nm
⟨θ⁴⟩ (rad⁴)
separation, d (nm)

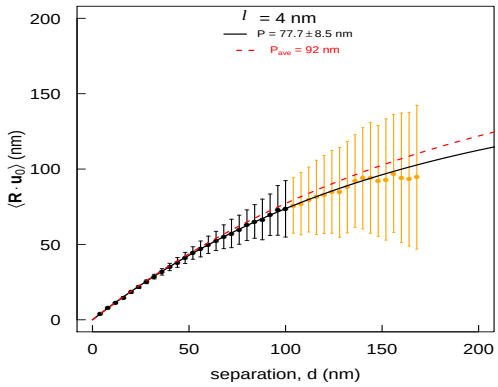
l = 4 nm
P = 77.7±8.5 nm
P_ave = 92 nm
⟨R · u₀⟩ (nm)
separation, d (nm)

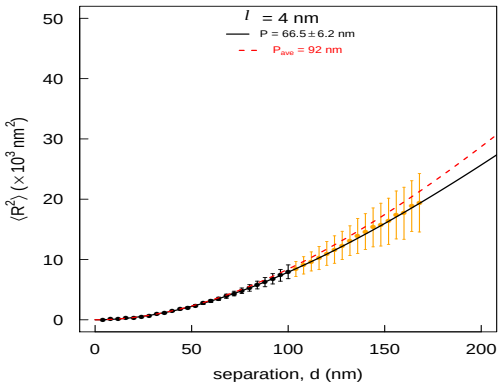
l = 4 nm
P = 66.5±6.2 nm
P_ave = 92 nm
⟨R²⟩ (×10³ nm²)
separation, d (nm)

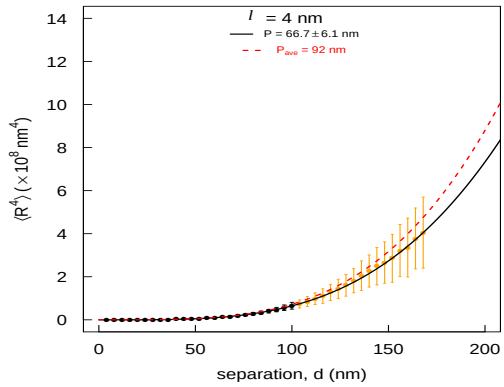
l = 4 nm
P = 66.7±6.1 nm
P_ave = 92 nm
⟨R⁴⟩ (×10⁸ nm⁴)
separation, d (nm)

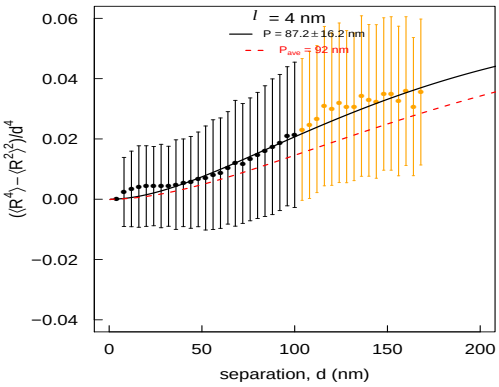
l = 4 nm
P = 87.2±16.2 nm
P_ave = 92 nm
(⟨R⁴⟩−⟨R²⟩²)/d⁴
separation, d (nm)

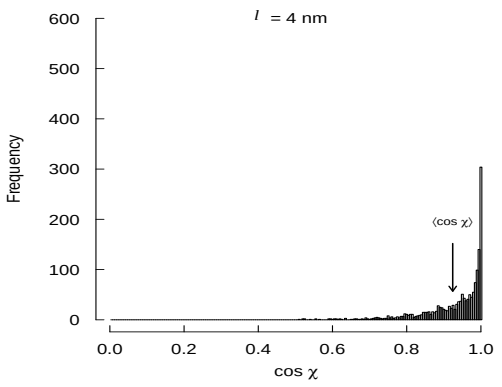
l = 4 nm
Frequency
⟨cos χ⟩
cos χ

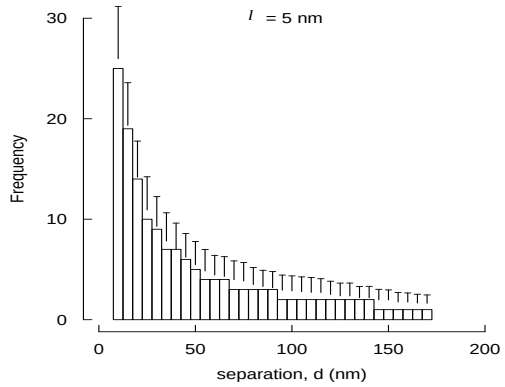
l = 5 nm
Frequency
separation, d (nm)

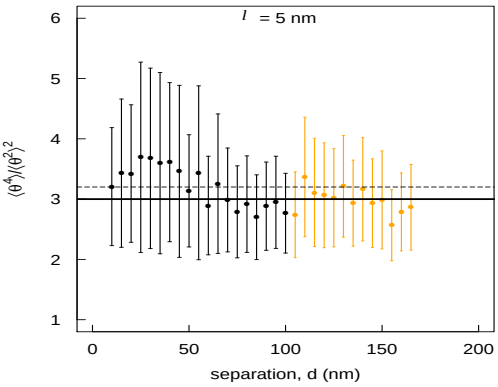
l = 5 nm
⟨θ⁴⟩/⟨θ²⟩²
separation, d (nm)

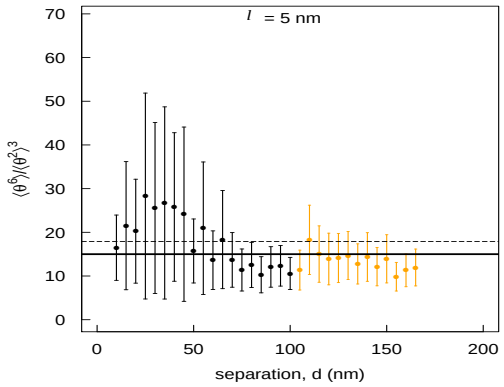
l = 5 nm
⟨θ⁶⟩/⟨θ²⟩³
separation, d (nm)

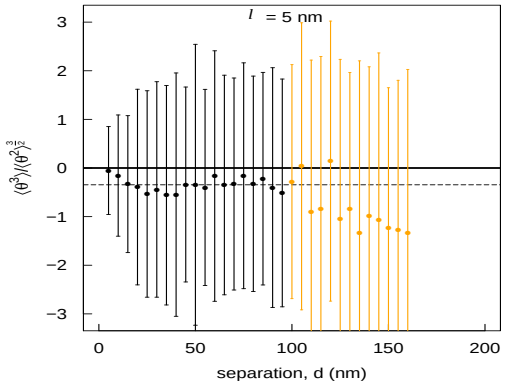
l = 5 nm
⟨θ³⟩/⟨θ²⟩^3/2
separation, d (nm)

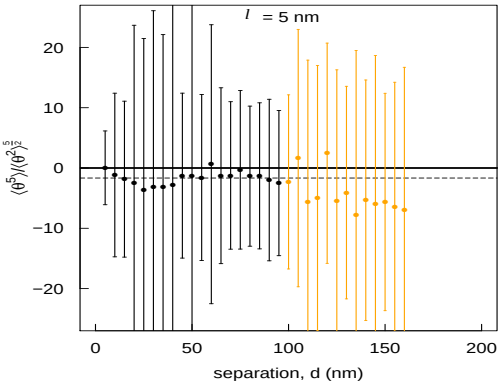
l = 5 nm
⟨θ⁵⟩/⟨θ²⟩^5/2
separation, d (nm)

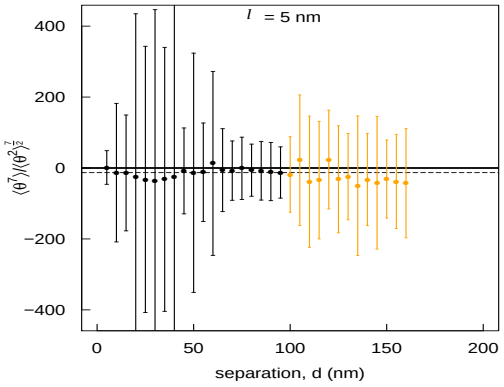
l = 5 nm
⟨θ⁷⟩/⟨θ²⟩^7/2
separation, d (nm)

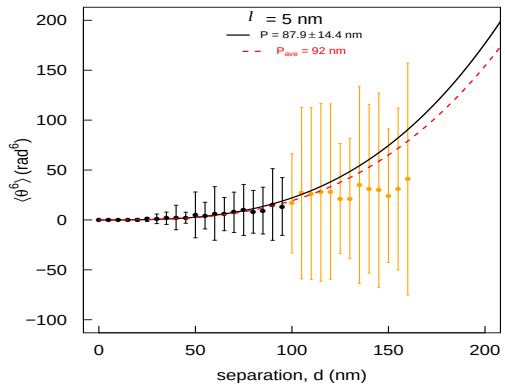
l = 5 nm
P = 87.9 ± 14.4 nm
P_ave = 92 nm
⟨θ⁶⟩ (rad⁶)
separation, d (nm)

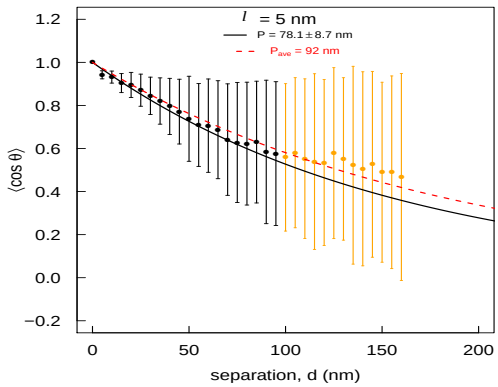
l = 5 nm
P = 78.1 ± 8.7 nm
P_ave = 92 nm
⟨cos θ⟩
separation, d (nm)

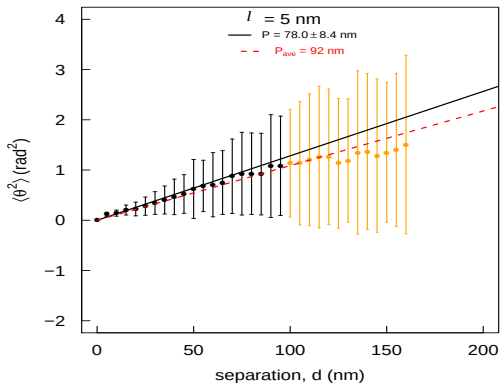
l = 5 nm
P = 78.0 ± 8.4 nm
P_ave = 92 nm
⟨θ²⟩ (rad²)
separation, d (nm)

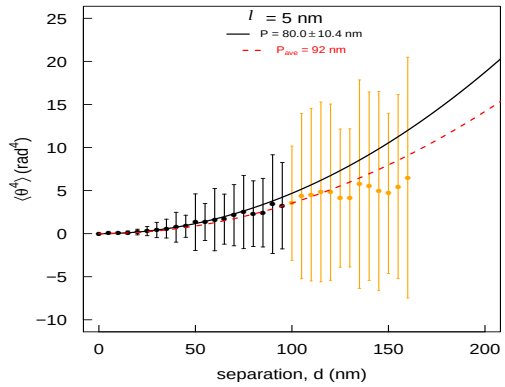
l = 5 nm
P = 80.0 ± 10.4 nm
P_ave = 92 nm
⟨θ⁴⟩ (rad⁴)
separation, d (nm)

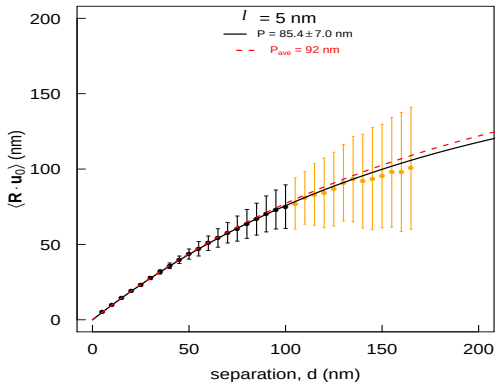
l = 5 nm
P = 85.4 ± 7.0 nm
P_ave = 92 nm
⟨R · u₀⟩ (nm)
separation, d (nm)

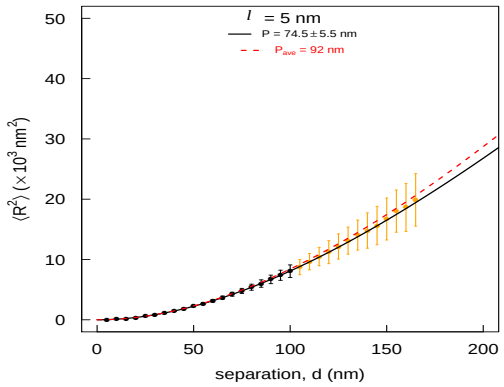
l = 5 nm
P = 74.5 ± 5.5 nm
P_ave = 92 nm
⟨R²⟩ (×10³ nm²)
separation, d (nm)

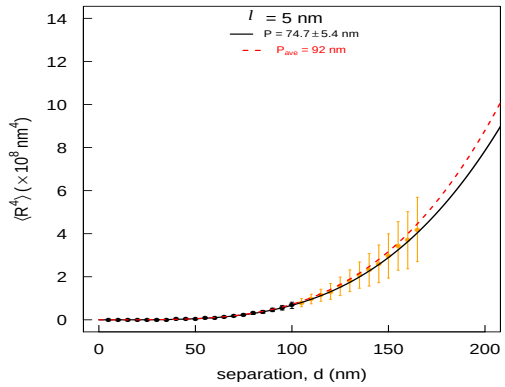
l = 5 nm
P = 74.7 ± 5.4 nm
P_ave = 92 nm
⟨R⁴⟩ (×10⁸ nm⁴)
separation, d (nm)

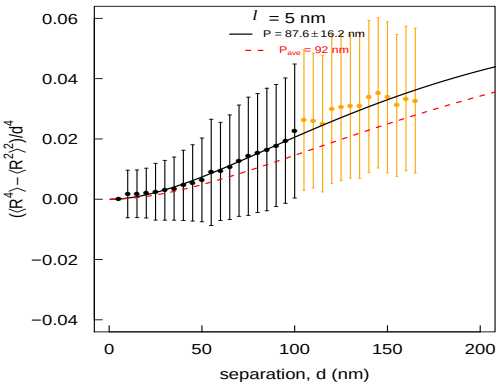
l = 5 nm
P = 87.6 ± 16.2 nm
P_ave = 92 nm
(⟨R⁴⟩ − ⟨R²⟩²)/d⁴
separation, d (nm)

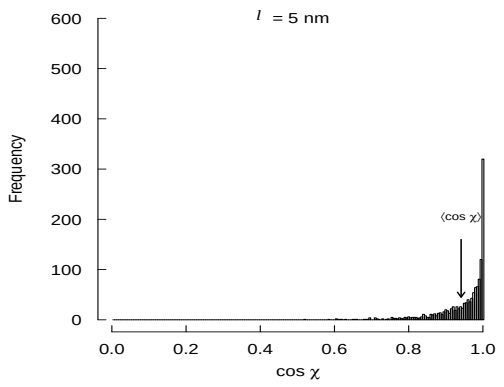
l = 5 nm
Frequency
⟨cos χ⟩
cos χ

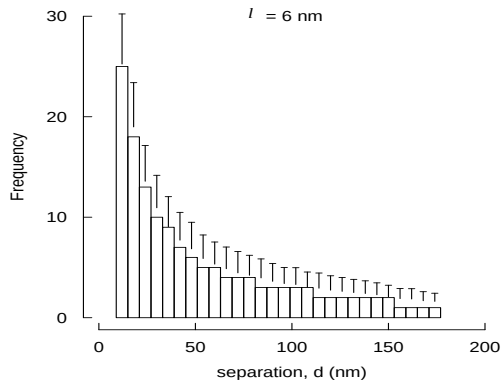
l = 6 nm
Frequency
separation, d (nm)

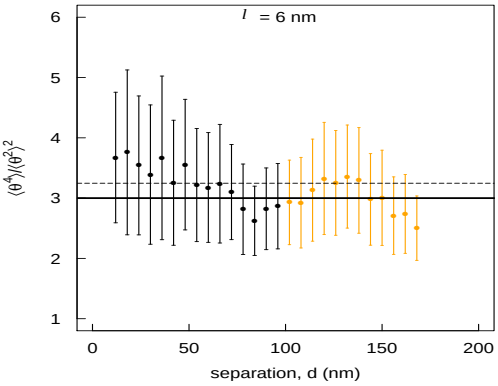
l = 6 nm
⟨θ⁴⟩/⟨θ²⟩²
separation, d (nm)

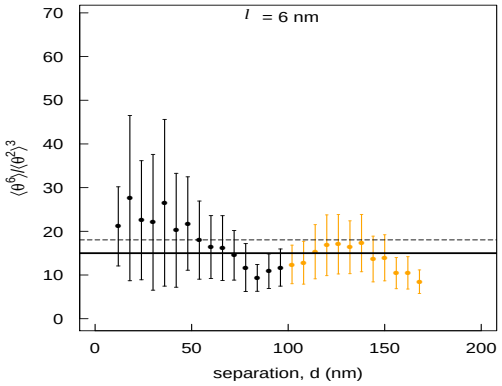
l = 6 nm
⟨θ⁶⟩/⟨θ²⟩³
separation, d (nm)

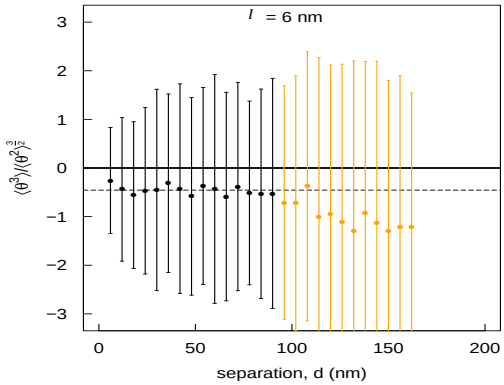
l = 6 nm
⟨θ³⟩/⟨θ²⟩^3/2
separation, d (nm)

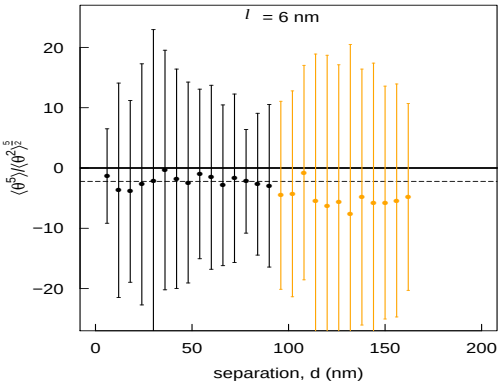
l = 6 nm
⟨θ⁵⟩/⟨θ²⟩^5/2
separation, d (nm)

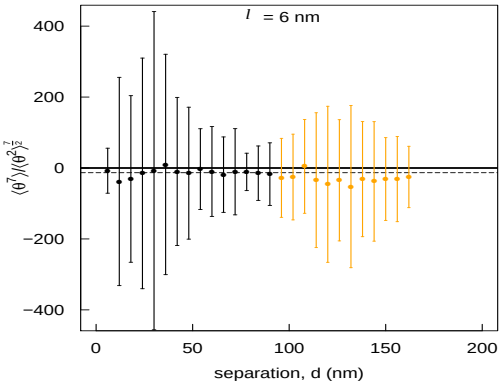
l = 6 nm
⟨θ⁷⟩/⟨θ²⟩^7/2
separation, d (nm)

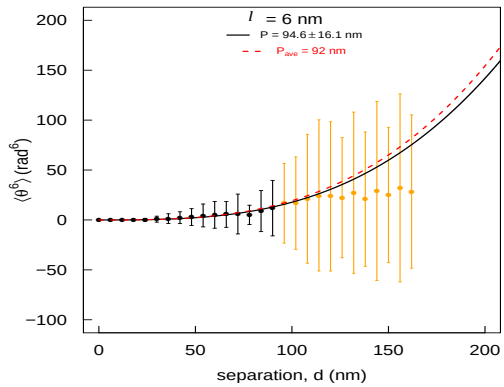
l = 6 nm
P = 94.6 ± 16.1 nm
P_ave = 92 nm
⟨θ⁶⟩ (rad⁶)
separation, d (nm)

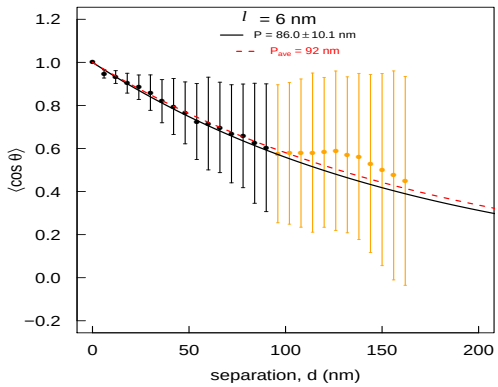
l = 6 nm
P = 86.0 ± 10.1 nm
P_ave = 92 nm
⟨cos θ⟩
separation, d (nm)

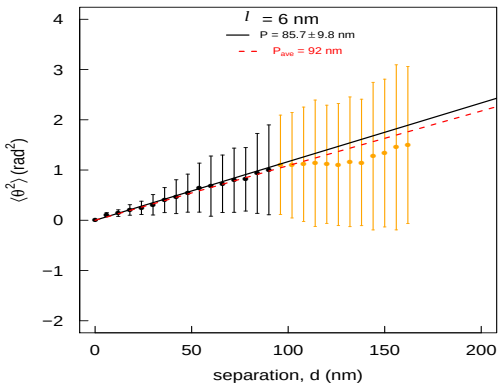
l = 6 nm
P = 85.7 ± 9.8 nm
P_ave = 92 nm
⟨θ²⟩ (rad²)
separation, d (nm)

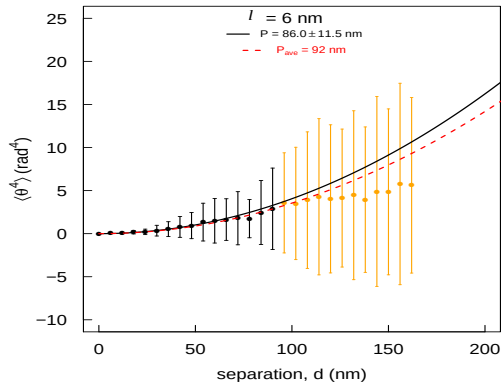
l = 6 nm
P = 86.0 ± 11.5 nm
P_ave = 92 nm
⟨θ⁴⟩ (rad⁴)
separation, d (nm)

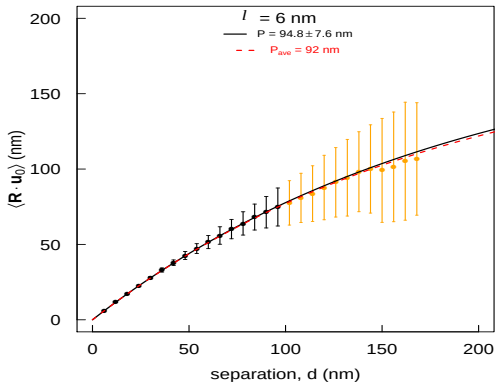
l = 6 nm
P = 94.8 ± 7.6 nm
P_ave = 92 nm
⟨R · u₀⟩ (nm)
separation, d (nm)

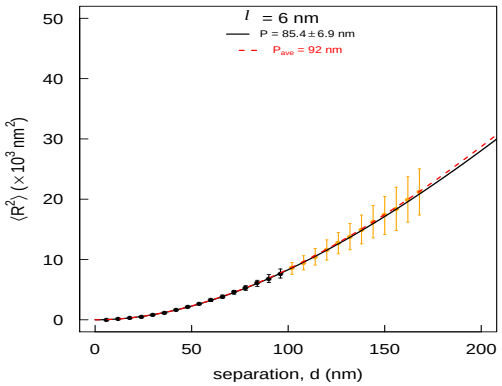
l = 6 nm
P = 85.4 ± 6.9 nm
P_ave = 92 nm
⟨R²⟩ (×10³ nm²)
separation, d (nm)

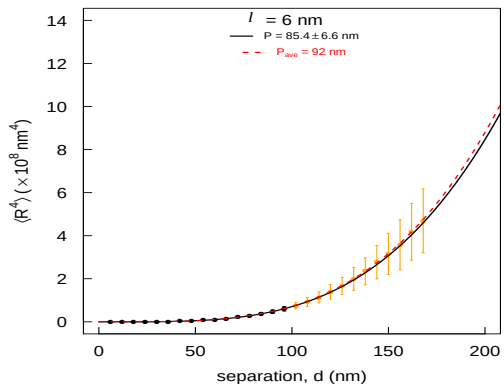
l = 6 nm
P = 85.4 ± 6.6 nm
P_ave = 92 nm
⟨R⁴⟩ (×10⁸ nm⁴)
separation, d (nm)

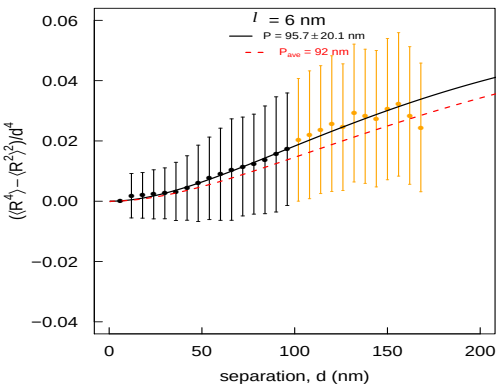
l = 6 nm
P = 95.7 ± 20.1 nm
P_ave = 92 nm
(⟨R⁴⟩ − ⟨R²⟩²)/d⁴
separation, d (nm)

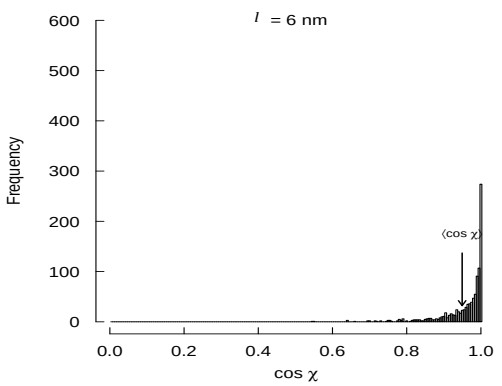
l = 6 nm
Frequency
⟨cos χ⟩
cos χ

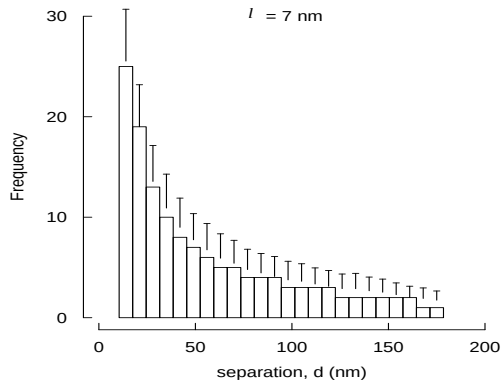
l = 7 nm
Frequency
separation, d (nm)

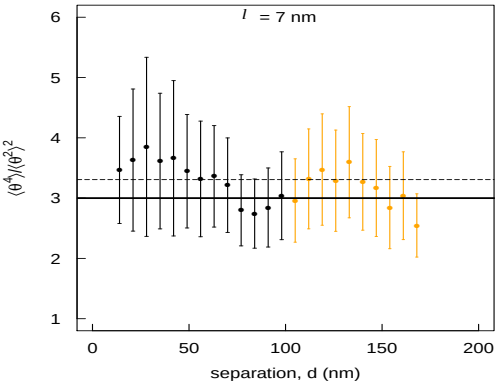
l = 7 nm
⟨θ⁴⟩/⟨θ²⟩²
separation, d (nm)

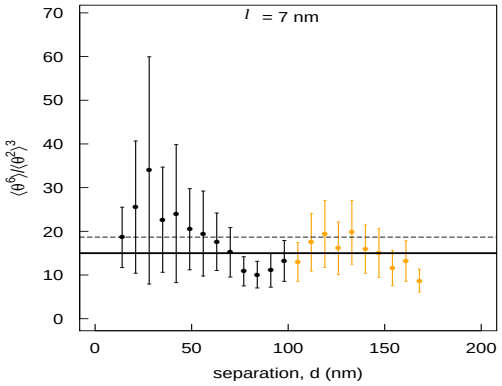
l = 7 nm
⟨θ⁶⟩/⟨θ²⟩³
separation, d (nm)

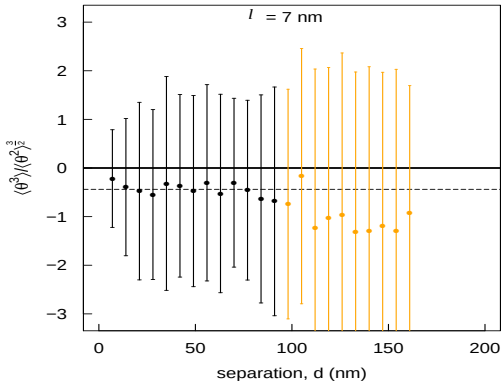
l = 7 nm
⟨θ³⟩/⟨θ²⟩^3/2
separation, d (nm)

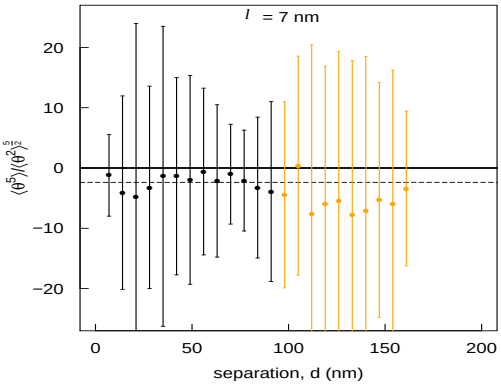
l = 7 nm
⟨θ⁵⟩/⟨θ²⟩^5/2
separation, d (nm)

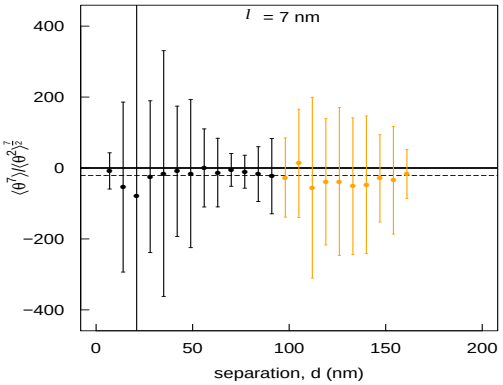
l = 7 nm
⟨θ⁷⟩/⟨θ²⟩^7/2
separation, d (nm)

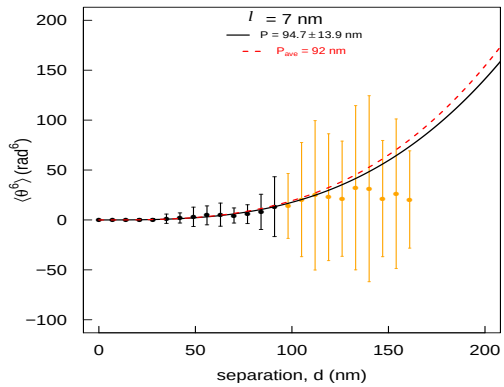
l = 7 nm
P = 94.7±13.9 nm
P_ave = 92 nm
⟨θ⁶⟩ (rad⁶)
separation, d (nm)

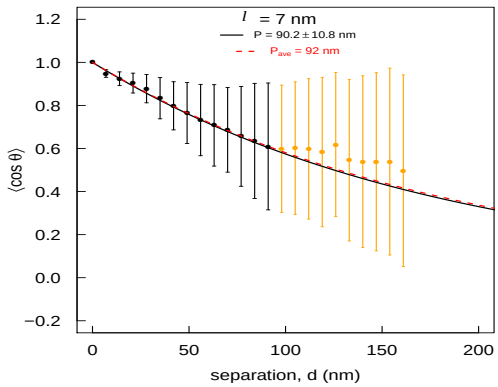
l = 7 nm
P = 90.2±10.8 nm
P_ave = 92 nm
⟨cos θ⟩
separation, d (nm)

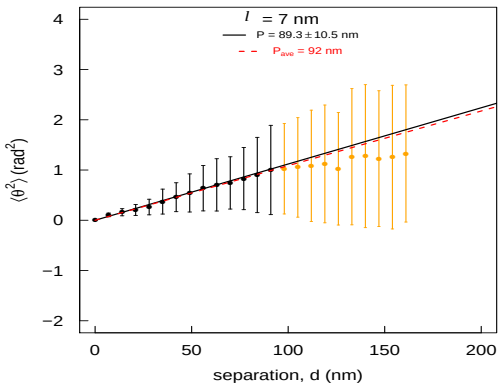
l = 7 nm
P = 89.3±10.5 nm
P_ave = 92 nm
⟨θ²⟩ (rad²)
separation, d (nm)

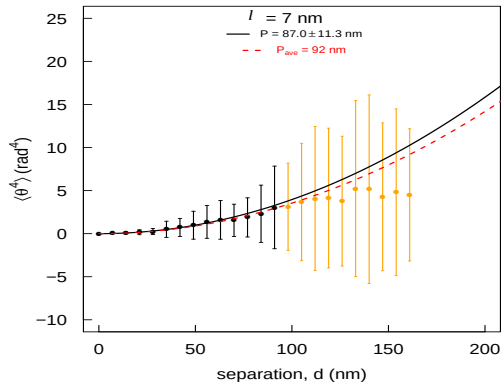
l = 7 nm
P = 87.0±11.3 nm
P_ave = 92 nm
⟨θ⁴⟩ (rad⁴)
separation, d (nm)

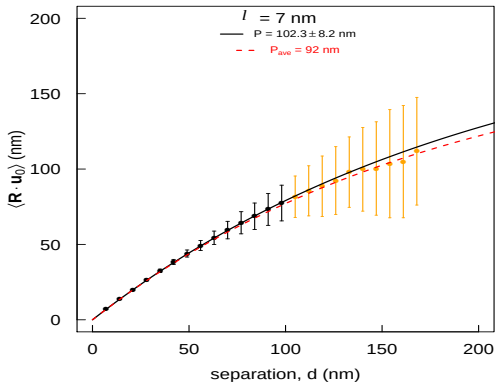
l = 7 nm
P = 102.3±8.2 nm
P_ave = 92 nm
⟨R · u₀⟩ (nm)
separation, d (nm)

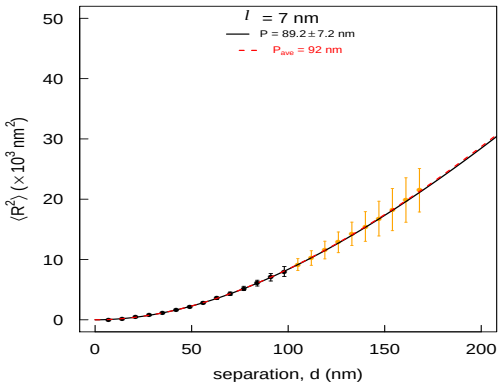
l = 7 nm
P = 89.2±7.2 nm
P_ave = 92 nm
⟨R²⟩ (×10³ nm²)
separation, d (nm)

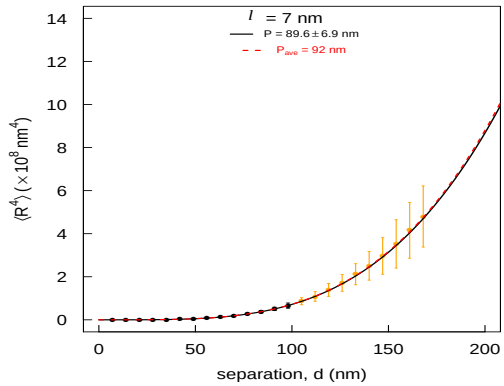
l = 7 nm
P = 89.6±6.9 nm
P_ave = 92 nm
⟨R⁴⟩ (×10⁸ nm⁴)
separation, d (nm)

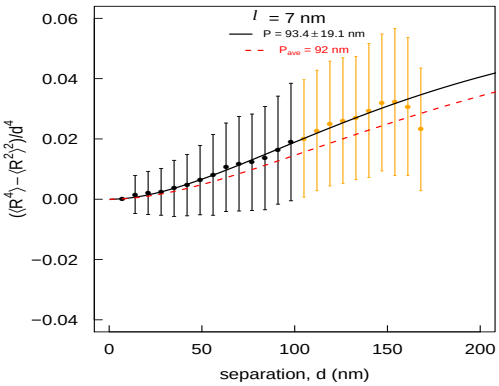
l = 7 nm
P = 93.4±19.1 nm
P_ave = 92 nm
(⟨R⁴⟩−⟨R²⟩²)/d⁴
separation, d (nm)

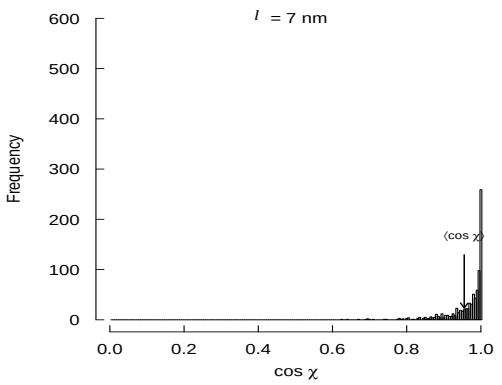
l = 7 nm
Frequency
⟨cos χ⟩
cos χ

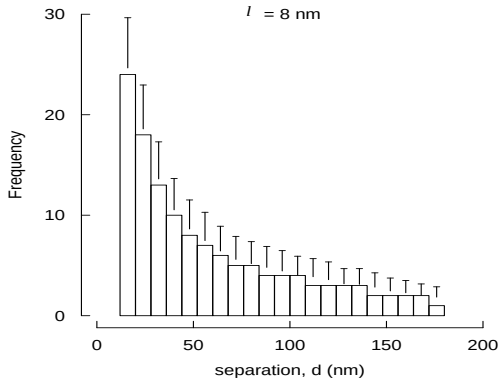
l = 8 nm
Frequency
separation, d (nm)

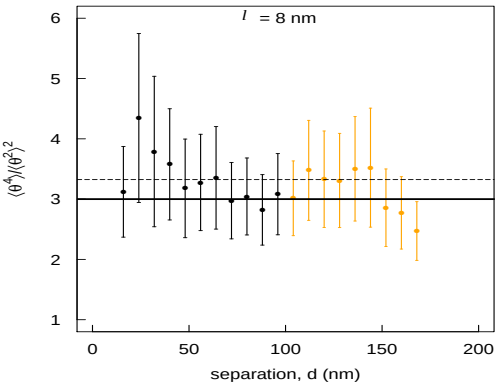
l = 8 nm
⟨θ⁴⟩/⟨θ²⟩²
separation, d (nm)

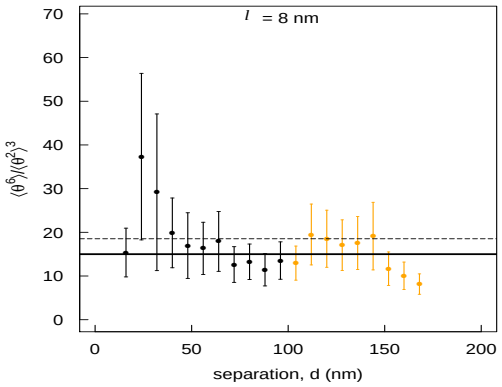
l = 8 nm
⟨θ⁶⟩/⟨θ²⟩³
separation, d (nm)

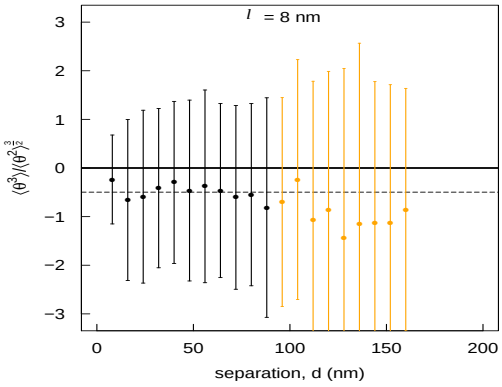
l = 8 nm
⟨θ³⟩/⟨θ²⟩^3/2
separation, d (nm)

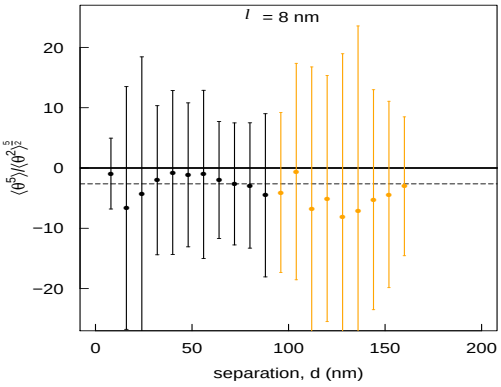
l = 8 nm
⟨θ⁵⟩/⟨θ²⟩^5/2
separation, d (nm)

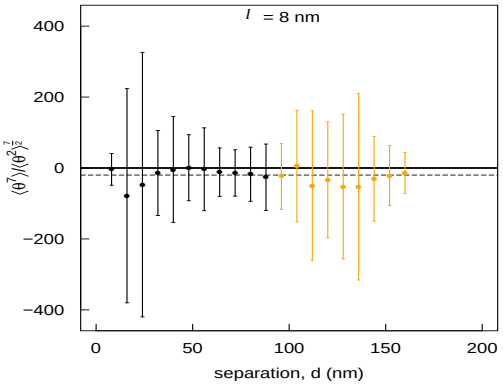
l = 8 nm
⟨θ⁷⟩/⟨θ²⟩^7/2
separation, d (nm)

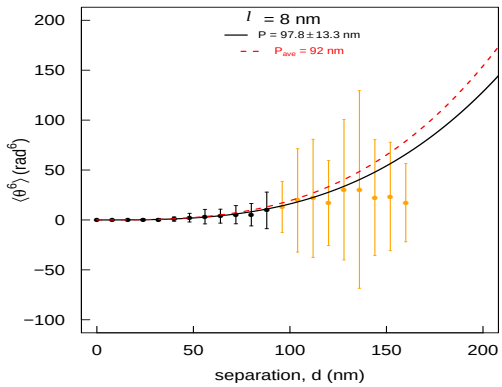
l = 8 nm
P = 97.8 ± 13.3 nm
P_ave = 92 nm
⟨θ⁶⟩ (rad⁶)
separation, d (nm)

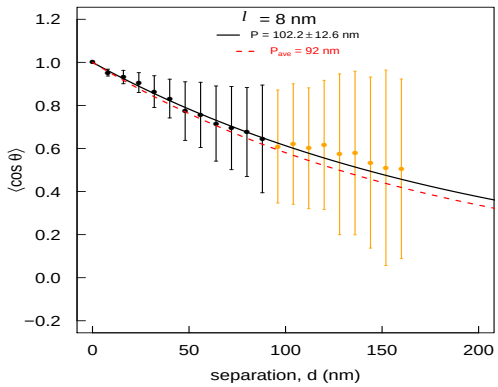
l = 8 nm
P = 102.2 ± 12.6 nm
P_ave = 92 nm
⟨cos θ⟩
separation, d (nm)

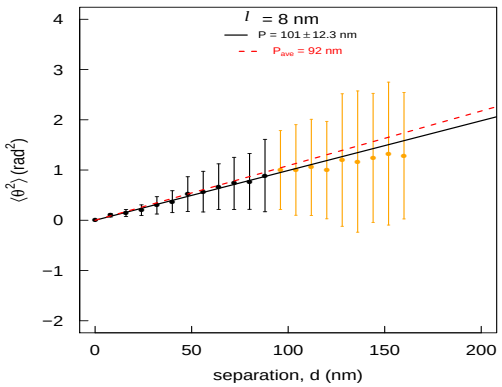
l = 8 nm
P = 101 ± 12.3 nm
P_ave = 92 nm
⟨θ²⟩ (rad²)
separation, d (nm)

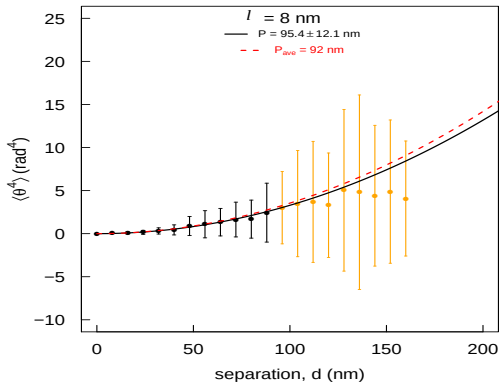
l = 8 nm
P = 95.4 ± 12.1 nm
P_ave = 92 nm
⟨θ⁴⟩ (rad⁴)
separation, d (nm)

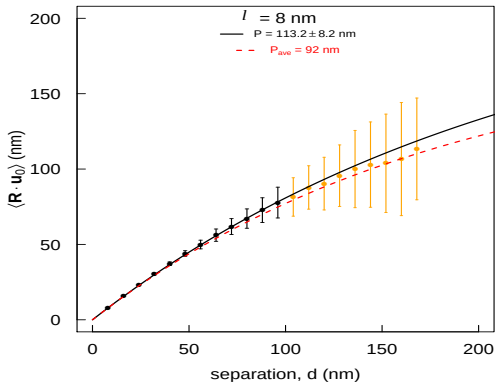
l = 8 nm
P = 113.2 ± 8.2 nm
P_ave = 92 nm
⟨R · u₀⟩ (nm)
separation, d (nm)

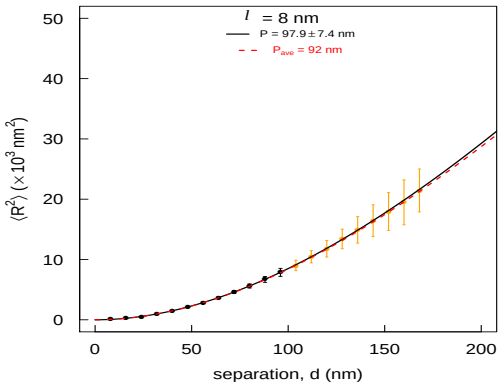
l = 8 nm
P = 97.9 ± 7.4 nm
P_ave = 92 nm
⟨R²⟩ (×10³ nm²)
separation, d (nm)

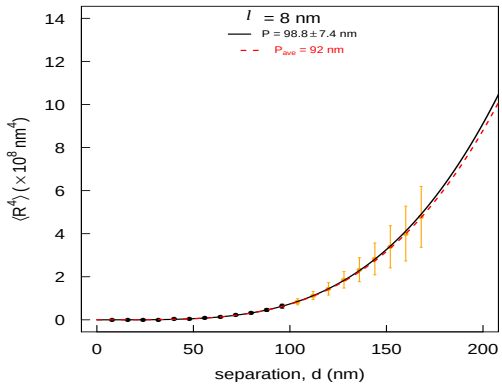
l = 8 nm
P = 98.8 ± 7.4 nm
P_ave = 92 nm
⟨R⁴⟩ (×10⁸ nm⁴)
separation, d (nm)

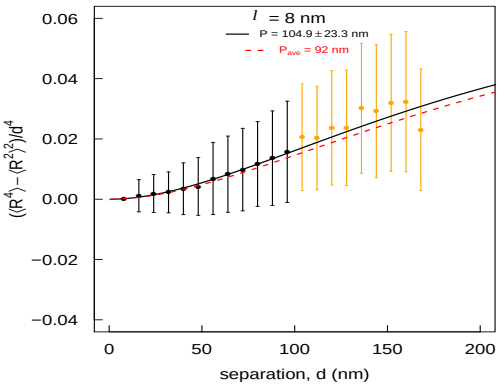
l = 8 nm
P = 104.9 ± 23.3 nm
P_ave = 92 nm
⟨⟨R⁴⟩ − ⟨R²⟩²⟩/d⁴
separation, d (nm)

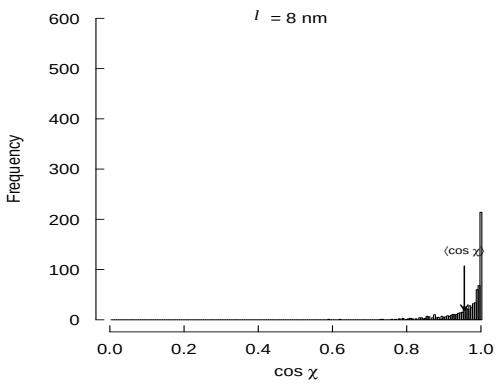
l = 8 nm
Frequency
⟨cos χ⟩
cos χ

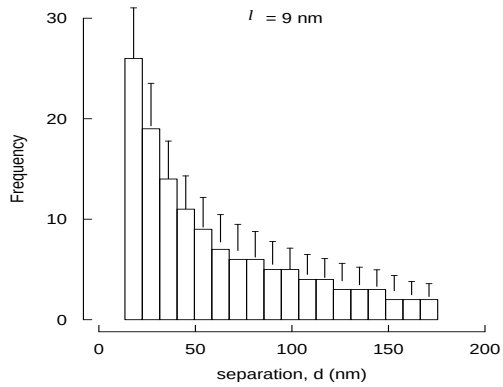
l = 9 nm
Frequency
separation, d (nm)

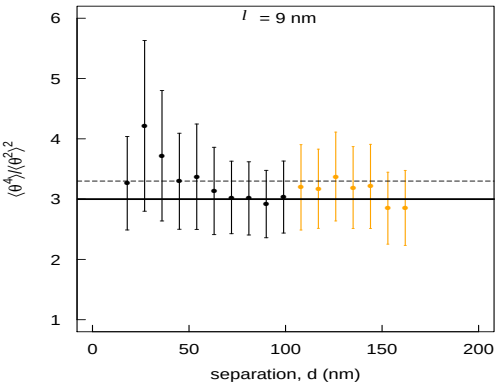
l = 9 nm
⟨θ⁴⟩/⟨θ²⟩²
separation, d (nm)

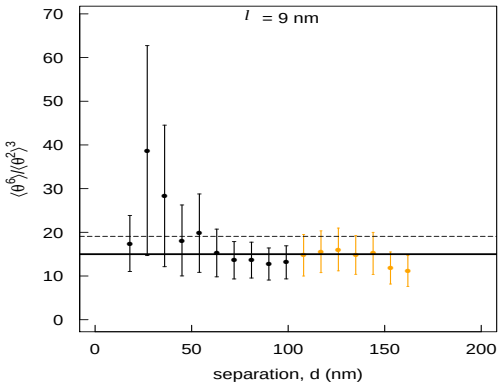
l = 9 nm
⟨θ⁶⟩/⟨θ²⟩³
separation, d (nm)

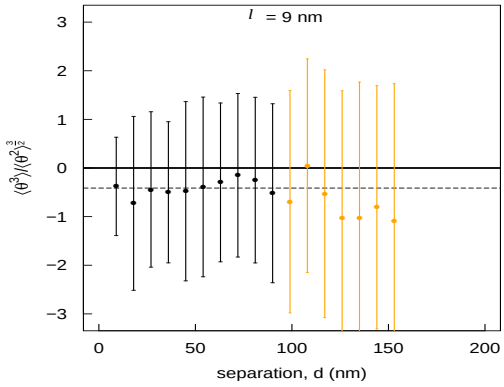
l = 9 nm
⟨θ³⟩/⟨θ²⟩^3/2
separation, d (nm)

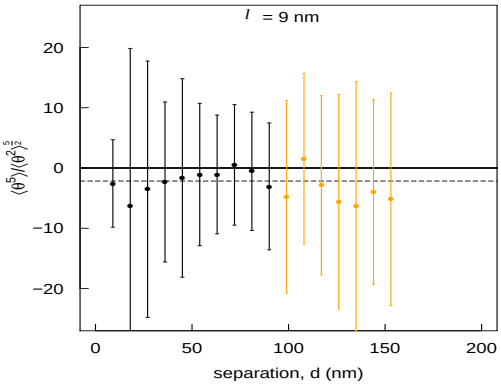
l = 9 nm
⟨θ⁵⟩/⟨θ²⟩^5/2
separation, d (nm)

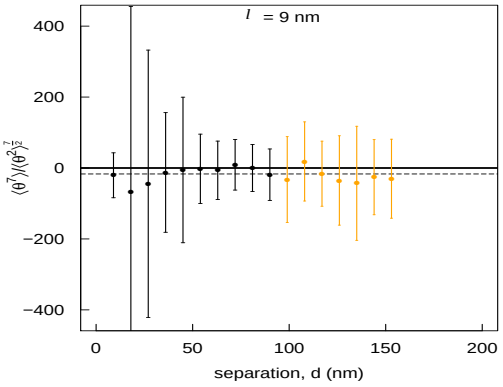
l = 9 nm
⟨θ⁷⟩/⟨θ²⟩^7/2
separation, d (nm)

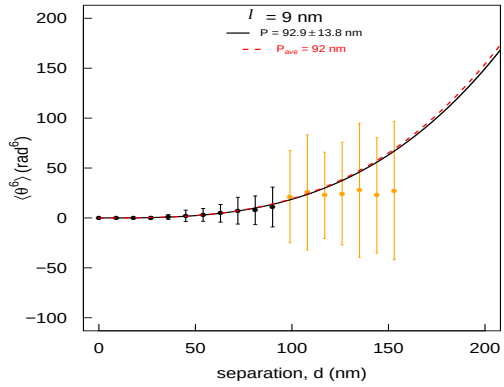
l = 9 nm
P = 92.9±13.8 nm
P_ave = 92 nm
⟨θ⁶⟩ (rad⁶)
separation, d (nm)

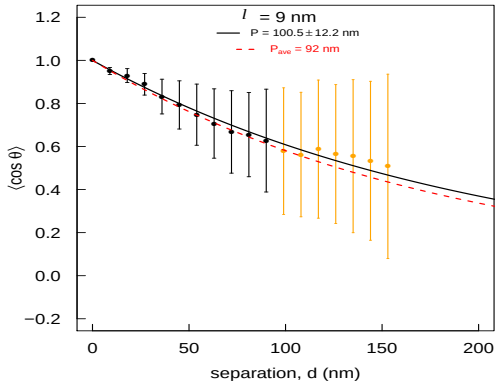
l = 9 nm
P = 100.5±12.2 nm
P_ave = 92 nm
⟨cos θ⟩
separation, d (nm)

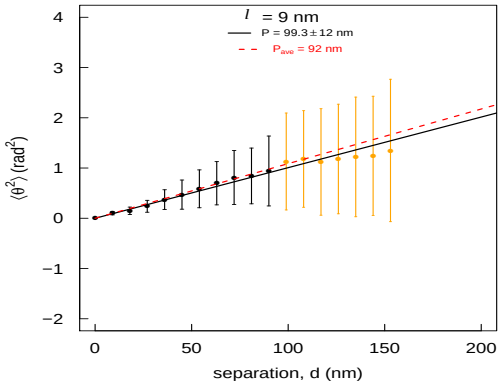
l = 9 nm
P = 99.3±12 nm
P_ave = 92 nm
⟨θ²⟩ (rad²)
separation, d (nm)

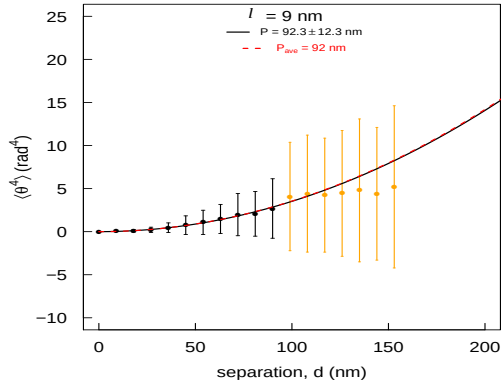
l = 9 nm
P = 92.3±12.3 nm
P_ave = 92 nm
⟨θ⁴⟩ (rad⁴)
separation, d (nm)

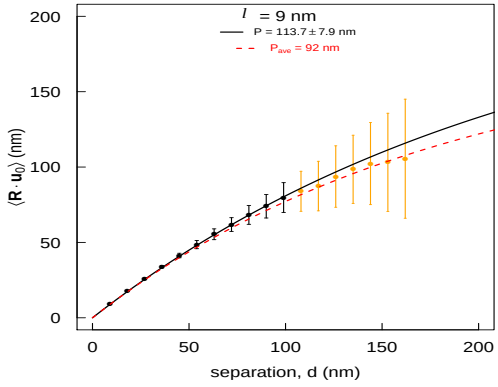
l = 9 nm
P = 113.7±7.9 nm
P_ave = 92 nm
⟨R · u₀⟩ (nm)
separation, d (nm)

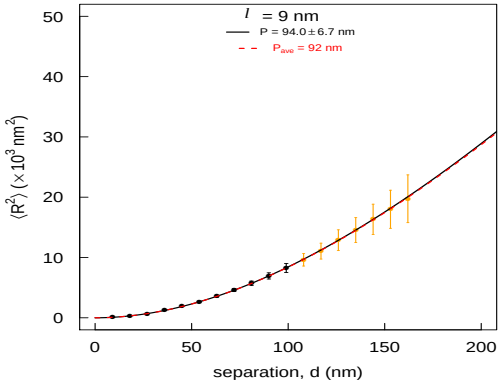
l = 9 nm
P = 94.0±6.7 nm
P_ave = 92 nm
⟨R²⟩ (×10³ nm²)
separation, d (nm)

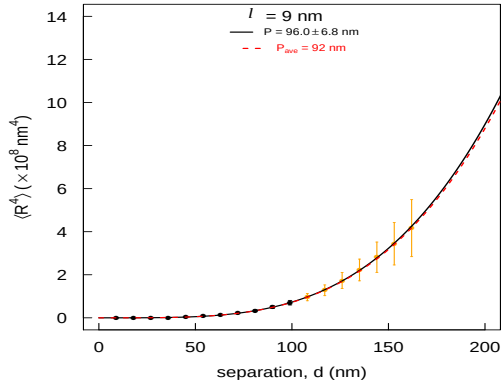
l = 9 nm
P = 96.0±6.8 nm
P_ave = 92 nm
⟨R⁴⟩ (×10⁸ nm⁴)
separation, d (nm)

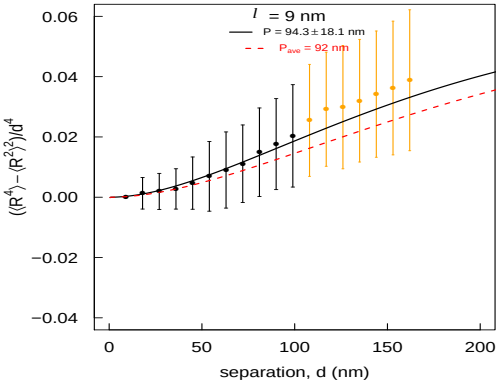
l = 9 nm
P = 94.3±18.1 nm
P_ave = 92 nm
(⟨R⁴⟩−⟨R²⟩²)/d⁴
separation, d (nm)

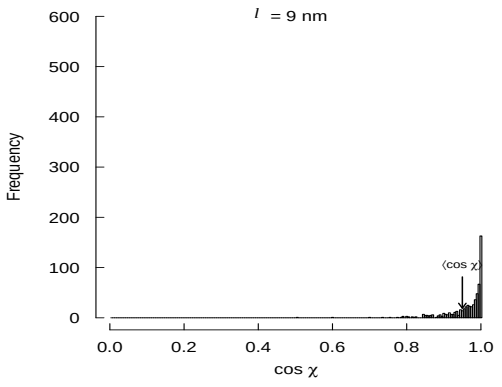
l = 9 nm
Frequency
⟨cos χ⟩
cos χ